Aus dem Institut für Immunologie

Institut der Universität München

Vorstand: Prof. Dr. Thomas Brocker


# *TCR functional avidity defines the size of the clonal $T_{reg}$ cell conversion niche*

Dissertation

zum Erwerb des Doktorgrades der Medizin

an der Medizinischen Fakultät der

Ludwig-Maximilians-Universität München

vorgelegt von

Emanuel Urmann

aus

Bad Soden

2022

Mit Genehmigung der Medizinischen Fakultät der

Ludwig-Maximilians-Universität zu München

| | |
|---|---|
| Erster Gutachter: | *Prof. Dr. Ludger Klein* |
| Zweiter Gutachter: | Prof. Dr. Stefan Endres |
| Dritter Gutachter: | Prof. Dr. David Anz |
| Weitere Gutachter: | Prof. Dr. Arthur Liesz |
| Dekan: | Prof. Dr. Thomas Gudermann |
| Tag der mündlichen Prüfung: | 30.06.2022 |

*Gewidmet meinen Eltern,*

*die mich immer unterstützt haben*

**Acknowledgments** **6**

**Summary** **8**

**Zusammenfassung** **9**

**1. Introduction** **11**

*1.1. T cell receptor and major histocompatibility complex* *11*

*1.2. TCR rearrangement* *13*

*1.3. T cell development* *14*

*1.4. Central tolerance induction* *16*

*1.5. The affinity model of thymocyte selection* *17*

*1.6. TCR-pMHC interaction* *19*

*1.7. PLP - a disease relevant tissue restricted antigen* *23*

*1.8. Mode of tolerance of representative TCRs* *25*

**2. Aim of this thesis** **29**

**3. Results** **30**

*3.1. Toxicity to E. coli of one soluble TCRα chain prevented TCR affinity measurements by SPR spectroscopy.* *30*

*3.2. TCR functional avidity* *39*

*3.3. Assessment of TCR binding characteristics using a tetramer-based approach* *43*

*3.4. Towards measuring TCR-PLP1-IA$^b$ interaction kinetics in situ using a FRET-based microscopy assay* *47*

**4. Discussion** **59**

*4.1. TCR affinity measurements by SPR were prevented by postinduction toxicity of the αTCR-F grey protein to E. coli.* *59*

*4.2. TCR functional avidity defines the size of the clonal $T_{reg}$ cell conversion niche.* *62*

*4.3. Biophysical characterisation of the T cell-APC interaction* *67*

**5. Conclusion and Outlook** **72**

**6. Methods & Material** **74**

*6.1. Protein production* *74*

*6.2. Protein analytics* *78*

*6.3. Stimulation assays of T hybridoma cells* *80*

*6.4. Tetramer assays* *84*

*6.5. Lipid bilayer experiments* *85*

*6.6. Statistical analysis* *85*

*6.7. Materials* *87*

**7. Supplement** **92**

*7.1. Cloning sequences for soluble TCR production* *92*

*7.2. Peptide sequences of myelin proteolipid protein (PLP)* *97*

*7.3. Protein sequences of FRET-IA$^b$ constructs* *98*

**8. References** **100**

**9. List of abbreviations** **110**

**10. Appendix** **112**

*10.1. List of figures* *112*

*10.2. List of tables* *113*

**11. Curriculum Vitae** **114**

**12. Affidavit** **115**

# Acknowledgments

I would like to thank everybody who helped me complete this thesis. It was a great experience that will for sure influence my future understanding of research and science. Without your help, this would not have been possible.

The first one to mention is **Prof. Ludger Klein**. You not only gave a medical student the chance to participate in an exciting research project, but you also personally supported me a lot by patiently explaining to me the "secrets of immunology". Furthermore, you gave me the opportunity to visit numerous retreats, schools, and congresses and helped me giving my work a clear structure. Your way of critically asking questions and breaking them down to clear experiments always impressed me. I hope that I can maintain this way of working for my future. It was a great pleasure being part of your team.

Dear **Christine Federle**, we all know that without your technical support I could never have implemented the complex techniques of this thesis. Your speed and your ability of multitasking were awe-inspiring. Moreover, your support reached far beyond technical assistance. You always encouraged me to overcome phases of little progress. I will miss your energy and pragmatism.

Dear **Dr. Tobias Hassler**, your work is not only the fundament for my thesis, but you also helped me a lot to get started in the beginning. Thank you for always supporting me with advice and PLP1-tetramer. The lab retreats you organized were awesome and one reason for the great atmosphere in our group.

Dear **Dr. Elisabetta Petrozziello**, **Madlen Steinert**, **Sebastian Teschner**, **Dr. Lena Wyss**, **Dr. Tomoyoshi Yamano** and all the other lab-members I had the pleasure of working with, it was a great time. I learned a lot from you and I am really thankful that I could always come to you with questions. I really hope that we stay in contact.

Particularly I want to thank **Prof. Johannes Huppa**, **Markus Kraller** and **Vanessa Mühlgrabner** from the Institute for Hygiene and Applied Immunology in Vienna for our great collaboration. Your FRET based technique to measure T cell receptor affinity is fascinating and offers a totally new perspective on the interaction of T cells with antigen presenting cells. With your help we were able to push the project forward!

Finally, I would like to thank all the people outside the laboratory who have contributed no less to this work. My whole **family** who always supported me and gave me the opportunity to find my way in life. All my **friends** who motivated me and cleared away the cobwebs in times of failure and disappointment that are unfortunately always a part of every research project.

This thesis is based on great teamwork and awesome friendships. I hope that we will all continue working together to understand the immune system and change the world to be a little bit of a better place. Thank you all.

# Summary

A characteristic of the adaptive immune system is the random composition of the antigen receptor repertoire. This potentially allows recognition of any pathogen. Yet statistically, autoreactive immune cells are also generated which, when not removed, can lead to autoimmunity. Therefore, tolerance induction is of major importance to prevent autoimmune diseases e.g., multiples sclerosis. For $CD4^+$ T cells, tolerance induction operates via two fundamentally different mechanisms: autoreactive T cells are either eliminated via apoptosis (negative selection/ clonal deletion) or are converted into regulatory T cells ($T_{reg}$) (clonal diversion).

By repertoire comparisons of mice that are tolerant or non-tolerant to myelin proteolipid protein (PLP) (a potential target molecule for multiple sclerosis), the Klein lab identified four *representative* T cell receptors (TCR) that behave either as PLP dependent deleters or PLP dependent $T_{reg}$ converters. The aim of this thesis was to investigate if TCR intrinsic binding parameters specify the cell fate decision between negative selection and clonal diversion.

TCR functional avidity was assessed by peptide stimulation assays. Furthermore, TCR binding kinetics were characterised using PLP1-tetramer staining capacity and dissociation half-lives. To investigate the molecular interactions in more details, we established cornerstones to measure isolated TCR affinities by surface plasmon resonance spectroscopy (SPR) and TCR *in situ* 2D interactions kinetics by a Förster resonance energy transfer (FRET) based approach.

Our findings support a model in which tolerance induction is mediated by TCR functional avidity. Negative selection was associated with high functional avidity above a certain threshold. For $T_{reg}$ cell induction below this threshold, we found a positive correlation between TCR functional avidity and $T_{reg}$ cell induction efficiency. Therefore, we propose a model where $T_{reg}$ cell conversion depends on a “niche” formed by thymic antigen presenting cells (APC) presenting the selecting antigen at stochastically distributed surface densities. T cells of high functional avidity are more efficiently converted into $T_{reg}$ cells because they can also be activated by APCs with a low antigen density resulting in an absolute larger “niche” size.

# Zusammenfassung

Eine Besonderheit des adaptiven Immunsystems ist das zufällig generierte Repertoire an Antigenrezeptoren. Dies ermöglicht es, potenziell alle Pathogene erkennen zu können. Statistisch entstehen dabei aber auch Rezeptoren, die gegen körpereigene Antigene gerichtet sind. Diese können zu Autoimmunität führen, wenn sie nicht entfernt werden. Aus diesem Grund ist ein Mechanismus zur Toleranzinduktion entscheidend, um die Entstehung von Autoimmunerkrankungen wie z.B. Multiple Sklerose zu verhindern. Für $CD4^+$ T-Zellen stehen hierfür zwei fundamental unterschiedliche Mechanismen zur Verfügung: autoreaktive T-Zellen werden entweder mittels Apoptose eliminiert (negative Selektion/ klonale Deletion) oder so umprogrammiert, dass sie sich in regulatorische T-Zellen ($T_{reg}$) differenzieren (klonale Diversion).

Mittels Repertoire-Analysen in Mäusen, die entweder tolerant oder nicht tolerant gegen Proteolipid-Protein (PLP) (ein potenzielles Zielprotein für Multiple Sklerose) sind, hat die Arbeitsgruppe von Prof. Klein vier *repräsentative* T-Zell-Rezeptoren identifiziert, die entweder PLP abhängig entfernt werden oder in regulatorische T-Zellen umgewandelt werden. Ziel dieser Arbeit war es zu überprüfen, ob T-Zell-Rezeptor-intrinsische Bindungsparameter das Toleranzverhalten zwischen negativer Selektion und klonaler Diversion beeinflussen.

Funktionale T-Zell-Rezeptor-Avidität wurde mittels Peptidstimulationsuntersuchungen analysiert. Des Weiteren wurde die Interaktionskinetik der T-Zell-Rezeptoren durch das Färbeverhalten mit einem PLP1-Tetramer und deren Dissoziationshalbwertszeiten charakterisiert. Um die molekulare Interaktion noch genauer zu untersuchen, haben wir darüber hinaus Grundlagen gelegt, um einerseits die Affinität von isolierten T-Zell-Rezeptoren mittels Oberflächenplasmonenresonanzspektroskopie (SPR) zu messen und andererseits 2D Interaktionskinetiken von T-Zell-Rezeptor *in situ* mittels eines Verfahrens basierend auf Förster-Resonanzenergietransfer (FRET) zu bestimmen.

Die Ergebnisse unserer Arbeit unterstützen ein Modell, in dem die zentrale Toleranzinduktion durch die funktionale T-Zell-Rezeptor Avidität kontrolliert wird. T-Zell-Rezeptoren mit einer hohen funktionalen T-Zell-Rezeptor Avidität über einem Schwellenwert werden negativ selektioniert. Unterhalb dieses Schwellenwertes haben

wir eine positive Korrelation zwischen T-Zell-Rezeptor Avidität und Effizienz der $T_{reg}$ Zell Induktion gefunden. Aus diesem Grund schlagen wir ein Model vor, in dem die $T_{reg}$ Zell Konversion von einer „Nische“ abhängt. Diese wird durch antigenpräsentierende Zellen im Thymus gebildet, die auf ihrer Zelloberfläche eine stochastisch verteile Dichte an selektionierenden Antigenen präsentieren. T-Zellen mit einer hohen funktionalen Avidität werden effizienter in $T_{reg}$ Zellen konvertiert, da sie bereits durch antigenpräsentierende Zellen mit einer geringen Antigendichte aktiviert werden, was zu einer größeren absoluten $T_{reg}$ Konversions-„Nische“ führt.

# 1. Introduction

T cells are specific lymphocytes and an important part of the adaptive immune system. Although T cells are initially derived from multipotent hematopoietic stem cells which are found in the bone marrow, their progenitor cells migrate to the thymus at an early stage of their development and mature there (Bhandoola et al., 2007). T cells get their name from this organ that is fundamental for their development und function. The importance of the thymus can be seen in infants affected by DiGeorge syndrome. Here the thymus is almost completely missing. Those patient suffer from extremely low T cell numbers resulting in recurrent severe infections (Fomin et al., 2010).

## 1.1. T cell receptor and major histocompatibility complex

T cells can be distinguished from other lymphocytes by the presence of the highly specialized T cell receptor (TCR) on the cell surface. Unlike antibodies, the TCR binds peptide fragments of partly degraded proteins that are bound to specialized cell-surface glycoproteins called major histocompatibility complexes (MHC). This phenomenon is referred to as MHC restricted antigen recognition (Yague et al., 1988). There are two classes of MHC molecules: MHC class I (MHC I) and MHC class II (MHC II). While both are important for peptide presentation, their peptides originate from different sources and are obtained via different pathways. For MHC I, peptides are mostly derived from intracellular sources, whereas for MHC II, they are mostly derived from exogenous sources (reviewed in (Neefjes et al., 2011)).

MHC I and MHC II share a similar overall structure. The characteristic MHC binding groove that allows antigen presentation is composed of a β-sheet and two semi-parallel α-helices (Bjorkman et al., 1987). In MHC I molecules, this binding groove is composed of the α chain domains 1 and 2. Each α domain is made of an α-helix and four stands of the β-sheet. In contrast, in MHC II molecules the binding groove is formed by two polypeptide chains. Here, the MHC binding groove is composed of an α1 and a β1 domain which are part of an α and a β chain, respectively (**Figure 1**) (Adams & Luoma, 2013).

MHC class I and class II proteins are highly polymorphic. This allelic variation mainly affects the peptide-binding groove and thereby affects the peptides that are presented on the cell surface. This makes it more difficult for pathogens to evade immune response (Rossjohn et al., 2015).

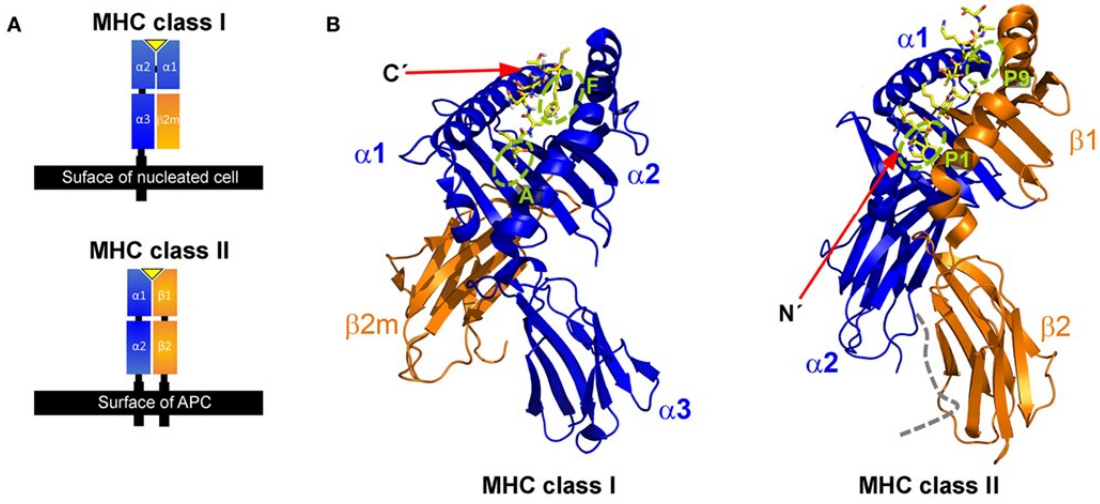


**Figure 1| Structure of MHC I and MHC II: A)** Schematic representation of peptide loaded MHC I and MHC II. **B)** Backbone ribbon representation of MHC I (HLA-A68 in complex with an HIV-derived peptide) and MHC II (HLA-DR1 in complex with a hemagglutinin-derived peptide). The peptide is shown in yellow. The N and C-terminus are highlighted. Relevant pockets of the MHC binding groove are labelled green. Figure was adapted from Adams & Luoma (Adams & Luoma, 2013).

TCRs are composed of a TCRα and a TCRβ chain (Marrack et al., 1983). Both α and β chains consist of an amino terminal variable (V) region followed by a constant (C) domain and a short stalk region containing cysteine residues forming an interchain disulphide bond. Each chain spans the membrane with a hydrophobic transmembrane region and ends in a short cytoplasmatic tail (**Figure 2**) (Murphy & Weaver, 2017).

The TCR overall structure resembles the antigen binding fragment (FAB) of an antibody and is composed of immunoglobulin superfamily domains forming antiparallel β-sheets. The antigen binding site of TCRs is formed by six complementarity determining regions (CDR). Three of these regions are part of the α chain and three are part of the β chain. These hypervariable regions are formed by the flexible loops that link the β-strands of the α and β variable domains. TCR specificity and affinity to antigens is determined by the specific residues at their surface sites and small differences in their relative positions (Al-Lazikani et al., 2000; Garboczi et al., 1996; Garcia et al., 1996; Kjer-Nielsen et al., 2002).

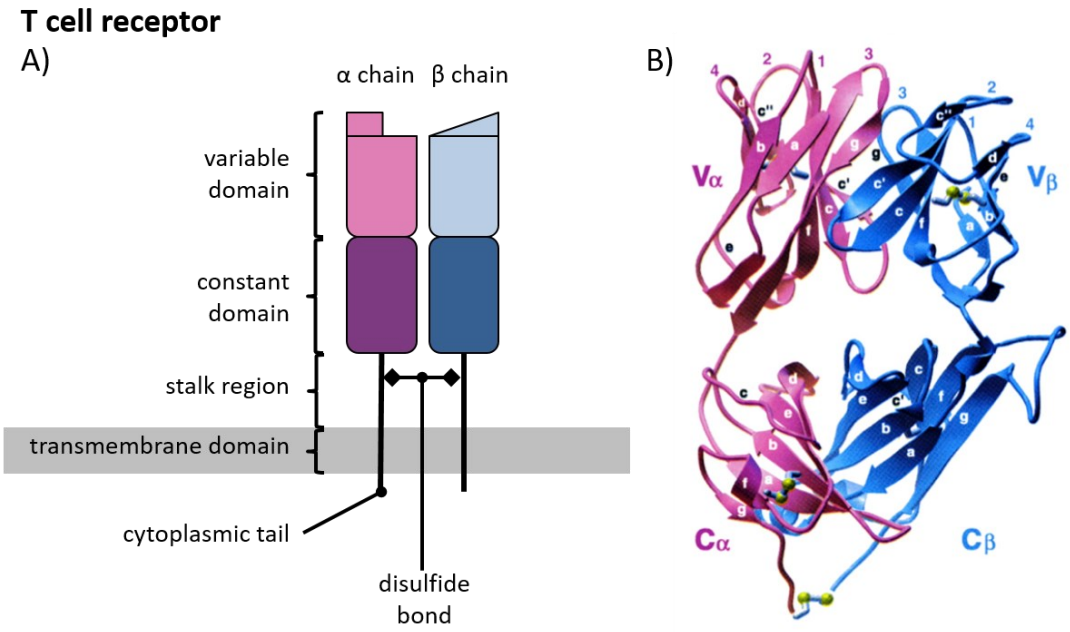


**Figure 2| T cell receptor: A)** Schematic representation of an αβ TCR **B)** Backbone ribbon representation of the 2C TCR. The α chain is shown in pink and the β chain is shown in blue. The sulfur atoms of the disulfide bond are highlighted in yellow. Backbone ribbon was adapted from Garcia et al. (Garcia et al., 1996).

## 1.2. TCR rearrangement

Human peripheral T cells express at least 25 x $10^6$ different TCRs (Arstila et al., 1999) - a repertoire to a large extent already shaped by the selection processes in the thymus. It is impossible for this amount of TCRs to be encoded directly in the genome. Instead, all TCRs are encoded by different combinations of gene segments each of which encodes only parts of the whole receptor. The TCRα variable domain is assembled from a variable (V) and a joining (J) segment. The TCRβ chain contains an additional diversity (D) segment and is assembled from a V, a D and a J segment (Davis & Bjorkman, 1988).

In a process termed V(D)J recombination which is specific for developing lymphocytes these segments are rearranged to form a complete TCR. It is initiated by a heterodimer of the protein products of the recombination activating genes 1 and 2 (RAG-1 and RAG-2) (van Gent et al., 1996). RAG-1 and RAG-2 are both essential for V(D)J recombination as can be seen in RAG-1 or RAG-2 knock out mice that show a total absence of mature B and T cell (Mombaerts et al., 1992). These mice suffer from a severe combined immunodeficiency (SCID).

Further TCR variability beyond the germline-encoded V, D and J repertoire results from DNA repair enzymes randomly adding and removing nucleotides in the process of TCR rearrangement (Bassing et al., 2002). These factors ultimately result in the enormous variability of the TCR.

## 1.3. T cell development

T cells are derived from self-renewing hematopoietic stem cells (HSCs). HSC can be found in the bone marrow and are multipotent cells with lineage potential for all blood cell types (Spangrude et al., 1988). Progenitors that still harbour multilineage potential enter the blood stream and migrate to the thymus. Here they commit to the T cell lineage and differentiate to functional T lymphocytes (Donskoy & Goldschneider, 1992). Those thymus seeding progenitors (TSP) enter the thymus at the corticomedullary junction (Lind et al., 2001) where they substantially proliferate in reaction to environmental signals (Bhandoola et al., 2007).

The earliest thymic progenitors in the thymus are termed double negative (DN) cells due to their lack of CD4 and CD8 surface proteins. They can be subdivided into four stages (DN1 to DN4) and can be distinguished by different expression of CD25, CD44 and CD117 (reviewed in (Koch & Radtke, 2011)). The heterogeneous DN1 subset contains the early thymic progenitors (ETP) that derive from the TSPs and are most efficient at generating T cells (Porritt et al., 2004). After proliferation, the ETPs start migrating deeper into the cortex towards the subcapsular zone. Here, they subsequently differentiate into DN2 thymocytes and become more confined to the T cell lineage and start expressing crucial genes for TCR rearrangement, assembly and signalling (Famili et al., 2017; Porritt et al., 2003). TCR rearrangement starts at the DN2 stage with some D-J rearrangements of the β locus and is continued at the DN3 stage within the subcapsular zone (Famili et al., 2017). Next, the rearranged TCR β chain is coupled to an invariant pre-TCRα chain and is expressed as pre-TCR on the cell surface. In a process called β-selection, successful rearrangement of the TCRβ gene is functionally tested: Ligand independent constitutive signalling through the pre-TCR induces a stop of the β chain rearrangement, proliferation, survival and further differentiation (von Boehmer, 2005). Cells that fail at successfully rearranging the β locus soon die. Thymocytes that pass β-selection mature

to the DN4 stage and begin migrating inwards towards the medulla (Koch & Radtke, 2011). During this process, they start upregulation of CD4 and CD8 and enter the double positive (DP) stage ($CD4^+$ $CD8^+$) (Porritt et al., 2003). At this stage, the TCRα locus is rearranged and a mature TCR is expressed for the first time on the T cell surface.

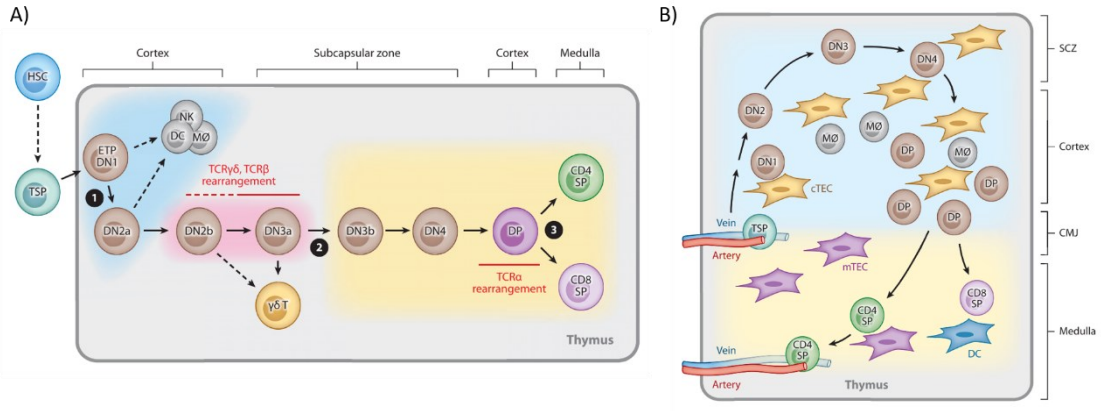


**Figure 3| Thymic T cell development: A)** Schematic representation of the steps of T cell maturation. Important T cell maturation checkpoints are highlighted by circled numbers. ❶ Notch signalling inhibits alternative cell fate potentials. ❷ Ligand independent constitutive signalling through the pre-TCR (rearranged TCRβ chain coupled to an invariant pre-TCRα chain) induces a stop of the β chain rearrangement, proliferation, survival and further differentiation along the αβ T cell lineage. ❸ Positive selection and CD4/CD8 lineage commitment of DP thymocytes. **B)** During T cell maturation T cells migrate through the thymus that can be subdivided into cortex (shown in blue) and the medulla (shown in yellow). SCZ: subcapsular zone; CMJ: corticomedullary junction. Figures were adapted from Koch & Radtke (Koch & Radtke, 2011).

### 1.3.1. Positive selection and CD4/CD8 lineage decision

In a process called positive selection, the TCR of DP thymocytes is functionally tested. Only T cells that express an MHC restricted TCR which induces signalling, survive and further differentiate into mature T cells. The α locus allows multiple rearrangements and thereby increases the chance to create a useful, MHC restricted TCR (Krangel, 2009). Still, a high number of DP cells are not able to produce an MHC restricted TCR and therefore die by neglect (Krueger et al., 2017).

Positively selected DP T cells finally differentiate into either CD4 or CD8 single positive (SP) T cells. The lineage fate is determined by the MHC class that is bound by their TCR. T cells that interact with MHC II differentiate into CD4 SP T cells. In contrast, T cells that interact with MHC I mature into CD8 SP T cells (Germain, 2002). The mechanism by which the TCR specificity determines the fate decision of CD4/CD8 lineage commitment

is still controversially discussed. A kinetic signalling model including co-receptor reversal is favoured at the moment (reviewed in (Singer et al., 2008)).

## 1.4. Central tolerance induction

The random rearrangement of TCRs should potentially allow for recognition of any pathogen. Inevitably, T cells are also generated that strongly react against host proteins. Those could potentially cause severe autoimmune reactions.

To efficiently avoid autoimmunity, the developing T cell repertoire is shaped in the thymus to be tolerant to self-antigens prior to release into the periphery (Kappler et al., 1987). For $CD4^+$ T cells, tolerance operates via two fundamentally different mechanisms: autoreactive T cells are either eliminated via apoptosis (negative selection) (Kisielow et al., 1988) or are reprogrammed to differentiate into $Foxp3^+$ regulatory T cells ($T_{reg}$) (clonal diversion) (Brunkow et al., 2001; Hori et al., 2003; Modigliani et al., 1995; Sakaguchi et al., 1995). Both mechanisms can generate tolerance as $T_{reg}$ cells suppress rather than induce an immune response against an antigen they bind to. They are an important additional tool of tolerance induction as can be seen in scurfy mice that carry a spontaneous loss of function mutation in the transcription factor Foxp3 and therefore lack $T_{reg}$ cells. These mice develop a fatal autoimmune-like lymphoproliferative disease (Vignali et al., 2008). A similar phenotype can be seen in patients suffering from immune dysregulation, polyendocrinopathy, enteropathy, X-linked (IPEX) syndrome. IPEX syndrome is a primary immunodeficiency syndrome which is caused by a mutated Foxp3 gene leading to multiorgan autoimmunity (e.g., severe enteropathy, type 1 diabetes, and eczema) (reviewed in (Bacchetta et al., 2018)).

Paradoxically, both tolerance mechanisms, negative selection and clonal diversion, can result from antigen encounter on thymic stromal cells (Jordan et al., 2001; Starr et al., 2003). Those cells display self-antigens to developing thymocytes and therefore have an important function in tolerance induction (reviewed in (Klein et al., 2014)). Thymic stromal cells can be subdivided into thymic epithelial cells (TECs) and cells of hematopoietic origin that mainly belong to the dendritic cell (DC) lineage. A unique feature of medullary thymic epithelial cells (mTECs) is the ectopic expression and presentation of otherwise tissue-restricted antigens (i.e., self-antigens with an

expression that is otherwise confined to one or a few anatomical sites) by a process termed “promiscuous gene expression” (Derbinski et al., 2001). The protein AIRE (autoimmune regulator) controls a large fraction of this promiscuously expressed gene pool (Anderson et al., 2002). AIRE seems to not act as a conventional sequence-specific transcription factor but instead acts on an epigenetic level via binding to hypomethylated histone 3 lysine 4 (H3L4) (Org et al., 2008). Apparently, it functions as a binding site for numerous protein complexes that are associated with chromatin binding, structure, transcription, and pre-mRNA processing (Anderson & Su, 2016). Interestingly, any given tissue restricted antigen is only expressed by a small fraction of mTECs (1-3 % in a protein approach (Cloosen et al., 2007) and 2-15 % in an mRNA based approach (Derbinski et al., 2008)). However, this mosaic like expression pattern seems to be sufficient to enforce tolerance induction in a physiological, polyclonal setting.

It is still actively debated which T cell intrinsic and extrinsic parameters such as TCR affinity, antigen presenting cells and co-stimulation specify the opposing cell fate decision between negative selection and clonal diversion of autoreactive T cells. However, it is likely that TCR reactivity to the antigens presented in the thymus has a major impact on this decision as it is not only the most obvious difference between thymocytes but also has a huge impact on their function (Hsieh et al., 2012; Josefowicz et al., 2012; Klein & Jovanovic, 2011; Klein et al., 2019; Wirnsberger et al., 2011).

## 1.5. The affinity model of thymocyte selection

The affinity model of thymocyte selection suggests that the strength of the interaction between a TCR and self-peptide-MHC complexes that are displayed on APCs in the thymus determines T cell fate. It was first proposed in the 1980s (Sprent et al., 1988) and was later modified to account for $T_{reg}$ cells within $CD4^+$ thymocytes. According to the modern model, weak interactions prevent that thymocytes die by neglect during positive selection. Thymocytes with weak affinity for self-peptide loaded MHC complexes are released into the periphery as conventional T cells. Strong interaction on the other hand causes negative selection by apoptosis. Clonal diversion (the rerouting of autoreactive thymocytes into $T_{reg}$ cells) is thought to occur in an affinity corridor between positive and negative selection (**Figure 4**) (Klein et al., 2014).

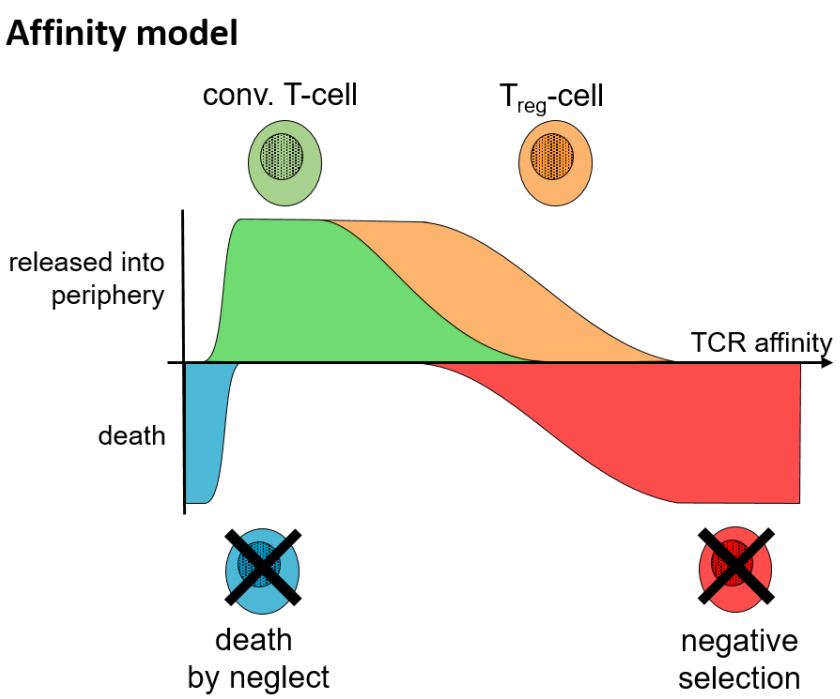


**Figure 4| Affinity model of thymocyte selection:** The affinity model of thymocyte selection suggests that TCR affinity for antigens presented in the thymus determines cell fate. T cells with low TCR affinity fail to complete positive selection and die in a process known as death by neglect. T cells that have a weak TCR affinity for self-peptide loaded MHC complexes are released into the periphery as conventional T cells. Strong interaction on the other hand causes negative selection by apoptosis. Clonal diversion (the rerouting of autoreactive thymocytes into $T_{reg}$ cells) is thought to occur in an affinity corridor between positive and negative selection.

For $CD8^+$ T cells, Naeher et al. found a constant functional avidity threshold between positive and negative selection (Naeher et al., 2007). However, for $CD4^+$ T cells, central tolerance induction is more complex due to the need to account for $T_{reg}$ cells. A study by Hinterberger et al. supported the hypothesis that $T_{reg}$ cells are selected within a corridor below negative selection. They demonstrated that knock-down of MHC II on mTECs decreased negative selection and increased $T_{reg}$ cell induction of an ovalbumin (OVA) specific TCR that, in presence of an AIRE-OVA fusion protein, was otherwise efficiently deleted (Hinterberger et al., 2010). Furthermore, Lee et al. demonstrated in TCR transgenic mice that at a fixed level of OVA expression under the control of the rat insulin promoter, the efficiency of $T_{reg}$ cell selection was correlated with the TCR responsiveness. Negative selection was observed with the more self-reactive TCRs (Lee et al., 2012). However, the affinity model of thymocyte selection still lacks validation in a polyclonal setting as most work was done in TCR transgenic mouse models. Furthermore, it is necessary to have a closer look at the biophysical interaction between

TCRs and peptide loaded MHC complexes as in most studies, T cell reactivity (i.e., the peptide responsiveness of a T cell expressing a given TCR) is used as an approximation of the TCR affinity.

## 1.6. TCR-pMHC interaction

The interaction between a T cell and an APC can be described by several different parameters. How these correlate with T cell function and in particular tolerance induction is incompletely understood and is one aim of this thesis.

### 1.6.1. TCR affinity

A simplified way to describe the interaction between a T cell and an APC is to focus only on the molecular interaction between one TCR and one peptide loaded MHC molecule (pMHC).

A) *TCR + pMHC* $\underset{\text{off rate} = k_{off}}{\overset{\text{on rate} = k_{on}}{\rightleftharpoons}}$ *TCR-pMHC*

B) **Law of mass:**

$$K_D = \frac{[TCR] \times [pMHC]}{[TCR - pMHC]} = \frac{k_{off}}{k_{on}}$$

C) **Kinetic of TCR-pMHC dissociation (1st order reaction)**

$$[TCR - pMHC] = [TCR - pMHC]_0 \times e^{-k_{off} \times t}$$

$$t_{1/2} = \frac{\ln(2)}{k_{off}}$$

**Figure 5| Interaction between TCR and peptide loaded MHC complex (pMHC): A)** Reaction equilibrium of the TCR-pMHC interaction: Bound (TCR-pMHC) and unbound (TCR) T cell receptors are in equilibrium under steady state conditions. For high affinity TCRs, the bound form dominates the equilibrium but low affinity TCRs favour the unbound form. On- and off-rate describe the constant formation and disruption of the TCR-pMHC interaction, respectively. **B)** Under steady state conditions, the law of mass can be used to describe the equilibrium. The dissociation constant ($K_D$) describes the ratio between bound and unbound TCR and correlates with the on ($k_{on}$) and off rate ($k_{off}$) of the interaction. **C)** The disruption of the TCR-pMHC interaction can be described as a first order reaction as indicated. $t_{1/2}$ is the half-life of the interactions.

The main parameters describing this interaction are association rate ($k_{on}$), dissociation rate ($k_{off}$) and dissociation constant ($K_D$) (Stone et al., 2009) (**Figure 5**). $k_{on}$ is the velocity with which the TCR-pMHC complex is formed. $k_{off}$ refers to TCR-pMHC interaction duration (dwell time) and is inversely correlated to the half-life ($t_{1/2}$) of the interaction. $K_D$ is defined as the occupancy of pMHC under equilibrium conditions and describes the strength/affinity of a single TCR-pMHC interaction. A lower $K_D$ correlates with a stronger interaction. Typically, TCR affinity "in isolation" can be measured by surface plasmon resonance spectroscopy (SPR-spectroscopy) (Stepanek et al., 2014).

### 1.6.2. TCR avidity

In contrast to affinity, which describes the strength of a single interaction, avidity refers to the accumulated strength of multiple protein interactions and accounts for the fact that T cells and APCs express multiple TCRs and pMHCs, respectively. An avidity-based model of tolerance induction postulates that in addition to TCR affinity, the density of pMHC ligands on thymic stromal cells is also crucial for tolerance induction. In fact, several studies indicate that the amount of presented antigen influences cell fate (Feuerer et al., 2007; Hinterberger et al., 2010; Lee et al., 2012).

### 1.6.3. Functional avidity / TCR responsiveness

*In vivo*, the interaction between a T cell and an APC also involves costimulatory interactions and adhesion molecules, all of which may play a role in signal integration. Therefore, the term "functional avidity" is often used to describe the overall responsiveness of a T cell to its antigen. Functional avidity is usually measured by *in vitro* T cell resposes to a given concentration of ligand in stimulation assays (Vigano et al., 2012).

### 1.6.4. *In situ* 2D interaction kinetics

As mentioned above, SPR-spectroscopy can be used to determine TCR-pMHC affinity. In this method, soluble unrestricted TCRs flow over pMHCs bound to a sensor in a three-dimensional (3D) environment (Garcia et al., 2001). In contrast to this reductionist setting, within the immunological synapse formed between a T cell and an APC, both

the TCR and the pMHC are embedded in complex membrane environments and are constrained to fewer degrees of freedom. In this setting the TCR-pMHC interaction is influenced by cell specific factors which include forces derived from cell-cell contacts and membrane protein interactions as well as geometrical constraints of the immunological synapse. The dissociation constant in this setting is referred to as two dimensional (2D)-$K_D$ (Axmann et al., 2015a; Kolawole et al., 2020).

To account for this and to describe the *in vivo* interactions more accurately, systems have been developed to study TCR-pMHC interactions in 2D systems where proteins are embedded in membranes and the TCR-pMHC interaction is part of an immunological synapse (Edwards et al., 2012). Those are often referred to as *in situ* measurements.

### 1.6.5. A FRET-based microscopical assays to measure TCR-pMHC binding kinetics *in situ*

Huppa et al. developed a microscopy assay based on Förster resonance energy transfer (FRET) to measure kinetics of the TCR-pMHC interaction *in situ* for peptides displayed on the MHC II molecule $IE^K$ (Axmann et al., 2015a; Huppa et al., 2010).

*Förster resonance energy transfer (FRET)*

FRET describes a mechanism of energy transfer between two chromophores with overlapping donor-emission und acceptor-absorption spectrums. During FRET, energy transfer occurs from a donor fluorophore to an acceptor fluorophore through dipole-dipole coupling. Importantly, the efficiency of this energy transfer critically depends on the distance between donor and acceptor fluorophore und decreases with the sixth power. This allows sensitive detection of small changes in distance. Typically, FRET signals can only be observed between fluorophores less than 100 Å apart. Site specific labelling of two proteins with the donor and the acceptor FRET fluorophore, respectively, can be used to determine whether the proteins are within a close distance of each other – a strong indication for their interaction (Zadran et al., 2012).

To detect TCR-pMHC interaction, Huppa et al. labelled TCRs with a single-chain variable fragment (scFv) derived from the monoclonal anti-TCRβ antibody H57 that was labelled with the FRET donor fluorophore Alexa 555. pMHCs were directly labelled with the corresponding FRET acceptor fluorophore Alexa 647 by maleimide-thiol reaction in a site-specific manner. The pMHC was reconstituted into a glass-supported lipid bilayer

via a lipid-anchor. This bilayer was functionalized with the adhesion molecule ICAM-1 and the co-stimulatory molecule B7-1, thus emulating the surface of an APC.

Upon addition of T cells to this functionalized lipid bilayer, formation of microclusters and immunological synapses were observed. The interaction between TCR and pMHC was displayed by FRET from the donor to the acceptor fluorophore and was visualized by high-resolution microscopy.

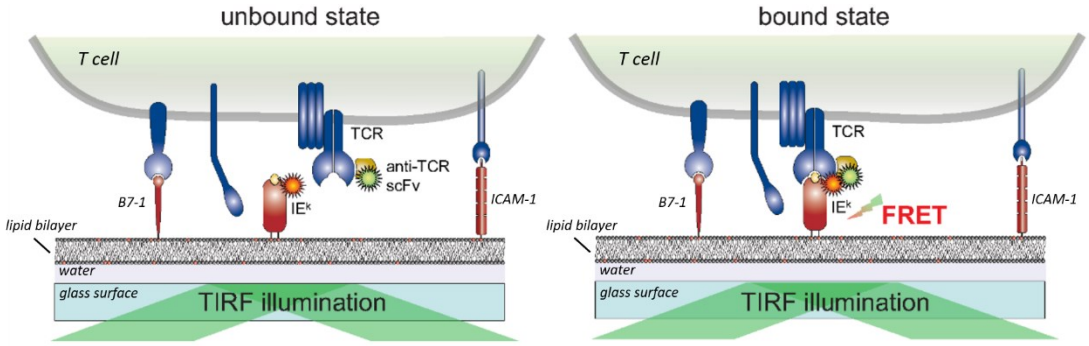


**Figure 6| FRET-based assay to quantify TCR-pMHC binding *in situ*:** The principle of detecting a TCR-pMHC interaction *in situ* is illustrated. The peptide loaded MHC II molecule $IE^K$ is stained with a FRET acceptor fluorophore and anchored to a lipid bilayer functionalized with B7-1 and ICAM-1. Thus, the lipid bilayer works as a model for an APC. The TCR is labelled with a FRET donor fluorophore that is attached to an anti-TCR single chain variable fragment (scFv). Upon interaction, energy is transferred from the donor to the acceptor fluorophore by FRET. This can be detected by high-resolution microscopy on a single molecule level. A special type of microscopy, total internal reflection fluorescence (TIRF) microscopy, was used to reduce cellular background as in TIRF illumination, only the basal cellular membrane in contact to the lipid bilayer is excited. Figure was adapted from Axmann et al. (Axmann et al., 2015a).

This setup allows measuring of *in situ* TCR affinity represented by 2D $K_D$ and kinetic off-rate $k_{off}$ of the TCR-pMHC interaction.

The 2D $K_D$ value of the TCR-pMHC interaction can be calculated from the FRET yield either of entire synapses or of TCR microclusters as determined by donor recovery after acceptor photobleaching. Basically, the FRET yield describes the amount of energy that is transferred from the FRET donor channel to the acceptor channel. It is directly proportional to the TCR occupancy. By comparing the FRET donor signal before and after photobleaching the FRET acceptor fluorophore, the FRET yield can be measured. Finally, 2D $K_D$ values can be calculated from FRET yield. $k_{off}$ was measured by tracking the lifetimes of individual single molecule TCR-pMHC interactions and mathematical modelling (Axmann et al., 2015a).

In summary, this method allows the precise description of the TCR-pMHC interaction in an immunological synapse and offers a remarkable potential to better understand the tolerance inducing interactions in the thymus under more physiological conditions.

## 1.7. PLP - a disease relevant tissue restricted antigen

To investigate tolerance induction of tissue restricted antigens, we chose to focus on myelin proteolipid protein (PLP) as a disease relevant autoantigen.

PLP is a hydrophobic transmembrane protein that is highly conserved between different mammals. It is one of the most abundant proteins in the myelin sheets of the central nervous system (reviewed in (Greer & Lees, 2002)). Furthermore, it can be used to induce experimental autoimmune encephalitis (EAE) in mice – a disease model for multiple sclerosis (Sobel et al., 1986). Remarkably, it can be knocked out without a major phenotype (Rosenbluth et al., 2006) making it an optimal target to investigate tolerance induction.

Klein et at. identified the $IA^b$ restricted target epitopes of PLP reactive $CD4^+$ T cells in $PLP^{knock\ out\ (KO)}$ C57BL/6 mice by re-stimulating T cells from mice immunized with PLP with an overlapping 25-mer peptide library reflecting the entire PLP protein (Klein et al., 2000). They found three immunogenic regions. In a next step, overlapping 12-mer peptides were used to fine-map these regions in order to identify the $IA^b$-restricted epitopes of PLP (**Figure 7**). By this, three 9-mer core epitopes could be identified that span the amino acids $PLP_{11\text{-}19}$ (PLP1), $PLP_{174–182}$ (PLP 2), and $PLP_{240–248}$ (PLP 3) (Wang et al., 2017). For analysis of central tolerance induction against the tissue restricted protein PLP, we decided to focus our analysis on the $PLP_{11\text{-}19}$ (PLP1) core epitope. Firstly, because of availability of a $PLP_{11\text{-}19}$-tetramer (see 1.7.1) that can be used to identify PLP1 specific T cells. Secondly, because C57BL/6 mice were mostly resistant to experimental autoimmune encephalitis (EAE) induction using this peptide (Wang et al., 2017) indicating a sufficient tolerance induction in $PLP^{wild\ type\ (WT)}$ mice.

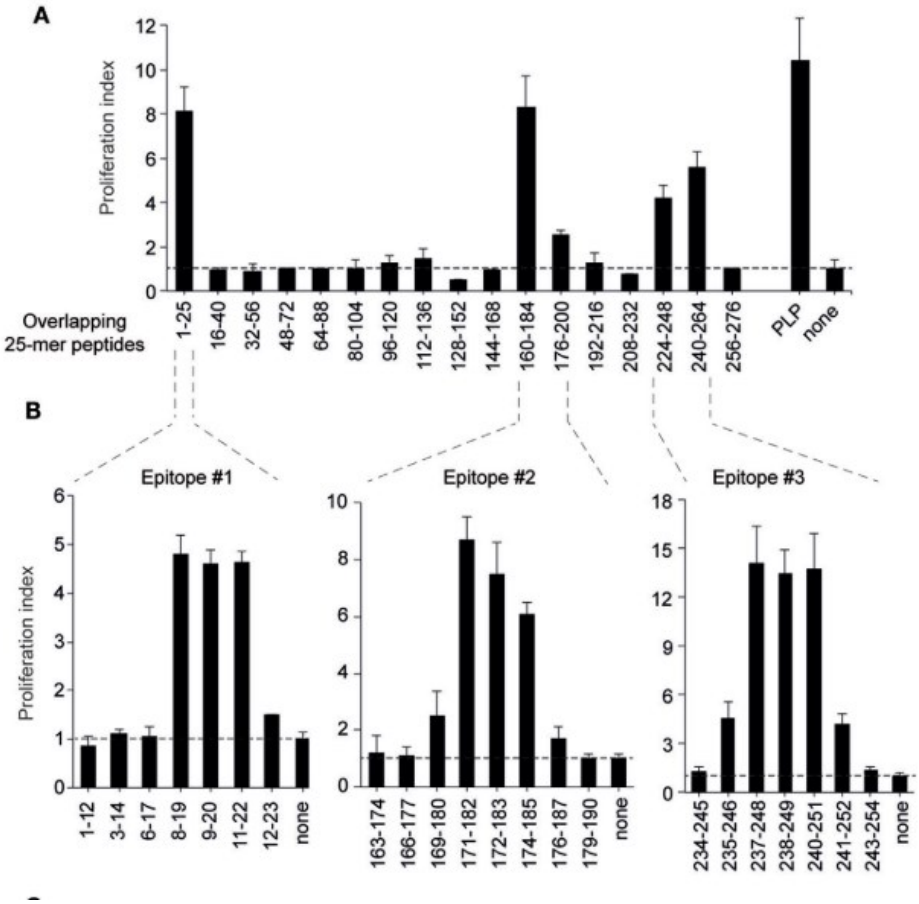


**Figure 7| IA$^b$ restricted epitopes of PLP: A)** PLP protein was used to immunize PLP$^{KO}$ C57BL/6 mice. After 9 days, cells derived from draining lymph nodes were isolated and re-stimulated with an overlapping 25-mer peptide library reflecting the entire PLP protein. **B)** Overlapping 12-mer peptides were used to fine-map and to identify the IA$^b$-restricted core epitopes of PLP. Figure was adapted from Wang et al. (Wang et al., 2017).

### 1.7.1. PLP1-tetramer

TCR-pMHC interactions are generally of low affinity (more than 1,000-fold weaker than a typical antibody–antigen interaction (Davis et al., 1998)) rendering it difficult to specifically identify TCRs using soluble peptide loaded MHC complexes (in analogy to the detection of specific B cells using fluorochrome labelled B cell antigens). MHC-tetramer technology was developed to overcome this hurdle. By coupling multiple pMHCs, the avidity of the interaction was increased allowing detection of peptide specific TCRs for instance by flow cytometry (Altman et al., 1996).

PLP$_{11-19}$-IA$^b$-tetramer (PLP1-Tet) can be used to detect PLP1 specific T cells (Hassler et al., 2019) in C57BL/6 mice expressing the MHC II molecule IA$^b$. In this construct, the PLP1 core epitope is covalently attached to the MHC II β chain via a linker region. The

construct contains an E. coli biotin ligase (BirA) signal sequence (Beckett et al., 1999) that allows site-specific biotinylation of the α chain, and a 6-His tag on the β chain. Both can be used for purification using an avidin column and nickel affinity chromatography, respectively. Furthermore, a Fos-Jun leucine zipper motif forces the MHCII α and β chains to dimerize.

The PLP1-tetramer is assembled from four $PLP_{11-19}$-$IA^b$-monomers (PLP1-$IA_b$). Tetramerization is mediated by biotin-streptavidin interactions (Hassler et al., 2019; Moon et al., 2007).

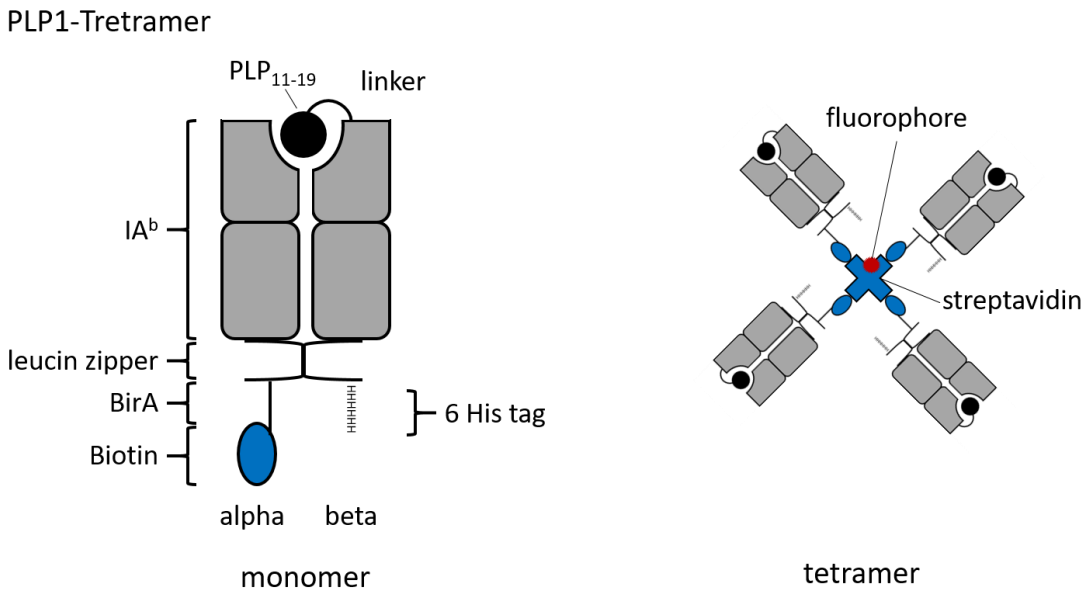


**Figure 8| Schematic representation of PLP1-tetramer.**

## 1.8. Mode of tolerance of *representative* TCRs

Hassler et al. addressed how the $CD4^+$ T cell repertoire of C57BL/6 mice is shaped by tolerance induction to PLP (Hassler et al., 2019). They could show that some PLP specific TCRs were deleted from the $CD4^+$ T cell repertoire, while others were differentiated into $T_{reg}$ cells.

In their approach, they used a PLP1-tetramer to select PLP1 specific $CD4^+$ T cells and compared the uncensored TCR repertoire of $PLP^{KO}$ mice with the tolerant TCR repertoire of $PLP^{WT}$ mice. Interestingly, $PLP^{WT}$ mice contained not less but even slightly higher numbers of PLP1-$Tet^+$ CD4 single positive (SP) cells ($PLP^{KO}$ vs. $PLP^{WT}$ 14.0±3.0 vs.

18.4±4.4). 30 %-40 % of those PLP1-Tet$^+$ cells expressed Foxp3 as a marker for $T_{reg}$ cells in PLP$^{WT}$ mice whereas Foxp3$^+$ cells were hardly detectable in PLP1-Tet$^+$ T cells of PLP$^{KO}$ mice.

In a fully polyclonal setting, the high number of TCRα and TCRβ chain combinations recognizing a given antigen (see 1.2) makes a comprehensive comparison of the PLP specific TCR repertoire of PLP$^{KO}$ and PLP$^{WT}$ mice by single-cell TCR sequencing impossible. Hassler et al. circumvented this inherent limitation by reducing the repertoire complexity to the diversity of TCRα chain by introduction of a transgenic TCRβ chain. This TCRβ chain was derived from a PLP1-specific TCR to bias the repertoire a little bit towards a higher number of PLP1-specific T cells.

In those "fixed-β" PLP$^{WT}$ mice, more than 57 % of the PLP1-Tet$^+$ cells were Foxp3$^+$ whereas in respective PLP$^{KO}$ mice only 5.8 % were $T_{reg}$ cells. By single cell TCRα sequencing of fixed-β PLP1-Tet$^+$ CD4$^+$ T cells from PLP$^{KO}$ and PLP$^{WT}$ mice Hassler et al. characterized the composition of the different TCR repertoires. The TCR repertoire of T cells derived from the thymus of PLP$^{KO}$ mice functioned as an uncensored reference library as these cells were neither shaped by PLP specific tolerance induction nor were influenced by peripheral homeostasis (**Figure 9A**). Analysis was focused on four *representative* TCRs (*TCR-A yellow*, *TCR-E salmon*, *TCR-F grey* and *TCR-L blue*) together accounting for app. 50 % of the PLP1-Tet$^+$ population.

The TCR repertoire of fixed-β PLP1-Tet$^+$ Foxp3$^-$ CD4 SP cells in the thymus of PLP$^{WT}$ mice resembled the distribution in the uncensored reference library of PLP$^{KO}$ mice. In contrast, the TCR composition of thymic PLP1-Tet$^+$ Foxp3$^+$ $T_{reg}$ cells was substantially different. For instance, *TCR-A yellow* was highly overrepresented. *TCR-E salmon* and *TCR-F grey* were missing or were significantly underrepresented, respectively. Only for *TCR-L blue* a similar abundancy was observed in the thymic TCR repertoire of PLP$^{WT}$ mice and in the reference library of PLP$^{KO}$ mice both for Foxp3$^+$ and Foxp3$^-$ T cells (**Figure 9B**).

The TCR repertoire of the peripheral PLP1-Tet$^+$ Foxp3$^+$ $T_{reg}$ cells in PLP$^{WT}$ mice was similar to the $T_{reg}$ cell repertoire in the thymus. *TCR-A yellow* was dominant and *TCR-L blue* was significantly abundant, *TCR-E salmon* was rare and *TCR-F grey* was absent. Interestingly,

the distribution of the *representative* TCRs among Foxp3$^-$ CD4$^+$ T cells was essentially the same as that of $T_{reg}$ cells (**Figure 9C**).

Hassler et al. concluded that *TCR-A yellow* acts as an efficient diverter TCR as in PLP tolerant mice *TCR-A yellow* was dominant in the $T_{reg}$ cell compartment. *TCR-L blue* also contributed to the $T_{reg}$ cell compartment although not as efficiently as *TCR-A yellow*. On the other hand, *TCR-F grey* was mostly absent in the tolerant peripheral repertoire, albeit being at least as abundant as *TCR-A yellow* in the uncensored reference repertoire. This suggests that *TCR-F grey* is deleted when PLP is expressed in mice classifying *TCR-F grey* as a deleter TCR. *TCR-E salmon* was difficult to classify from this repertoire analysis itself. It was not found in the repertoire of PLP$^{WT}$ Foxp3$^+$ thymocytes and Foxp3$^-$ peripheral CD4$^+$ T cells but could be found at a low frequency in PLP$^{WT}$ Foxp3$^+$ peripheral repertoire. Thereby *TCR-E salmon* behaved like a low potency diverter with reduced frequency in the peripheral Foxp3$^-$ compartment.

| *Representative* TCR | Classification of tolerance induction mode |
|---|---|
| TCR-A yellow | efficient diverter |
| TCR-E salmon | low efficient diverter + reduced frequency |
| TCR-F grey | deleter |
| TCR-L blue | less efficient diverter |

**Table 1| Classification of *representative* TCRs:** The classification of tolerance induction against PLP of the *representative* TCRs is based on the repertoire analysis by Hassler et al. (Hassler et al., 2019).

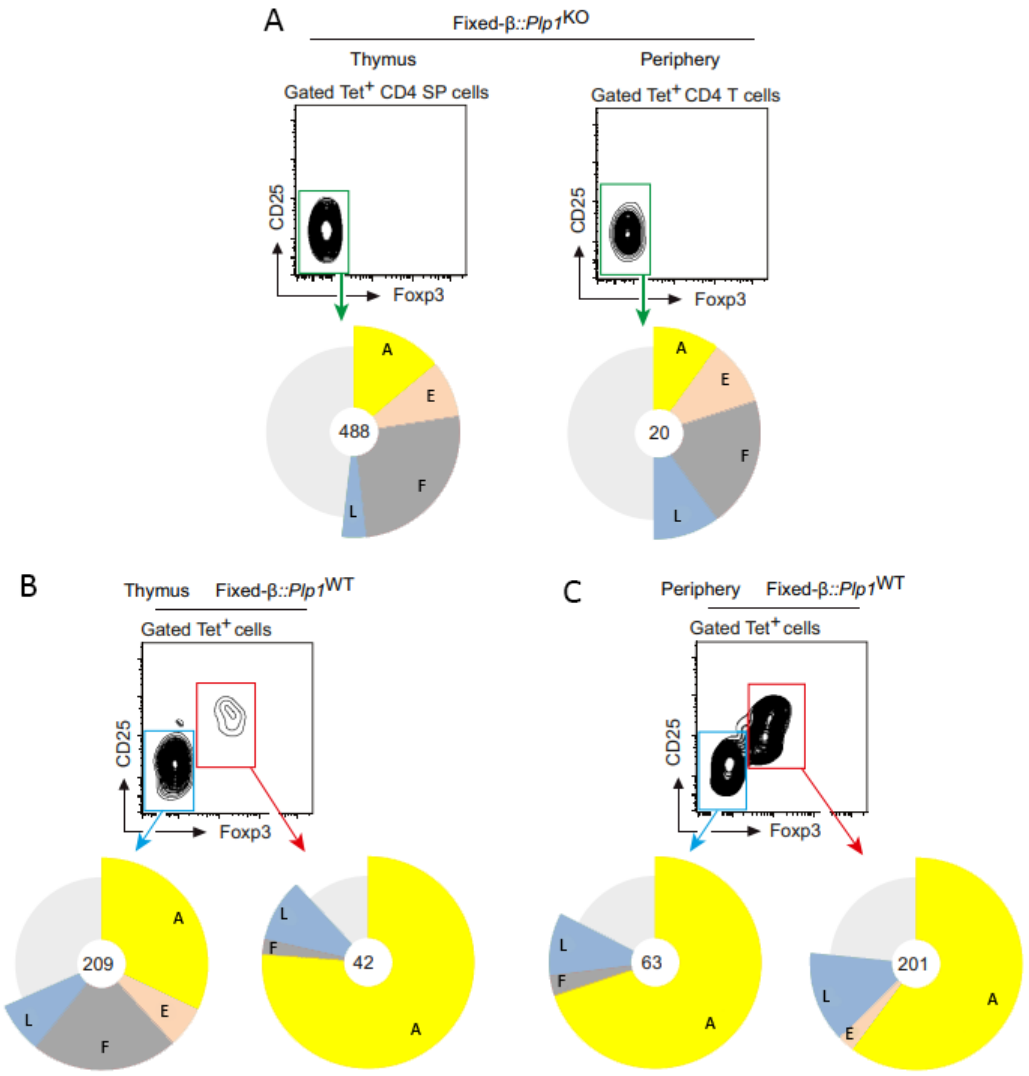


**Figure 9| PLP1-tetramer specific repertoire analysis:** T cells specific for PLP were isolated from mice expressing a fixed TCRβ chain using the PLP1-tetramer. Alpha chains of PLP1-Tet$^{+}$, CD4$^{+}$ thymic and peripheral T cells were sequenced to generate the PLP specific TCR repertoires of PLP$^{KO}$ and PLP$^{WT}$ mice. **A)** PLP specific TCR repertoire of PLP1$^{KO}$ mice: Frequency of the four *representative* TCRs A, E, F, and L in thymus and periphery. The colourless sector summarizes all other PLP specific TCRs which could be detected with a frequency of >1 %. The total number of cells that were included in the respective TCR repertoire can be found in the centres of the pie chart. **B/C)** PLP specific TCR repertoire of PLP1$^{WT}$ mice separated in Foxp3$^{+}$ and Foxp3$^{-}$ T cell: Frequency of the four *representative* TCRs A, E, F, and L in the **B)** thymus and **C)** periphery. Figure was adapted from Hassler et al. (Hassler et al., 2019).

# 2. Aim of this thesis

The generation of the receptor pool of the adaptive immune system contains random elements. Therefore, central tolerance induction is of major importance to prevent autoimmune diseases. For $CD4^+$ T cells, tolerance induction operates via two fundamentally different mechanisms: autoreactive T cells are either eliminated via apoptosis (negative selection or clonal deletion) or are reprogrammed to differentiate into regulatory T cells (clonal diversion). However, which cell intrinsic and extrinsic parameters specify this important cell fate decision remains largely elusive.

By repertoire comparisons of mice that are tolerant or non-tolerant to PLP, the Klein lab identified four *representative* TCRs that behave either as PLP dependent deleters or PLP dependent $T_{reg}$ cell converters. Aim of this thesis was to investigate if TCR intrinsic binding parameters specify the cell fate decision between negative selection and clonal diversion. To do so, we will use SPR-spectroscopy, peptide stimulation assays and tetramer-based approaches to measure different parameters of TCR binding. Furthermore, we want to establish a new technique to investigate the T cell-APC interaction *in situ*, in an immunological synapse, to study kinetics of the TCR-pMHC interactions under more physiological conditions. Ultimately, we will check for correlations between the measured TCR binding characteristics and the observed mode of tolerance in the PLP repertoire analysis and we will test if the affinity-model of thymocyte selection correctly predicts mode of tolerance of the four *representative* TCRs.

# 3. Results

## 3.1. Toxicity to E. coli of one soluble TCRα chain prevented TCR affinity measurements by SPR spectroscopy.

To measure the affinity of the interaction between a TCR and a PLP loaded MHC complex by SPR spectroscopy, a soluble version of the TCR is needed. The soluble versions of the TCRs were designed as chimeric proteins by linking the TCRα and TCRβ variable (V) domains to corresponding human constant (C) domains. Conserved amino acids between human and mice functioned as a linker between the mice V and the human C region. To achieve solubility of the complexes, TCR transcription was designed to stop directly before the position where the α and β chain normally form an interchain disulphide bond (**Figure 10**) (Steele et al., 2003).

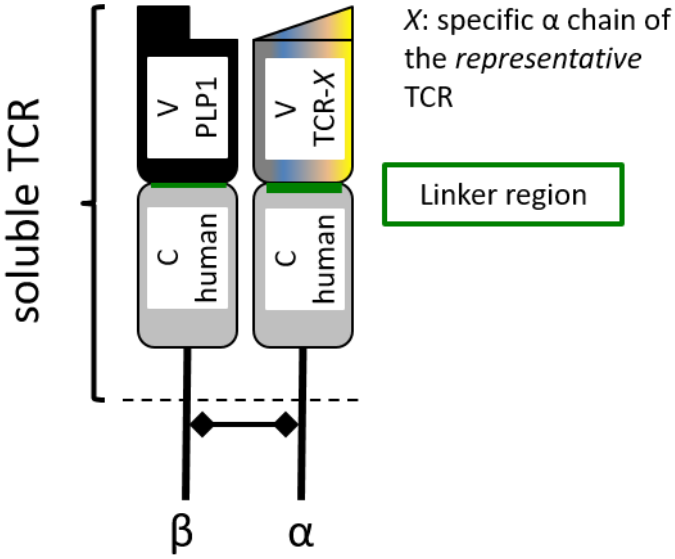


**Figure 10| Schematic representation of a soluble TCR:** Soluble TCRs were designed as chimeric proteins. TCRα and TCRβ variable (V) domains were linked to corresponding human constant (C) domains. All of the TCRs used in the present study contain the same β chain (β*TCR-PLP1*) paired to a different α chain. Transcription of soluble TCRs was designed to terminate directly before the position where the α and β chain normally form an interchain disulphide bond.

### 3.1.1. Successful expression of three α chains and the common β chain in E. coli

All of the TCRs employed in the present study comprise the same β chain (β*TCR-PLP1*) paired to a different α chain. Expression of the common β chain and the four TCRα chains was performed in BL21(DE3) E. coli using an isopropyl-β-D-thiogalactopyranosid (IPTG) inducible T7 RNA polymerase expression system under the control of the lac I operator.

The common β*TCR-PLP1* chain and three out of four α chains (α*TCR-A yellow*, α*TCR-E salmo*n and α*TCR-L blue*) were successfully expressed in inclusion bodies of E. coli with high yields of estimated 100-150 mg protein per litre LB culture. This was validated using sodium dodecyl sulfate polyacrylamide gel electrophoresis (SDS page) and protein quantification. However, expression of α*TCR-F grey* was unsuccessful under standard conditions (induction at 37 °C with 1 mM IPTG for 4 h in presence of kanamycin) in BL21(DE3) E. coli. Neither SDS page analysis of the total bacterial lysate (data not shown) nor analysis after inclusion body isolation revealed a band at 23 kDa (i.e., the expected weight of the α chain), indicating a lack of proper recombinant production of the α*TCR-F grey* chain (**Figure 11A**). Along these lines, the collected α*TCR-F grey* pellet after inclusion body isolation was much smaller and more gelatinous compared to the other TCRs indicating that indeed a much smaller amount of protein was produced (**Figure 11B)**.

For an adequate analysis of tolerance induction against PLP, it would be important to collect affinity data for all four *representative* TCRs. For this reason, we used different approaches to improve α*TCR-F grey* expression.

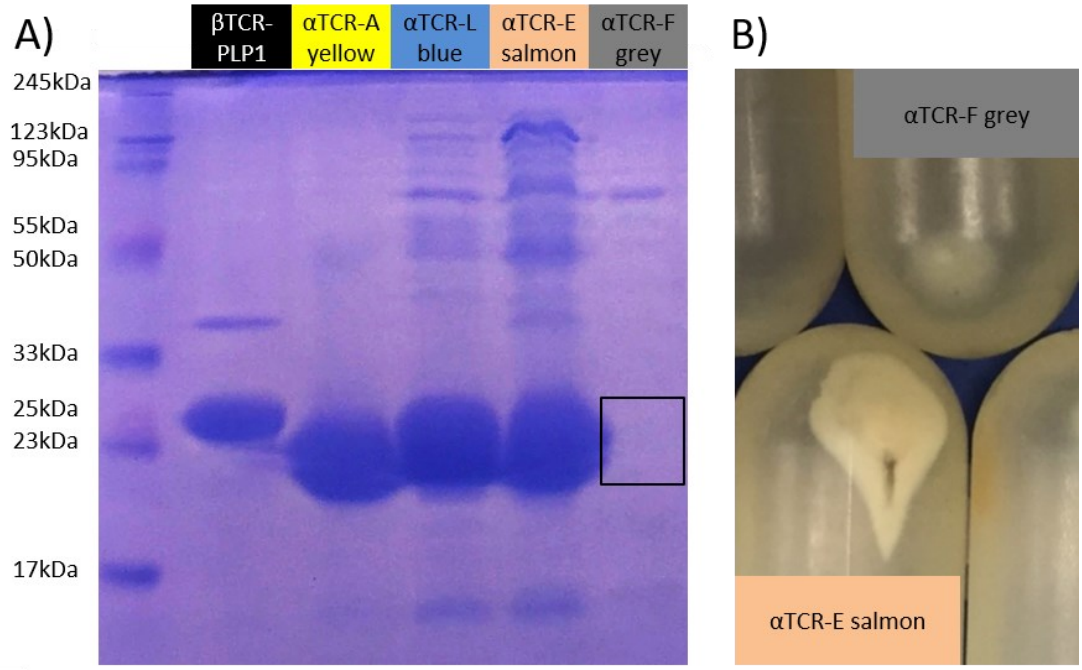


**Figure 11| Expression of soluble TCRs under "standard" conditions:** TCR α and β chains were expressed in inclusion bodies of BL21(DE3) E. coli using a T7 RNA polymerase expression system. Inclusion bodies were isolated by centrifugation. **A)** 15 % SDS page of the resuspended inclusion bodies revealed successful expression of the common β chain β*TCR-PLP1* (27,6 kD) and the α chains α*TCR-A yellow*, α*TCR-E salmon* and α*TCR-L blue* (22,8 kDa). Expression of α*TCR-F grey* could not be verified (box). Samples that corresponded to 1 ml induced LB medium were loaded. SDS page was stained with Coomassie brilliant blue. **B)** Inclusion body pellets after cell lysis and washing. The collected α*TCR-F grey* pellet after inclusion body isolation was much smaller and more gelatinous compared to other TCR chains as for example α*TCR-E salmon*.

### 3.1.2. Altering codon usage does not lead to successful expression of α*TCR-F grey.*

Rare codon usage could have been a possible explanation for the insufficient expression of α*TCR-F grey* (Saida, 2007). Rare codon usage means that some codons are rarely used in E. coli and only small amounts of corresponding transfer-RNAs (tRNAs) exist resulting in an ineffective translation of the protein. To overcome potential problems of codon usage, a codon-optimised version was generated by exchanging rare codons for more common codons in E. coli. In addition, plasmids were transformed into the Rosetta 2(DE3) E. coli strain that contains tRNAs for seven rare codons. However, neither of these two approaches nor the combination of both led to successful expression of the *TCR-F grey* α chain (Data not shown).

### 3.1.3. α*TCR-F grey* is toxic to BL21(DE3) E. coli.

Toxicity was another possible explanation for the insufficient expression of α*TCR-F grey*. Some proteins interfere with vital functions of the bacteria leading to the death of the production organism before adequate amount of recombinant protein can be produced. To check for problems in the growth of the transformed E. coli cultures upon protein induction, culture density was monitored using optical density measurements at a wavelength of 600 nm (OD600). Strikingly, BL21(DE3) E. coli cultures transformed with α*TCR-F grey* collapsed upon induction with 1 mM IPTG and did not grow denser than OD600 = 1.0 when induced at OD600 = 0.5. In contrast, E. coli transformed with α*TCR-E salmo*n only began to saturate at OD600 > 2.0 4 h after induction (**Figure 12**). Before and without induction the two cultures grew similarly.

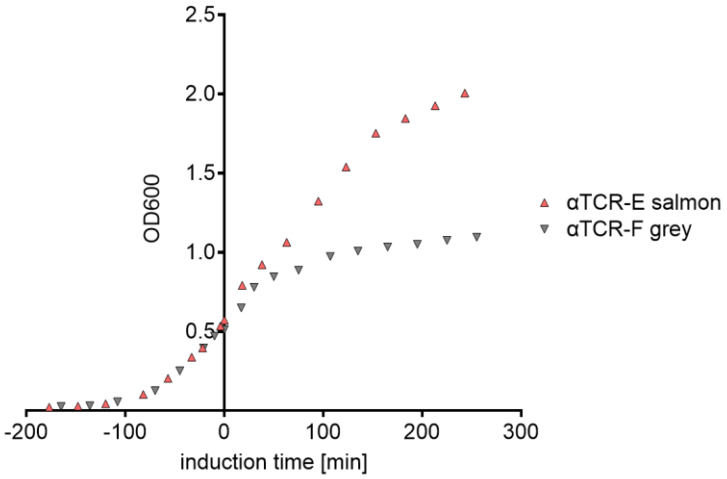


**Figure 12| Collapse of α*TCR-F grey* cultures upon induction:** Density of BL21(DE3) E. coli cultures transformed with either α*TCR-F grey* or α*TCR-E salmo*n was monitored by OD600 measurements. Upon induction, the α*TCR-F grey* culture collapsed. It grew slower and saturated at an unusually low OD600 ≈ 1.0. Negative time refers to the phase before induction.

In addition to that, stability and toxicity of the plasmid encoding α*TCR-F grey* was tested and compared to the plasmid encoding α*TCR-E salmo*n. For this, a similar number of bacteria from an LB-kanamycin pre-culture were placed on three sets of LB-agar plates containing kanamycin, kanamycin and 1 mM IPTG or no antibiotic. IPTG is used to induce the T7 RNA polymerase expression system. Kanamycin functioned as a transformation marker as the resistance gene for kanamycin is encoded together with the protein sequence in the pET-30a (+) vector (see 7.1.6).

Plasmid stability, describing the percentage of E. coli maintaining the TCR encoding plasmid upon induction, was measured by comparing the number of colonies on an LB plate without antibiotic with the number of colonies on a kanamycin-LB plate. Bacteria that lose the plasmid also lose resistance to kanamycin and die. The loss of colonies was larger for the α*TCR-F grey* encoding plasmids (plasmid stability quotient = 46 %) than for α*TCR-E salmo*n (plasmid stability quotient = 73 %) (**Figure 13B**).

Plasmid toxicity was defined as the ratio of colonies on plates containing kanamycin and the inducer (1 mM IPTG) to the number of colonies in the presence of only kanamycin. Strikingly, for both plasmids the amounts of colonies were substantially reduced. For the α*TCR-E salmo*n encoding plasmid, 340 times fewer colonies were found on plates containing IPTG/kanamycin compared to the LB-agar plates containing only kanamycin (toxicity quotient of 99.7 %). However, essentially no colonies of α*TCR-F grey* transformed *E. coli* were detectable on the kanamycin-LB plate when IPTG was also present even when a one hundred times higher number of bacteria were spread out. This indicates that the toxicity quotient of the α*TCR-F grey* encoding plasmid was close to 100 % (**Figure 13C**).

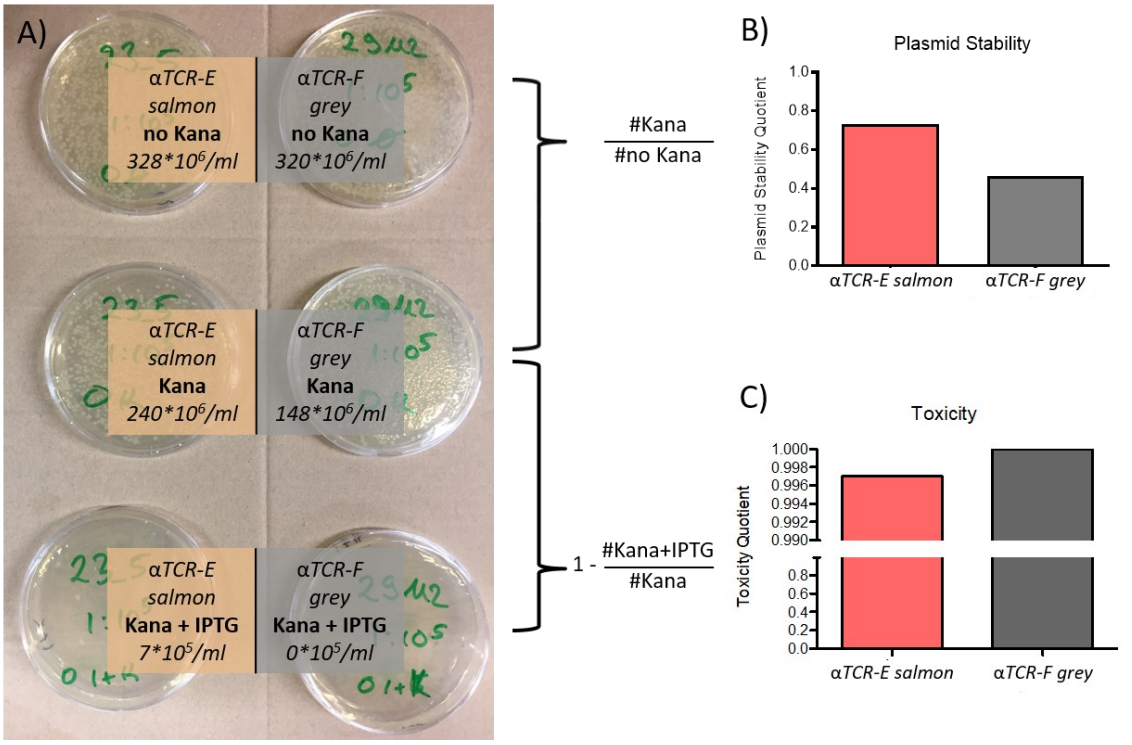


**Figure 13| Plasmid stability and toxicity in BL21(DE3) E. coli:** α*TCR-E salmo*n and α*TCR-F grey* transformed BL21(DE3) E. coli were incubated in kanamycin-LB pre-cultures. **A)** Similar number of bacteria were placed on three sets of LB-agar plates containing no antibiotic (1st row), kanamycin (kana) (2nd row) or kanamycin and 1 mM IPTG (3rd row). After incubation overnight, colonies on the plates were counted and normalized to 1ml LB-culture. **B)** Plasmid stability and **C)** toxicity quotients were calculated as indicated.

### 3.1.4. Altering expression conditions did not solve the expression problem of α*TCR-F grey*.

To overcome the problem that α*TCR-F grey* was not expressed under standard settings, expression was tested under various conditions. For instance, bacteria were induced at higher bacterial densities (OD600 of 0.7-1.5 vs. standard 0.5) or for a reduced time (1 h or 2 h vs. standard 4 h). In addition, induction was tried with and without kanamycin and with reduced concentration of IPTG (0.01 mM vs. standard 1 mM). Finally, the temperature was lowered to 30 °C and expression at 16 °C overnight was tested. However, neither of these approaches nor various combinations resulted in successful expression of the *TCR-F grey* α chain. In contrast, expression of α*TCR-E salmo*n was consistently observed.

### 3.1.5. Toxicity tolerant *OverExpress™* E. coli are not beneficial for α*TCR-F grey* expression.

*OverExpress™* cells (C41, C43) are E. coli strains that have been selected from BL21(DE3) and are reported to be able to express proteins that are toxic for other E. coli strains assumably because they have a slower rate of mRNA accumulation resulting in a slower but metabolically better controlled expression of otherwise toxic proteins (Dumon-Seignovert et al., 2004; Miroux & Walker, 1996). The *OverExpress™* cells C41pLys and C43pLys additionally carry a plasmid encoding a lysozyme that is a natural inhibitor of the T7 RNA polymerase. The lysozyme inactivates the T7 RNA polymerase to further reduce basal protein expression and therefor toxic stress during growth phase. After induction the lysozyme inhibition is overcome by the high expression levels of T7 RNA polymerase allowing expression of the target gene (Saida, 2007).

Expression of α*TCR-F grey* was tested in these E. coli strains. In contrast to BL21(DE3) E. coli, α*TCR-F grey* transformed *OverExpress™* bacterial cultures did not collapse upon induction with IPTG (**Figure 14**).

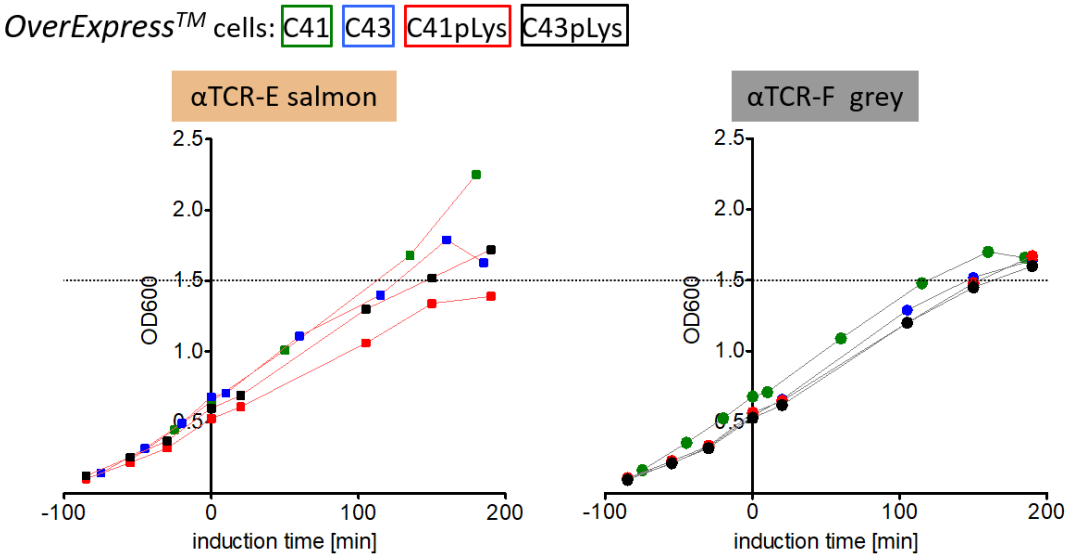


**Figure 14| Stable *OverExpress™* E. coli cultures upon induction:** Density of *OverExpress™* E. coli cultures transformed with either α*TCR-E salmon* or α*TCR-F grey* was monitored by OD600 measurements. In contrast to α*TCR-F grey* transformed BL21(DE3) cultures, the *OverExpress™* cultures did not collapse upon induction. Growth of α*TCR-F grey and* α*TCR-E salmon* transformed cultures was similar and only slightly saturated at OD600 = 1.5 (dotted line) after 4 h of stimulation. Negative times refer to the period before induction.

Concordantly with this observation, the toxicity quotients of both α*TCR-E salmon* and α*TCR-F grey* plasmids were substantially lower than the values that we were previously

observed with BL21(DE3) E. coli. For all tested *OverExpress*$^{TM}$ strains, the number of colonies on the LB plates containing kanamycin and IPTG was comparable to the number of colonies on the kanamycin-LB plates (**Figure 15C**). Meanwhile, plasmid stability in *OverExpress*$^{TM}$ cells was equivalent to BL21(DE3) E. coli. For instance, using CD41pLys *OverExpress*$^{TM}$ cells, plasmid stability of the α*TCR-F grey* encoding plasmid was even slightly higher (plasmid stability quotient = 77 %) than of the α*TCR-E salmo*n encoding plasmid (plasmid stability quotient = 62 %) (**Figure 15B**).

Despite this promising resilience of the *OverExpress*$^{TM}$ *cells,* expression of α*TCR-F grey* was not detectable in any of the *OverExpress*$^{TM}$ strains. Neither SDS page of total bacteria lysate nor SDS page after inclusion body isolation revealed an adequate band (**Figure 16**). It is noteworthy that in *OverExpress*$^{TM}$ CD41pLys and C43pLys strains that additionally contain the lysozyme plasmid, even expression of α*TCR-E salmo*n failed.

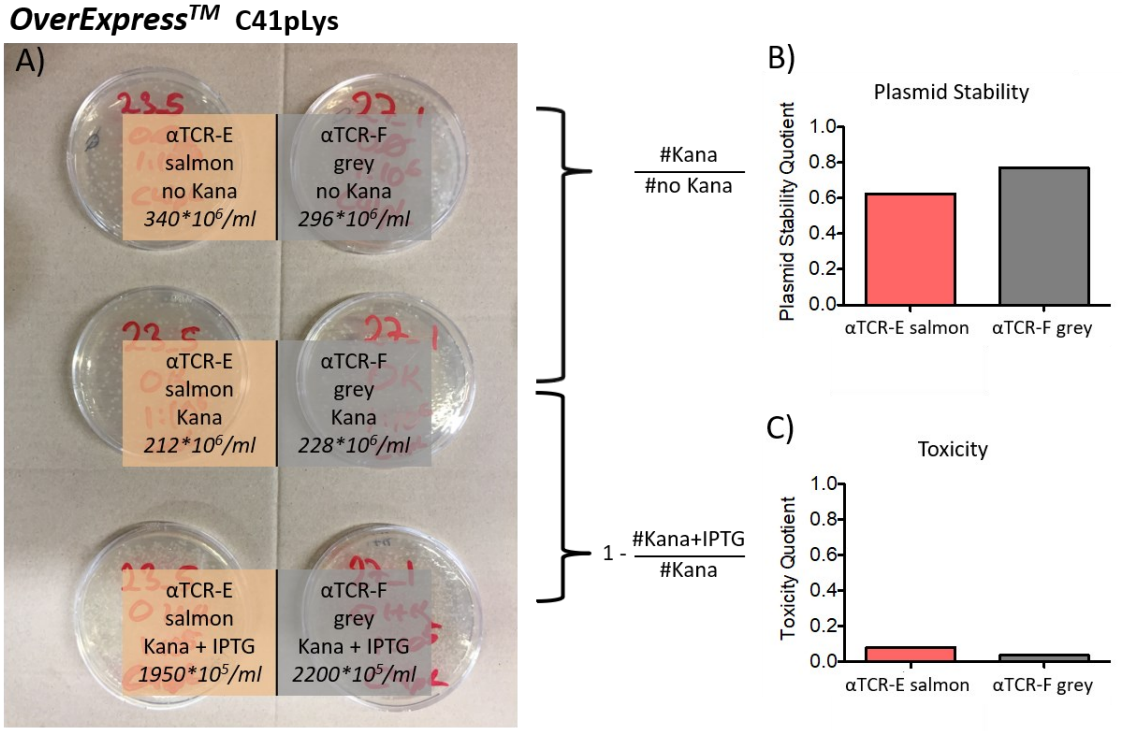


**Figure 15| Plasmid stability and toxicity in OverExpress™ C41pLys E. coli:** α*TCR-E salmon* and α*TCR-F grey* transformed OverExpress™ C41pLys E. coli were incubated in kanamycin-LB pre-cultures. **A)** Similar number of bacteria were placed on three sets of LB-agar plates containing no antibiotic (1st row), kanamycin (kana) (2nd row) or kanamycin and 1 mM IPTG (3rd row). After incubation overnight, colonies on the plates were counted and normalized to 1 ml LB-culture. **B)** Plasmid stability and **C)** toxicity quotients were calculated as indicated.

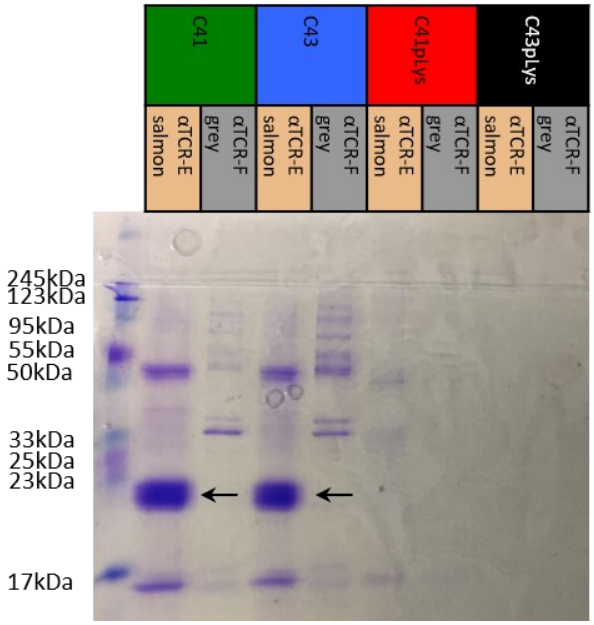


**Figure 16| Expression of α*TCR-F grey* was not detectable in OverExpress™ cells:** Expression of α*TCR-F grey* and α*TCR-E salmon* in *OverExpress™* C41, C43, C41pLys and C43pLys E. coli was tested. Inclusion bodies were isolated by centrifugation. 15 % SDS page of the resuspended inclusion bodies revealed that α*TCR-F grey* was not sufficiently produced in any of those toxicity tolerant strains. α*TCR-E salmon* could be detected in inclusion bodies of C41 and C43 *OverExpress™* cells (←) but not of C41pLys and C43pLys *OverExpress™* cells.

## 3.2. TCR functional avidity

To measure TCR functional avidity, the four *representative* TCR were reexpressed in BW58 T hybridoma cells. Those hybridoma cells carry an NFAT-GFP reporter system. Stimulation of the TCR initiates a signal transduction cascade and ultimately triggers transcription of genes relevant for T cell activation. The transcription factor nuclear factor of activated T cells (NFAT) plays a crucial role in the induction of gene transcription in T cells (Macian, 2005). NFAT-GFT reporter hybridoma cells carry a retroviral vector containing multiple NFAT-binding sites, followed by the minimal interleukin 2 promoter and the reporter gene for green fluorescent protein (GFP) (Hooijberg et al., 2000). Upon TCR stimulation, NFAT is produced and induces GFP production that can be measured and quantified by flow cytometry. This allows detection of activated T hybridoma cells.

### 3.2.1. Characterisation of reporter hybridoma cells carrying the TCRs of interest

To validate the quality of the hybridoma cells, surface expression was evaluated by surface staining for CD3, CD4, the common β chain βTCR-PLP1 (stained with AntiVb6) and human CD2 (huCD2), a co-transfected marker for expression of the specific α chains which cannot be stained directly due to the lack of a corresponding antibody. When checked by flow cytometry, all these surface markers were expressed in a comparable manner (**Figure 17A**). Furthermore, the four hybridoma cell lines behaved alike upon TCR independent stimulation with anti-CD3 (**Figure 17B**). Half maximal effective concentration (EC50) for anti-CD3 was app. 12 ng/ml for all four *representative* TCR hybridoma cell lines. Tukey's multiple comparison test did not reveal any significant differences between the cell lines ($p>0.05$, $n=6$). LgEC50 and not EC50 was used for statistical analysis to account for serial dilution of the stimulant (see 6.6.1 for more details on statistical analysis).

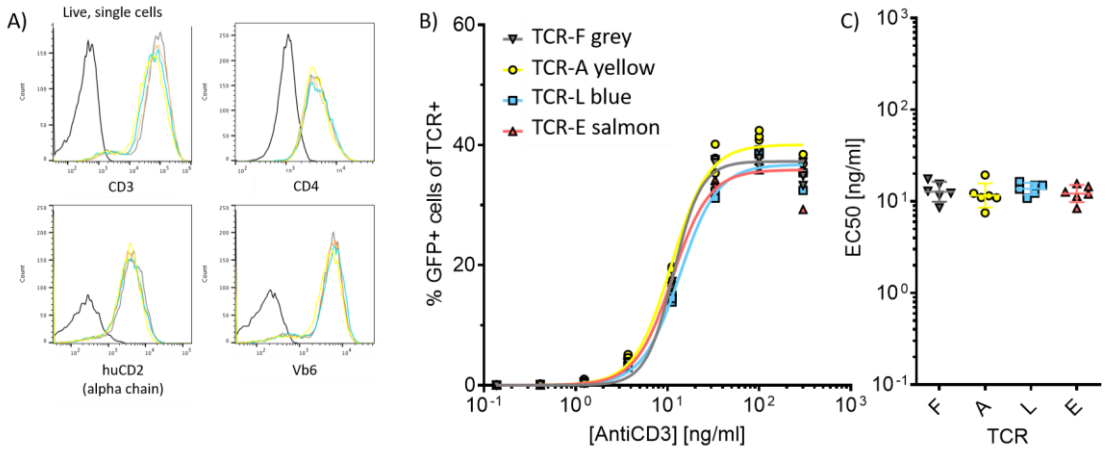


**Figure 17| Quality control of T hybridoma cell lines: A)** Surface analysis by flow cytometry of hybridoma cells each expressing a *representative* TCR (color-coded: *TCR-F grey*; *TCR-A yellow*; *TCR-L blue*; *TCR-E salmon*; BmDCs were used as control: black). CD3, CD4, huCD2 (a co-transfected marker for the specific α chain) and the common β chain βTCR-PLP1 (stained with AntiVb6) were comparably expressed. Plots are gated on live, single cells **B)** *In vitro* TCR independent stimulation with anti-CD3 of the NFAT-GFP reporter T hybridoma cells. Data was interpolated with a four-parameter sigmoid dose response curve and lgEC50 was calculated. **C)** Calculated EC50 for anti-CD3-stimulation of each *representative* TCR is displayed. LgEC50 (concentration of half response) was not significantly different between the hybridoma cell lines (Tukey's multiple comparison test p> 0.05). Lines indicate mean with SD of lgEC50. The data is representative for six independent experiments.

### 3.2.2. Peptide-specific stimulation assays revealed a hierarchy of TCR functional avidity.

TCR functional avidity was measured by *in vitro* stimulation of the T hybridoma cell lines with PLP peptide in the presence of APCs. Activation was measured by detecting GFP expression by flow cytometry. As we were interested in the influence of neighbouring amino acids of $PLP_{11-19}$ core epitope, we used two different peptide versions, a shorter $PLP_{9-20}$ version and a longer $PLP_{1-24}$ version (amino acid sequences can be found in supplement 7.2). All four T hybridoma cell lines expressing one of the four *representative* TCRs could be stimulated by both peptides but could not be stimulated by peptides unrelated to PLP (e.g., LLO) (**Figure 18 A&D**).

Interestingly, stimulation with the longer $PLP_{1-24}$ peptide led to higher activation plateaus compared to the $PLP_{9-20}$ peptide) (**Figure 18 C&F**). This was most significant for *TCR-E salmon* that was only inefficiently stimulated by the shorter $PLP_{9-20}$ peptide. However, the relative stimulatory hierarchy of both peptides was the same. Irrespective of whether the shorter or the longer PLP peptide was used, hybridoma cells expressing

*TCR-F grey* reacted strongest. Concentrations of 3 pmol/ml $PLP_{9-20}$ and 32 pmol/ml $PLP_{1-24}$ were sufficient to induce half maximum response (EC50). In contrast, hybridoma cells expressing *TCR-E salmon* were stimulated weakest. Concentrations of 2,586 pmol/ml $PLP_{9-20}$ and 583 pmol/ml $PLP_{1-24}$ were needed for half maximum response. This was about 850-fold ($PLP_{9-20}$) or 18-fold ($PLP_{1-24}$) higher than the concentrations that were needed for *TCR-F grey*. Hybridoma cells expressing *TCR-A yellow* (EC50 $PLP_{9-20}$= 104 pmol/ml; EC50 $PLP_{1-24}$=69 pmol/ml) and *TCR-L blue* (EC50 $PLP_{9-20}$=476 pmol/ml; EC50 $PLP_{1-24}$=139 pmol/ml) had an intermediate responsiveness.

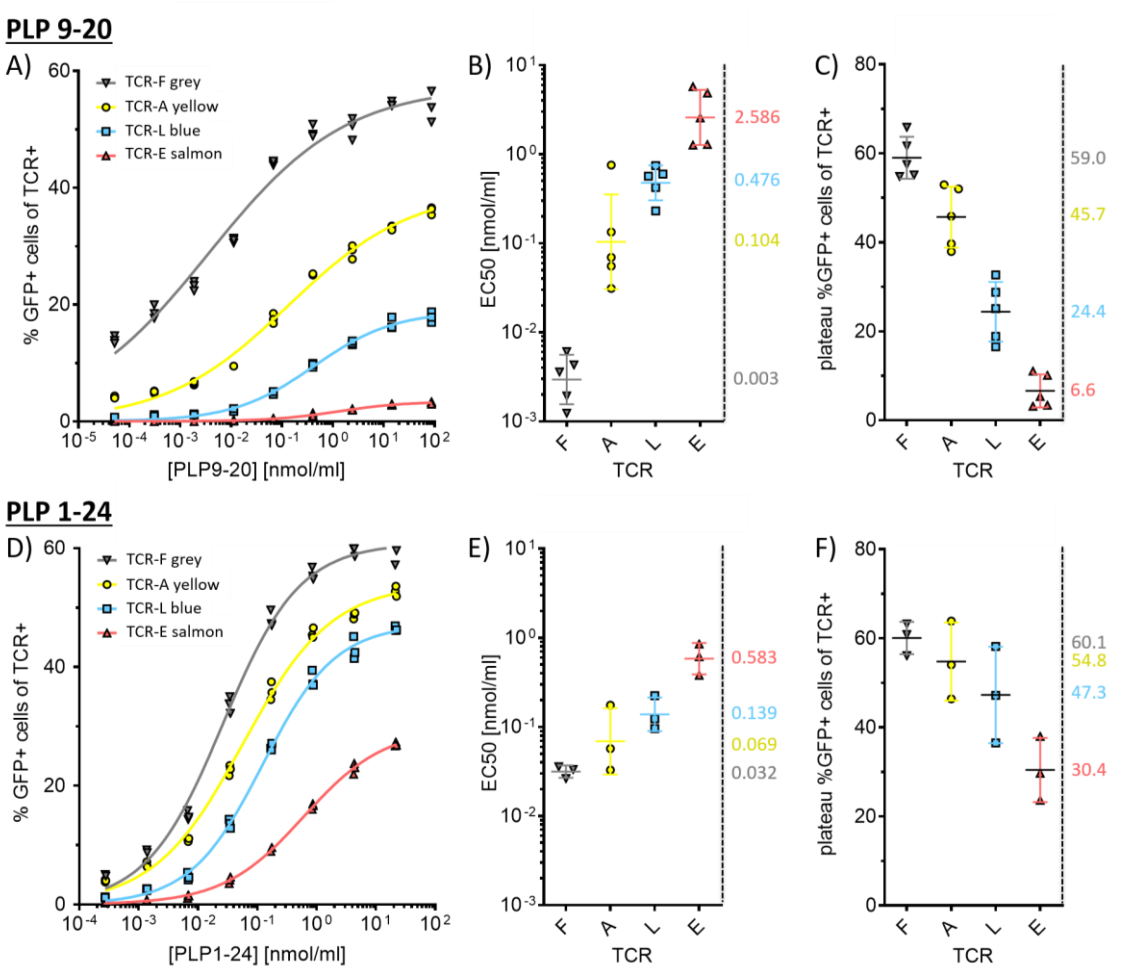


**Figure 18| *In vitro* stimulation assay with PLP peptide:** *In vitro* stimulation with **A)** $PLP_{9-20}$ or **D)** $PLP_{1-24}$ peptide of NFAT-GFP reporter T hybridoma cells each expressing a *representative* TCR. Data was interpolated with a four-parameter sigmoid dose response curve and lgEC50 was calculated. Calculated EC50 for stimulation with **B)** $PLP_{9-20}$ and **E)** $PLP_{1-24}$ peptide of each *representative* TCR is displayed. Lines and numbers indicate mean with SD of lgEC50. Stimulation with **C)** $PLP_{9-20}$ reached lower plateaus than stimulation with **F)** $PLP_{1-24}$. Lines and numbers indicate mean with SD of plateau. Data is representative for five ($PLP_{9-20}$) or three ($PLP_{1-24}$) independent experiments.

Statistical evaluation of lgEC50 (to account for serial dilution of the stimulant) with Tukey's multiple comparison test revealed the following levels of significance:

**Tukey's multiple comparisons test of lgEC50**

| TCR | Adjusted p value $PLP_{9-20}$ | Summary $PLP_{9-20}$ | Adjusted p value $PLP_{1-24}$ | Summary $PLP_{1-24}$ |
|---|---|---|---|---|
| **A VS. L** | 0.0678 | ns | 0.1971 | ns |
| **A VS. E** | 0.0004 | *** | 0.0016 | ** |
| **A VS. F** | 0.0001 | *** | 0.1402 | ns |
| **L VS. E** | 0.0397 | * | 0.0123 | * |
| **L VS. F** | <0.0001 | **** | 0.0107 | * |
| **E VS. F** | <0.0001 | **** | 0.0003 | *** |

**Table 2| Statistical comparison of lgEC50:** Using Tukey's multiple comparison test, significance levels of the differences between the four *representative* TCRs in lgEC50 of the stimulation assays with $PLP_{9-20}$ and $PLP_{1-24}$ were calculated. ns: $p \geq 0.05$; *: $p \leq 0.05$; **: $p \leq 0.01$; ***: $p \leq 0.001$; ****: $p \leq 0.0001$

In summary, functional avidity was highest for *TCR-F grey*, followed by *TCR-A yellow* and *TCR-L blue*. It was lowest for *TCR-E salmon*.

## 3.3. Assessment of TCR binding characteristics using a tetramer-based approach

MHC-tetramers have been developed to visualize TCR-pMHC interactions by flow cytometry despite their relatively low affinity by using the avidity effect achieved by coupling multiple pMHCs. Their binding characteristics are an additional useful parameter to describe the TCR-pMHC interaction considering the important role of avidity in T cell stimulation (Holmberg et al., 2003; Savage et al., 1999).

### 3.3.1. PLP1-tetramer staining capacity of TCR-F grey is considerably lower compared to the other *representative* TCRs.

PLP1-tetramer surface staining capacity of hybridoma cells each expressing one of the four *representative* TCRs was analysed by flow cytometry (**Figure 19**). *TCR-A yellow* had the highest staining capacity followed by *TCR-L blue* and *TCR-E salmon*. Interestingly, *TCR-F grey* had a considerably lower staining capacity compared to the other TCRs.

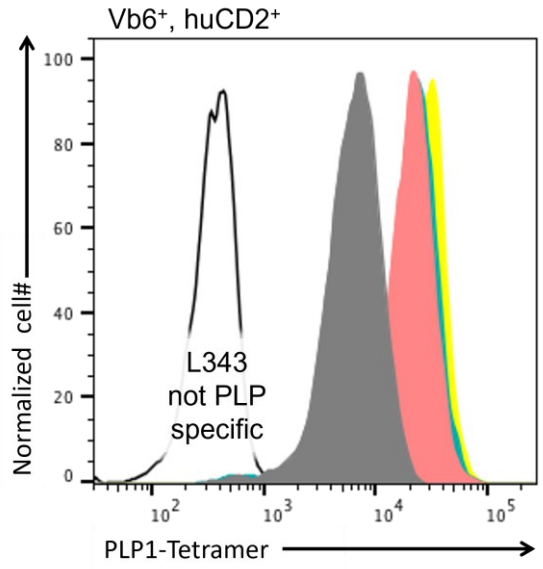


**Figure 19| PLP1-tetramer surface staining of T hybridoma cells:** PLP1-tetramer staining of hybridoma cells each expressing one of the four *representative* TCRs (color-coded: *TCR-F grey*; *TCR-A yellow*; *TCR-L blue*; *TCR-E salmon*). Data is generated by flow cytometry and the samples were gated on Vb6$^+$ huCD2$^+$ cells. All four hybridoma cell lines expressed comparable amounts of CD3, CD4, Vb6 and huCD2 (see 3.2.1.).

### 3.3.2. Half-life of tetramer dissociation

Dissociation rates of the PLP1-tetramer are an interesting parameter that expands our understanding of the kinetics of the TCR-pMHC interactions. To measure PLP1-Tet interaction half-lives, hybridoma cells were first stained with PLP1-tetramer under precisely controlled conditions. Directly before long term measurement by flow cytometry was started, an excess of MHCII capturing antibody was added to capture unbound PLP1-tetramer. This prevented rebinding of dissociated tetramer to the TCRs creating a sink for unbound tetramer. Measurement of the decreasing mean fluorescent intensity (MFI) over time now allowed the calculation of the dissociation-rate of the PLP1-tetramer from the TCRs. After adding the MHC II capturing antibody, which marked $t_0$ of the experiment, the measured MFI declined asymptotically and stabilized after approximately 10 min at a plateau that was significantly lower than the starting $MFI_0$ that was measured directly before adding the capturing antibody. The relative order of $MFI_0$ values that were measured in this experiment confirmed results of the previous experiment. The $MFI_0$ was highest for *TCR-A yellow* (3,888) followed by *TCR-L blue* (3,849) and *TCR-E salmon* (3,633). The $MFI_0$ was lowest for the *TCR-F grey* (845) (**Figure 21B**). $MFI_{Plateau}$ was measured 45 min after adding the capturing antibody and ΔMFI was calculated (**Table 3**).

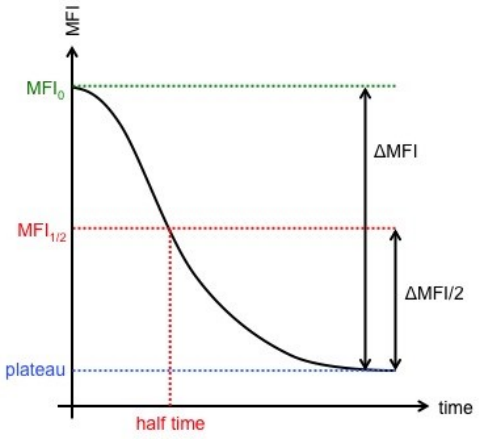


**Figure 20| Schematic representation of tetramer dissociation.**

Tetramer-half-life was determined by interpolation with a third order polynomial function and mathematical modelling (see 6.4.2.). In summary, tetramer half-life was highest for *TCR-A yellow* (374 s), followed by *TCR-F grey* (334 s) and *TCR-E blue* (253 s) and shortest for *TCR-E salmon* (199 s).

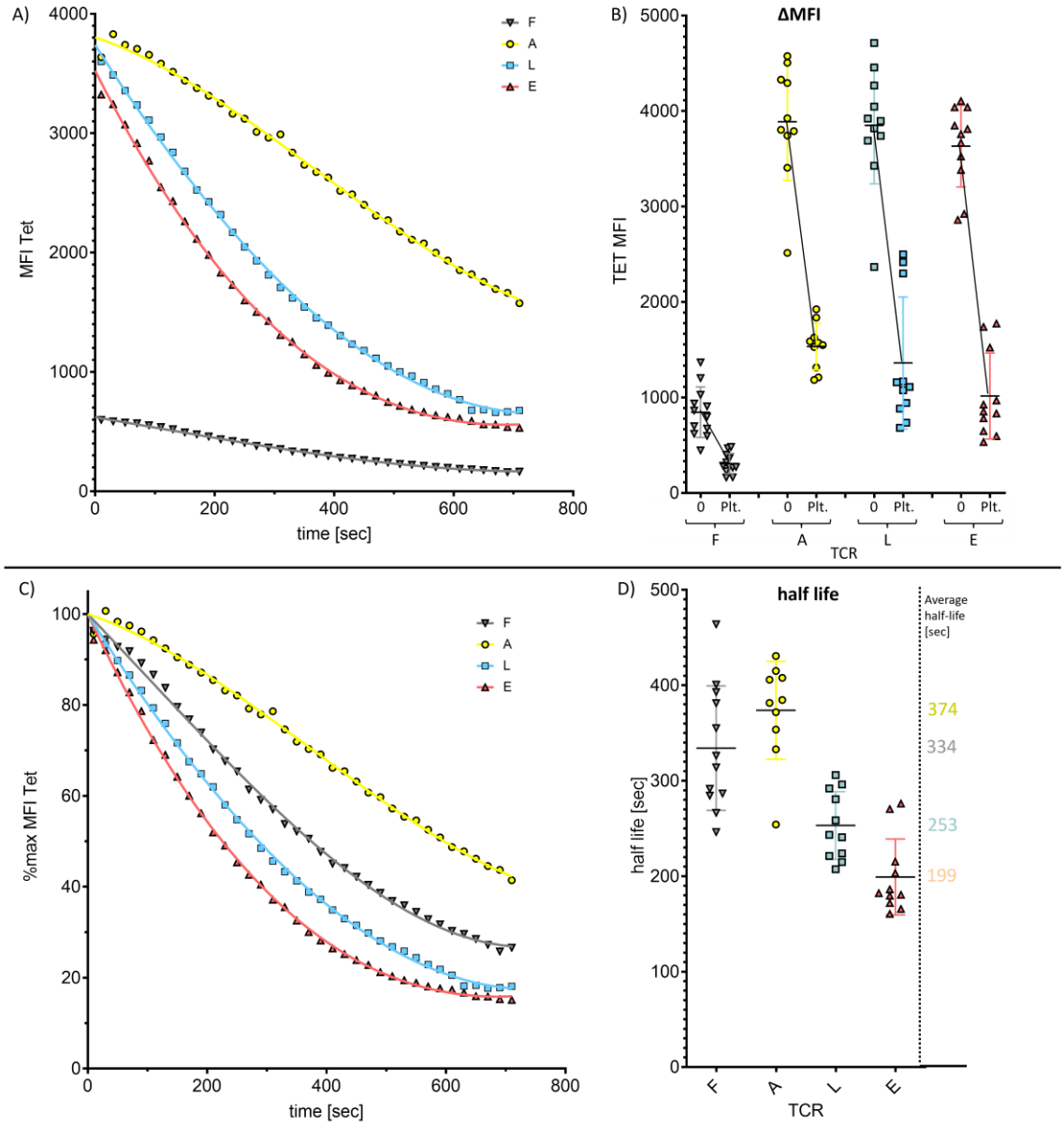


**Figure 21| PLP1-tetramer dissociation: A)** T hybridoma cells each expressing one of the four *representative* TCRs were stained with PLP1-tetramer. $MFI_0$ was determined directly before an excess of MHCII capturing antibody was added at time point zero. This prevented rebinding of dissociated tetramer to the TCRs creating a sink for unbound tetramer. Measurement of the decreasing mean fluorescent intensity (MFI) over time reflected the dissociation of the PLP1-tetramer from the TCRs. The data was interpolated with a third order polynomial (cubic) function. **B)** MFI of tetramer measured by flow cytometry before (0) and 45 min after (Plt.) adding the MHC II capturing antibody. **C)** MFI of PLP1-Tet dissociation was normalized to corresponding $MFI_0$ **D)** Half-life of tetramer dissociation. Lines indicate mean with SD ($n \geq 10$). Data is representative for three independent experiments.

| | TCR-A yellow | TCR-L blue | TCR-E salmon | TCR-F grey |
|---|---|---|---|---|
| **$MFI_0$** | 3,888 | 3,849 | 3,633 | 845 |
| **$MFI_{plateau}$** | 1,534 | 1,361 | 1,016 | 307 |
| **ΔMFI** | 2354 | 2,488 | 2,617 | 538 |
| **$\Delta MFI/MFI_0$** | 60.5% | 64.6% | 72.0% | 63.6% |
| **half-life** | 373.8 | 253.2 | 199.2 | 334.2 |

**Table 3| Summary of mean of measured tetramer dissociation parameters:** (n≥10) Data is representative for three independent experiments.

## Tukey's multiple comparisons test of $MFI_0$ and half-life

| TCR | p value of $MFI_0$ | Summary of $MFI_0$ | p value of half-life | Summary of half-life |
|---|---|---|---|---|
| **A vs. L** | 0.9794 | ns | <0.0001 | **** |
| **A vs. E** | 0.0189 | * | <0.0001 | **** |
| **A vs. F** | <0.0001 | **** | 0.0917 | ns |
| **L vs. E** | 0.0379 | * | 0.0108 | * |
| **L vs. F** | <0.0001 | **** | <0.0001 | **** |
| **E vs. F** | <0.0001 | **** | <0.0001 | **** |

**Table 4| Statistical comparison of $MFI_0$ and half-life:** Using Tukey's multiple comparison test, significance levels of the differences between the four *representative* TCRs in $MFI_0$ and half-life of the tetramer dissociation assays were calculated. ns: $p \geq 0.05$; *: $p \leq 0.05$; **: $p \leq 0.01$; ***: $p \leq 0.001$; ****: $p \leq 0.0001$

## 3.4. Towards measuring TCR-PLP1-IA$^b$ interaction kinetics *in situ* using a FRET-based microscopy assay

*In vivo*, both the TCR and the pMHC are embedded in complex membrane environments. They are influenced by cell specific factors which include forces derived from cell-cell contacts and membrane protein interactions as well as geometrical constraints of the immunological synapse. The dissociation constant in this setting is referred to as two dimensional (2D)-$K_D$ (Axmann et al., 2015a; Kolawole et al., 2020) (see 1.6.4).

To describe the interactions that occur under 2D settings more accurately, Axmann et al. developed a system to study TCR-pMHC interactions *in situ* where both proteins are anchored in membranes and the interaction occurs across the intercellular junction (Axmann et al., 2015a) (see 1.6.5). In this model system, the membrane of an APC is mimicked by a glass supported planar lipid bilayer that is functionalized with an MHC complex that is labelled with a FRET acceptor. In this thesis we wanted to use this technology to measure *in situ* interaction kinetics of the four *representative* PLP1 specific T cells. For this, it was necessary to generate a novel PLP1-IA$^b$ FRET construct that can be labelled site specifically with a FRET acceptor.

### 3.4.1. PLP1-IA$^b$ has physiological stimulatory potency.

The PLP1-IA$^b$-tetramer (see 1.7.1) is a versatile tool to stain PLP1 reactive T cells. It is composed of four PLP-IA$^b$ monomers. We wondered whether this monomer can also be used as surrogate ligand to stimulate PLP specific T cells and could be useful as a FRET probe. For this, the monomeric PLP1-IA$^b$ construct was tested in different experiments.

#### 3.4.1.1. Plate bound PLP1-IA$^b$ monomer efficiently stimulates PLP specific T hybridoma cells.

We first tested PLP1-IA$^b$ monomer stimulatory capacity. To do so, culture plates were coated with the monomer at varying concentrations to function as a simplified model of an APC. NFAT-GFP reporter T hybridoma cells expressing the four *representative* TCRs were then incubated for 12h in those prepared culture plates. After this time, GFP expression levels as a marker for activation were analysed by flow cytometry.

T hybridoma cell lines could efficiently be activated by the PLP1-IA$^b$ monomer. Hybridoma cells expressing *TCR-F grey* reacted most efficiently against PLP1-IA$^b$ monomer and EC50 was on average 8 ng/ml. *TCR-E salmon* was stimulated weakest with a 13-fold higher EC50 of 104 ng/ml. T hybridoma cells expressing *TCR-A yellow* and *TCR-L blue* demonstrated an intermediate responsiveness with an EC50 of 10 ng/ml and 21 ng/ml, respectively (**Figure 22C**). As a negative control we used T hybridoma cells L343 expressing a TCR not specific for PLP. As expected, these cells could not be activated by PLP1-IA$^b$. For comparison, a PLP$_{1\text{-}24}$ peptide stimulation assay with "normal" (bone marrow derived) APCs was performed in parallel. Both assay systems led to the same functional avidity hierarchy of the *representative* TCRs (**Figure 22A**).

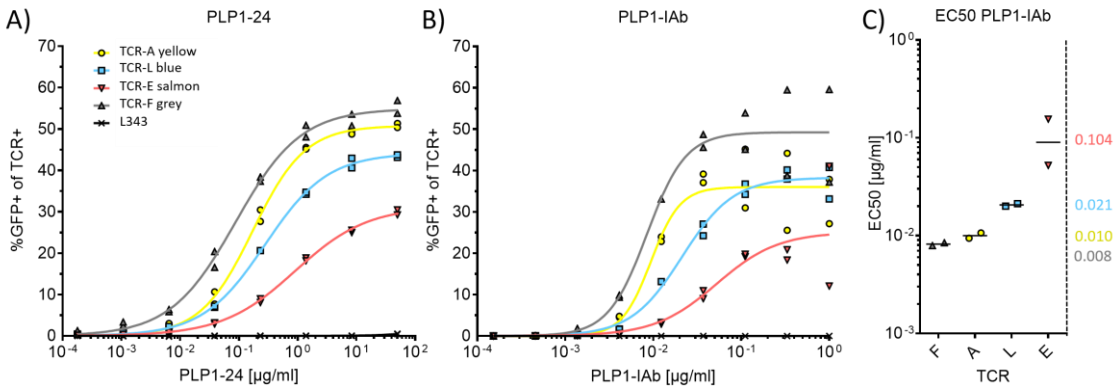


**Figure 22| PLP1-IA$^b$ monomer stimulates T hybridoma cells:** Stimulation assays of NFAT-GFP reporter T hybridoma cells each expressing one of the four *representative* TCRs. T hybridoma cells were either **A)** "classically" stimulated with APCs loaded with PLP$_{1\text{-}24}$ peptide or **B)** in wells that have been coated with PLP1-IA$^b$ monomer at varying concentrations. After 12 h stimulation, GFP expression as a marker for activation was analysed by flow cytometry. Data was interpolated with a four-parameter sigmoid dose response curve and lgEC50 was calculated. **C)** Calculated EC50 of PLP1-IA$^b$ monomer stimulation for each *representative* TCR is displayed. Lines und numbers indicate mean. Data is representative for 2 independent experiments.

### 3.4.1.2. Synapse formation and $Ca^{2+}$-flux upon interaction of *TCR-F grey* T cells with lipid bilayers loaded with PLP1-IA$^b$ monomer.

We next asked whether stimulatory potency of PLP1-IA$^b$ monomer can also be observed in a lipid bilayer setting. To do so, PLP1-IA$^b$ monomer was labelled non-site specifically with an amine-reactive Alexa 647 fluorophore. Glass-supported planar lipid bilayers that were functionalized with adhesion molecule ICAM-1 and co-stimulatory molecule B7-1 were loaded with the labelled PLP1-IA$^b$ monomer using an unpublished streptavidin

binding platform that was kindly provided by Prof. Johannes Huppa. Finally, *TCR-F grey* transgenic T cells were stained using an H57 single chain variable fragment linked to Cy3 fluorophore (H57 scFv-Cy3) and were placed on the lipid bilayer.

The interaction between the *TCR-F grey* T cells and the lipid bilayer (as a surrogate antigen presenting cell surface), was observed by total internal reflection (TIRF) microscopy. When T cells were placed on a "control" lipid bilayer without PLP1-IA$^b$ monomer, *TCR-F grey* and ICAM-1 were evenly distributed over the entire contact interface of the T cell and the lipid bilayer (**Figure 23A**). Upon interaction with a PLP1-IA$^b$ functionalized lipid bilayer, *TCR-F grey* and PLP1-IA$^b$ clustered and became surrounded by a ring of ICAM-1 (**Figure 23B**). This is often described as bull's eye arrangement which is the typical organization of an immunological synapse that is formed between activated T cells and APCs (Bromley et al., 2001; Dustin, 2014).

We then asked whether the observed interaction also results in activation of the T cells. To do so, a fura-2AM based assay was used to measure the intracellular $Ca^{2+}$-levels in the T cells as a means to verify the stimulatory potency of the functionalized lipid bilayer. Fura-2AM is a calcium indicator whose relative fluorescence at 340 nm vs. 380 nm is dependent on intracellular $Ca^{2+}$ levels. This allows calculation of intracellular calcium concentrations based on the 340 nm/380 nm fluorescent emission ratio. Rapidly after contact with the functionalized lipid bilayer loaded with 70 ng PLP1-IA$^b$ monomer, *TCR-F grey* T cells displayed elevated intracellular $Ca^{2+}$-levels (**Figure 24A**). From a total of 1500 cells that were observed in a steady state situation 15 min after deposition onto the lipid bilayer, roughly 80 % were scored as "activated" as evident from stably elevated intracellular $Ca^{2+}$ levels. A five-fold reduction of the PLP1-IA$^b$ monomer concentration only slightly reduced stimulatory potency of the functionalized lipid bilayer (**Figure 24B**). Together, these observations indicated that PLP1-IA$^b$ monomer has physiological stimulatory potency and is well suited as a basic structure for lipid bilayer experiments.

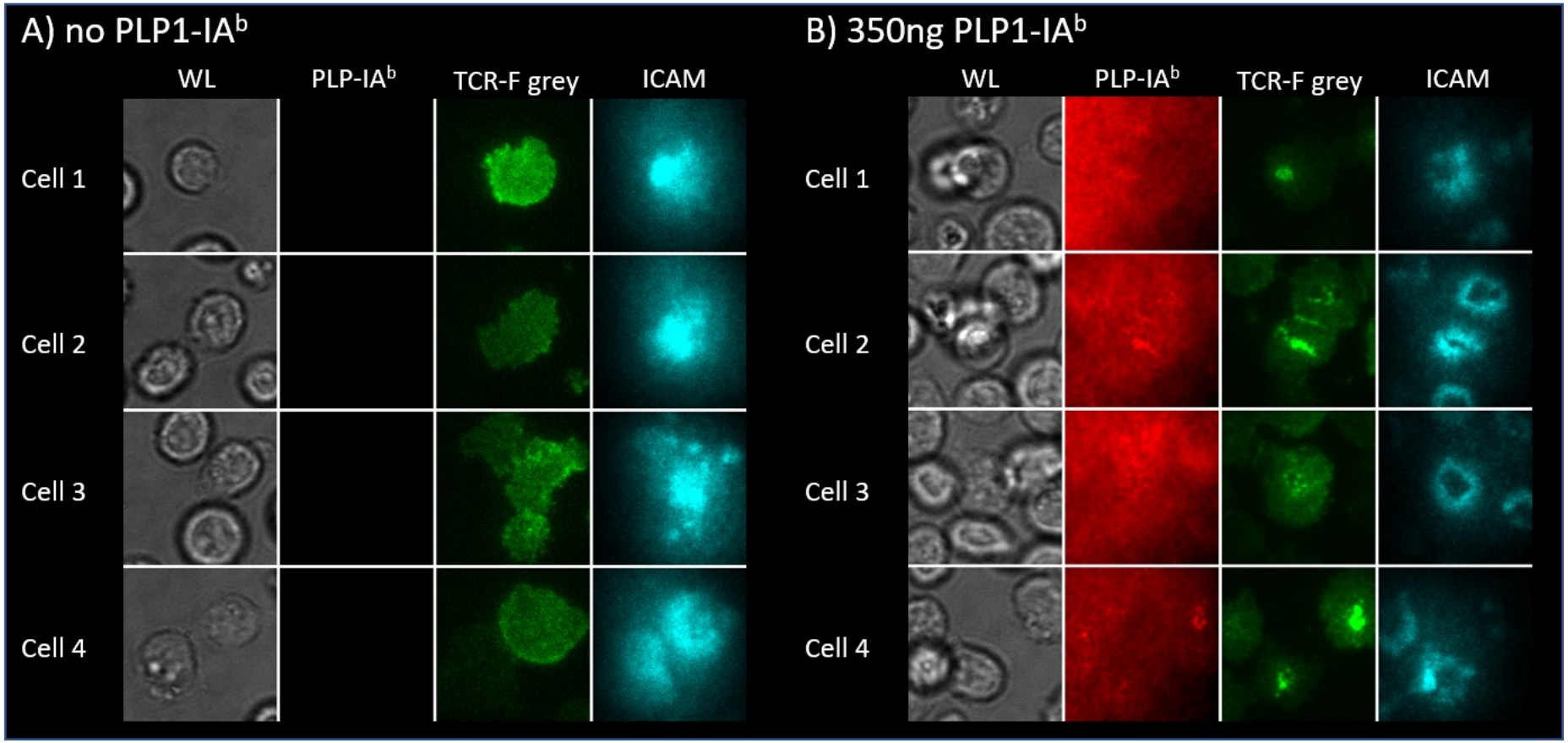


**Figure 23| Interaction of *TCR-F grey* T cells with a functionalized, glass supported lipid bilayer with or without PLP1-IA$^b$ monomer:** *TCR-F grey* on T cells was labelled using H57 scFv-Cy3. Interaction with a functionalized lipid bilayer (loaded with ICAM-1 and B7-1) was observed by TIRF microscopy in **A)** absence and in **B)** presence of PLP1-IA$^b$ monomer. **A)** When no PLP1-IA$^b$ monomer was present in the lipid bilayer, *TCR-F grey* and ICAM-1 were evenly distributed on the T cell surface and in the lipid bilayer, respectively. **B)** Upon presence of PLP1-IA$^b$ monomer in the lipid bilayer, *TCR-F grey* and PLP1-IA$^b$ monomer clustered and became surrounded by a ring of ICAM -1 ("bull's eye arrangement"). Pictures were generated in collaboration with Markus Kraller.

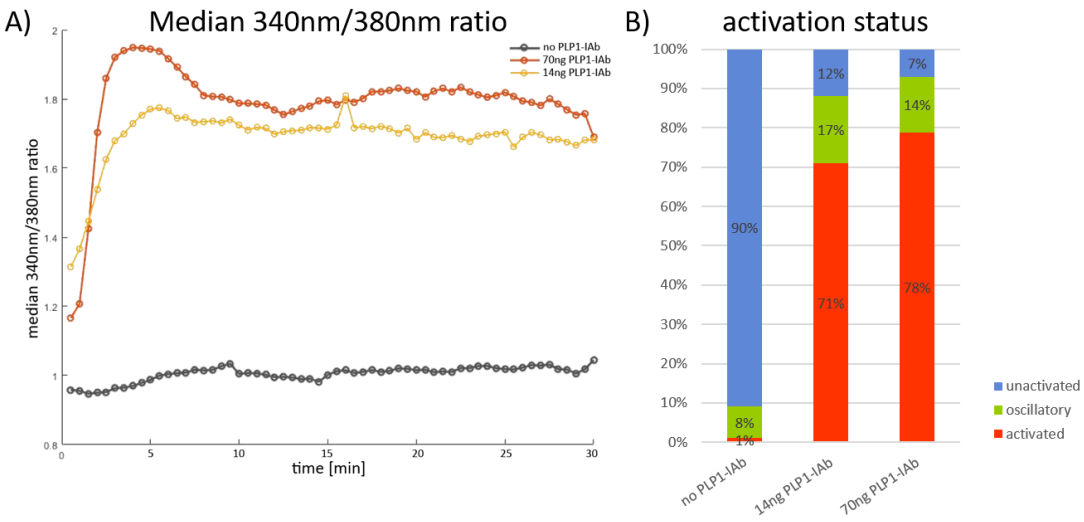


**Figure 24| A lipid bilayer functionalized with PLP1-IA$^b$ monomer activates T cells:** T*CR-F grey* T cells were labelled with fura-2AM to measure intracellular $Ca^{2+}$ concentrations based on 340 nm/380 nm ratio. Labelled T cells were placed on a functionalized lipid bilayer loaded with no, 14 ng or 70 ng PLP1-IA$^b$ monomer. Upon contact of the T cell cells with the lipid bilayer, absorption at 340 nm and 380 nm was measured by inversed microscopy. **A)** Median 340 nm/380 nm absorption ratio was calculated. **B)** Based on 340 nm/380 nm ratio, 1500 cells were characterized as activated, oscillatory or unactivated. Data was generated in collaboration with Markus Kraller.

### 3.4.2. Successful expression of three PLP1-IA$^b$ FRET constructs in Schneider cells that can be labelled site specifically.

For FRET experiments, it is necessary to label PLP1-IA$^b$ monomer site specifically with a FRET acceptor. Commonly, thiol-reactive fluorophores as for example Alexa fluor 647 $C_2$-maleimide can be used for this approach. For this, it was necessary to generate a PLP1-IA$^b$ FRET construct with one free cysteine group at an appropriate position for FRET effects upon interaction with a FRET donor labelled TCR (via H57 scFv).

### 3.4.2.1. Mutation of $Cys_{-2}$ in PLP1-$IA^b$ monomer does not disrupt stimulatory potency.

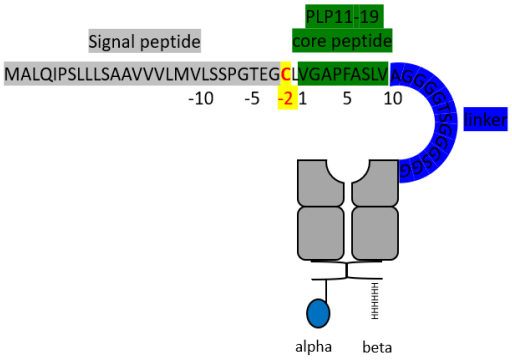


**Figure 25| Partial amino acid sequence PLP1-IAb:** Cysteine at position -2 is highlighted in red.

PLP1-$IA^b$ monomer contains a free cysteine at position -2 (**Figure 25** high-lighted in red) of the β chain between the signal peptide and the $PLP_{11-19}$ core peptide. This free cysteine would disturb site specific labelling. Therefore, it was necessary to mutate this cysteine into alanine for the PLP1-$IA^b$ FRET constructs. However, before starting the time-consuming recombinant production of the PLP1-$IA^b$ FRET constructs we first wanted to test if this mutation would have a detrimental effect on stimulatory potency. For this, in a preliminary system the stimulatory potency of a model peptide $PLP_{FRET}$ which represents the amino acid -2 to 14 of the PLP1-$IA^b$ monomer but contains the mutated cysteine at position -2 was compared to $PLP_{9-20}$.

In essence, the results of stimulation assays using $PLP_{9-20}$ and $PLP_{FRET}$ were comparable: Hierarchy of TCR functional avidity was not altered and calculated EC50s were similar between $PLP_{9-20}$ and $PLP_{FRET}$ (**Figure 26**). Thus, it is unlikely that mutation of $Csy_{-2}$ into alanine disrupts stimulatory potency of the PLP-$IA^b$ FRET constructs.

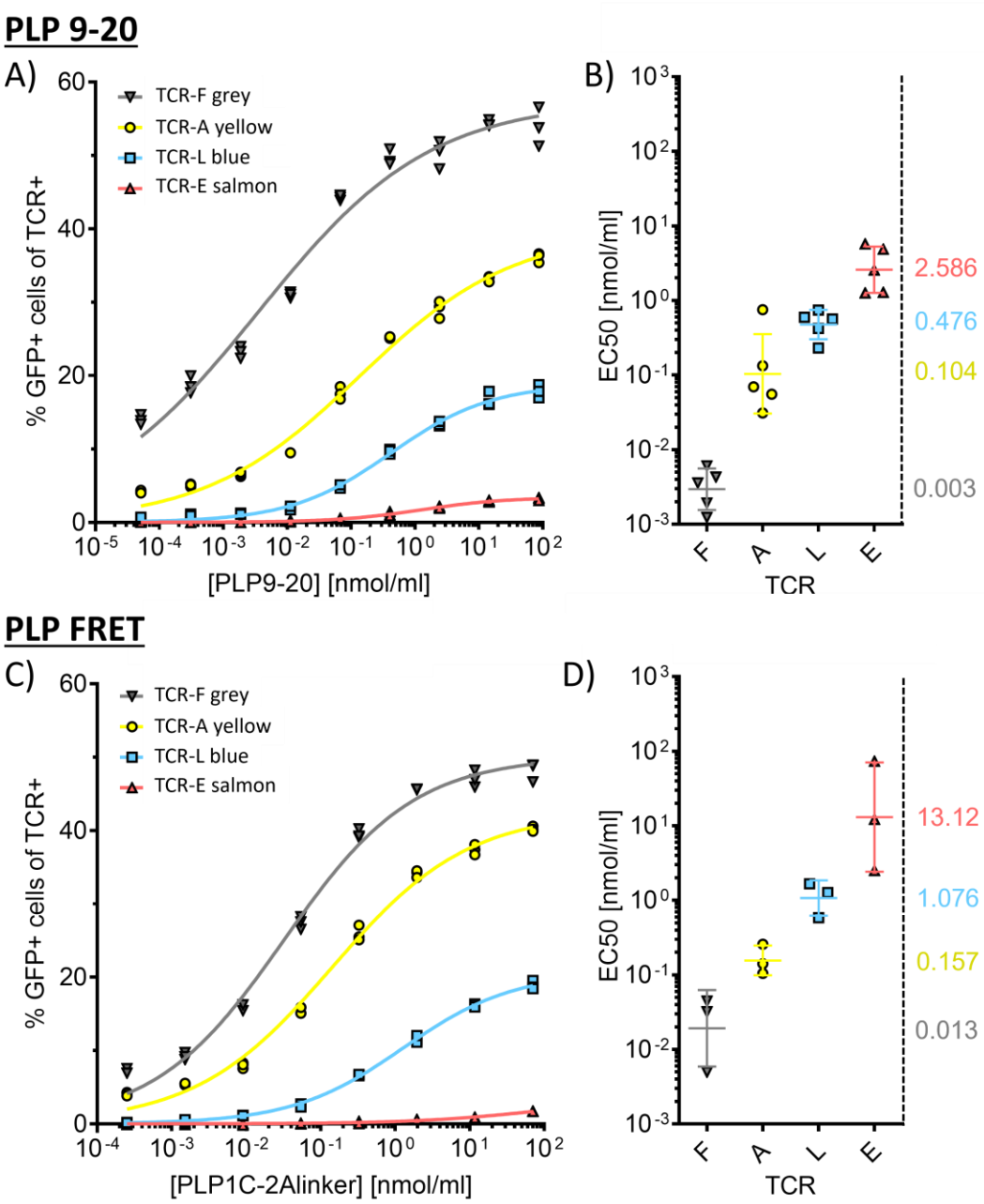


**Figure 26| Mutation of cysteine at position -2 of PLP-IA$^b$ monomer does not influence stimulatory potency:** *In vitro* stimulation with **A)** $PLP_{9\text{-}20}$ or **C)** $PLP_{FRET}$ of NFAT-GFP reporter T hybridoma cells each expressing a *representative* TCR. Data was interpolated with a four-parameter sigmoid dose response curve and lgEC50 was calculated. Calculated EC50 for **B)** $PLP_{9\text{-}20}$ and **D)** $PLP_{FRET}$ stimulation of each *representative* TCR is displayed. Lines and numbers indicate mean with SD of lgEC50. Data is representative for five ($PLP_{9\text{-}20}$) or three ($PLP_{FRET}$) independent experiments.

### 3.4.2.2. Prediction of three potential FRET acceptor fluorophore positions in PLP1-IA$^b$ monomer.

Next, we predicted mutation sites in PLP-IA$^b$ monomer as anchor point for the FRET probe which would allow a suitable inter-dye distance. As no structural data of IA$^b$ binding to a TCR labelled with H57 scFv is available a crystal structure of a respective IE$^K$ complex (Huppa et al., 2010) was used as surrogate (**Figure 27A**). As optimal positions for the FRET acceptor are difficult to predict a priori from in silico modelling, we decided to generate and test three different constructs. Based on this modelling work, positions αS90, αG28 of the α chain and βG23 in the linker region of the β chain were selected as promising attachment points for the FRET acceptor. Inter-fluorophore distance was predicted to be 35.1 Å for PLP1-IA$^b$ αG28C, 48.1 Å for PLP1-IA$^b$ βG23C and 51.5 Å for PLP1-IA$^b$ αS90C (**Figure 27**).

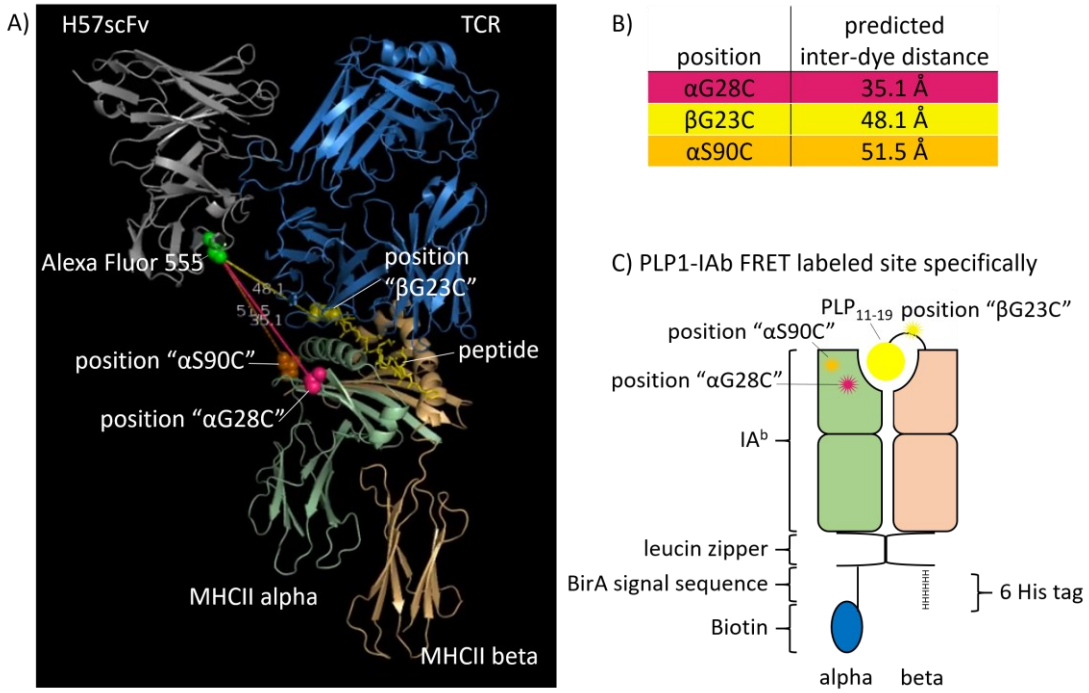


**Figure 27| Prediction of 3 potential FRET acceptor fluorophore positions in PLP1-IA$^b$ monomer: A)** A composite crystal structure model of the MHC II IE$^K$ interacting with an H57 scFv labelled TCR was used to predict potential FRET acceptor fluorophore positions in the PLP1-IA$^b$ monomer and their corresponding inter-fluorophore distances. **B)** Predicted inter-fluorophore distances **C)** Schematic representation of the PLP1-IA$^b$ FRET constructs that contain one free cysteine either at position αS90 or αG28 of the α chain or at position βG23 in the linker region of the β chain. Furthermore, the constructs contain a BirA signal sequence that allows site-specific *in vivo* biotinylation of the α chain, a 6-His tag and a leucine zipper motif that forces the MHCII α and β chain to dimerize.

### 3.4.2.3. Successful expression of PLP1-IA$^b$ FRET constructs that can be labelled with Alexa Fluor 647 $C_2$-maleimide

Plasmids for production of the three PLP1-IA$^b$ FRET constructs that each contain only one free cysteine group either at position αS90 or αG28 of the α chain or at position βG23 in the linker region of the β chain were generated by site directed mutagenesis. Using Schneider S2 cells, all three Cys-modified PLP1-IA$^b$ FRET constructs could be expressed and purified successfully. SDS page analysis indicated high purity (**Figure 28**). This was confirmed by size exclusion chromatography using Superdex™ 200 columns (data not shown). Notably, α and β chain were separated in the 12 % SDS page both under reducing and nonreducing conditions. The α chain could be identified by its biotinylated BirA signal sequence (**Figure 29**). The 6-His tag of the β chain could be identified by western blot staining against 6-histidine (**Figure 30**). After labelling with Alexa Fluor 647 C2-maleimide, the degree of labelling was determined. It was 70 % for PLP1-IA$^b$ αG28C, 75 % for PLP1-IA$^b$ αS90C and 95 % for PLP1-IA$^b$ βG23C.

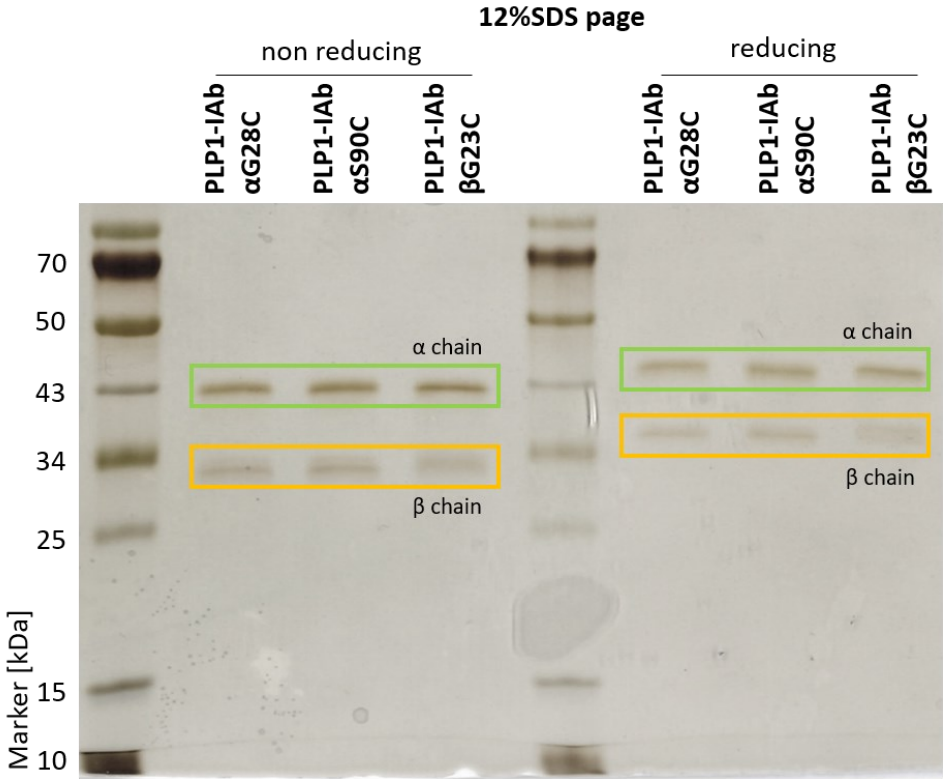


**Figure 28| 12% SDS page of PLP1-IA$^b$ FRET constructs:** α chain (orange) and β chain (green) are separated both under reducing (right) and non-reducing (left) conditions. Picture was generated in collaboration with Markus Kraller.

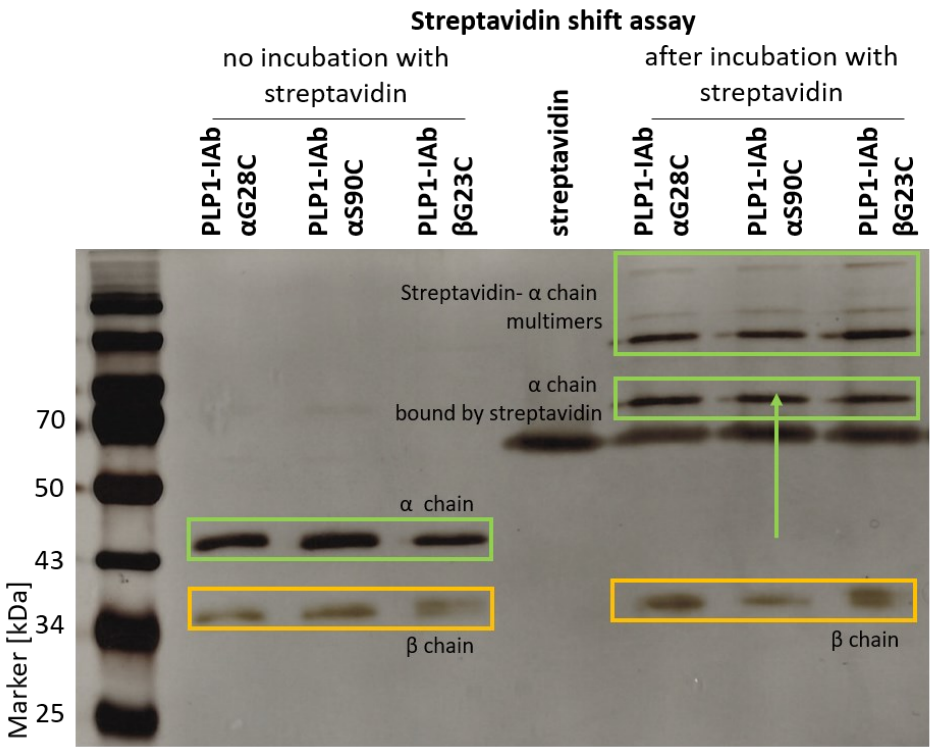


**Figure 29| Identification of the α chain by streptavidin shift assay:** 12 % SDS page of PLP1-IA$^{b}$ FRET constructs without (left) or after (right) incubation with streptavidin. The α chain contains a biotinylated BirA signal sequence that binds streptavidin. Upon incubation with streptavidin, the α chain is bound by streptavidin and therefore increases in weight. As streptavidin has 4 binding sites, also α-chain-streptavidin multimers can be found. The β chain is not shifted. Picture was generated in collaboration with Markus Kraller.

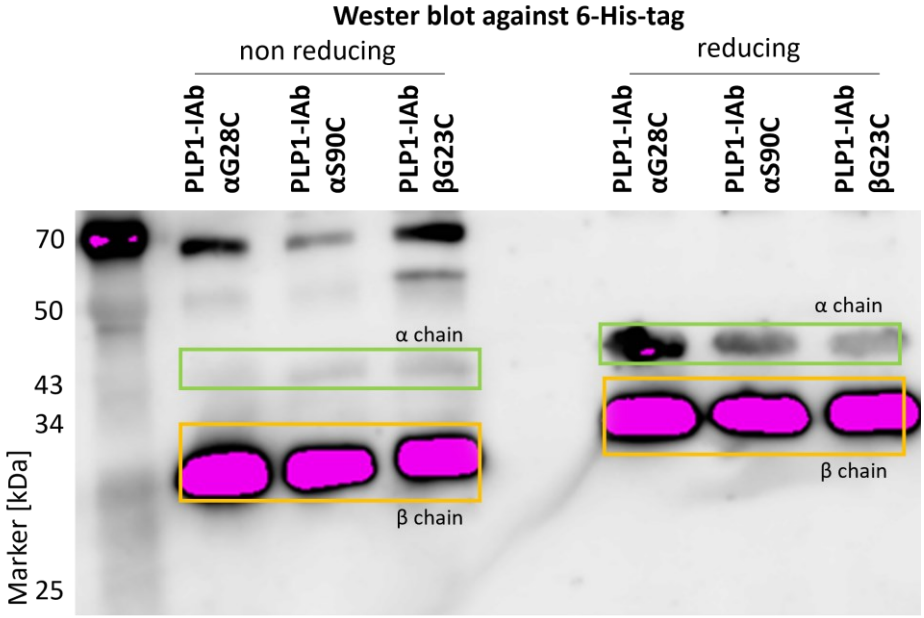


**Figure 30| Identification of the β chain by western plot:** Western plot of PLP1-IA$^{b}$ FRET constructs with anti-6-His-tag. The β chain was identified by its 6-His-tag. Picture was generated in collaboration with Markus Kraller.

### 3.4.3. PLP1-IA$^b$ FRET constructs were functional *in vitro* and *in situ.*

We next wanted to test function of the novel PLP1-IA$^b$ FRET constructs. To do so, culture plates were coated with the PLP1-IA$^b$ FRET constructs at varying concentrations. Those coated wells were used to stimulate *TCR-A yellow* T hybridoma cells containing an NFAT-GFP reporter system. After 12 h of stimulation, GFP expression as a marker for activation was analysed by flow cytometry (**Figure 31A**). All three novel PLP-IA$^b$ FRET constructs were able to stimulate the hybridoma cells with an EC50 below 1 ng/ml. Furthermore, the stimulatory potency of the three PLP1-IA$^b$ FRET constructs were highly similar and comparable to stimulatory potency of the original PLP1-IA$^b$ monomer.

To test function in the lipid bilayer system, functionalized lipid bilayers were loaded with PLP1-IA$^b$ FRET constructs and were used to stimulate fura-2AM labelled *TCR-A yellow* T cells. For all three PLP1-IA$^b$-FRET constructs elevated intracellular $Ca^{2+}$-levels were detectable and more than 64% of the T cells interacting the with PLP1-IA$^b$-FRET loaded lipid bilayer were classified "activated (**Figure 31B**).

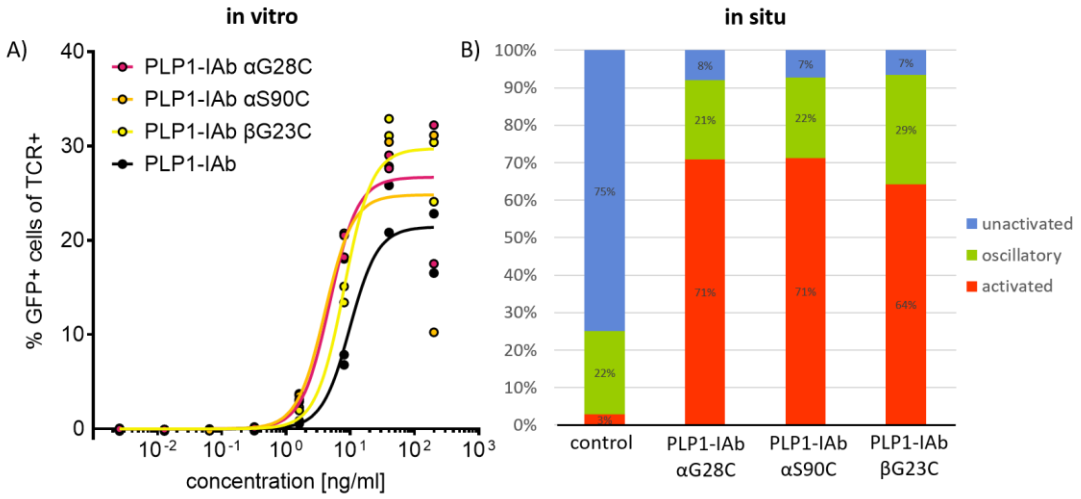


**Figure 31| PLP1-IA$^b$ constructs were functional: A)** Stimulation assays of NFAT-GFT reporter T hybridoma cells expressing *TCR-A yellow*. T hybridoma cells were stimulated in wells that had been coated with PLP1-IA$^b$ FRET constructs at varying concentrations. After 12 h stimulation, GFP expression as a marker for activation was analysed by flow cytometry. Data was interpolated with a four-parameter sigmoid dose response curve. **B)** fura-2AM labelled T*CR-A yellow* T cells were placed on functionalized lipid bilayers that were loaded with 100 ng Alexa Fluor 647 $C_2$-maleimide labelled PLP1-IA$^b$ FRET constructs. A functionalized lipid bilayer without MHC II functioned as control. Based on intracellular $Ca^{2+}$ concentration, 1500 cells were characterized as either activated, oszillatory or unactivated. $Ca^{2+}$-flux data was generated in collaboration with Vanessa Mühlgrabner.

### 3.4.4. PLP1-IA$^b$ FRET constructs caused only low FRET signals.

Finally, we wanted to check if the interaction between *TCR-A yellow* and the novel PLP1-IA$^b$-FRET constructs could be visualised by a FRET signal. To do so, interactions of *TCR-A yellow* T cells labelled with a FRET donor by H57 scFv-Cy3, and functionalized lipid bilayers loaded with different concentrations of the three novel PLP1-IA$^b$ FRET constructs, labelled with the FRET acceptor Alexa 647, were observed by TIRF microscopy. Despite clustering of TCRs with MHC II complexes and observed formation of immunological synapses, only weak FRET signals were observed even at high concentrations of PLP1-IA$^b$-FRET constructs. Bulk FRET yield of an entire immunological synapse, determined by donor recovery after acceptor photobleaching, was less than 2 % (**Figure 32**). Unfortunately, these FRET yields were too low to perform any quantitative *in situ* affinity measurements.

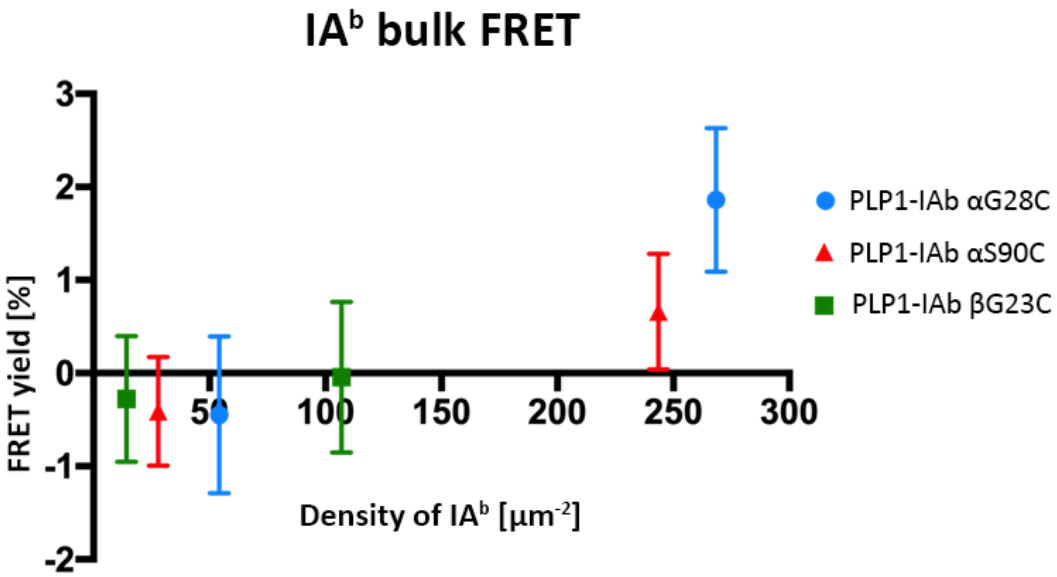


**Figure 32| PLP1-IA$^b$ FRET constructs resulted in low FRET signals:** Functionalized lipid bilayers were loaded with PLP1-IA$^b$ FRET constructs and interactions with H57 scFv-Cy3 labelled *TCR-A yellow* T cells were observed by TIRF microscopy. FRET yield of at least 30 interactions was determined by donor recovery after acceptor photobleaching at varying densities of PLP1-IA$^b$ FRET constructs. Dots and lines indicate mean with SD. Data was generated in collaboration with Vanessa Mühlgrabner.

# 4. Discussion

## 4.1. TCR affinity measurements by SPR were prevented by postinduction toxicity of the α*TCR-F grey* protein to E. coli.

Through repertoire comparisons of mice that are tolerant or non-tolerant to PLP, the Klein lab identified four *representative* TCRs that function either as PLP dependent deleters or PLP dependent $T_{reg}$ cell converters. Aim of this thesis was to investigate if TCR intrinsic binding parameters specify the cell fate decision between negative selection and clonal diversion. To do so, we wanted to use SPR spectroscopy to measure kinetics of TCR-PLP1-$IA^b$ interactions. For this approach soluble TCRs were needed.

Three out of four TCRα chains and the common β chain could be expressed successfully in E. coli (**Figure 11**). Unfortunately, expression of the deleter α*TCR-F grey* proved challenging and was not achieved. Information regarding the properties of this TCR would be crucial for a comprehensive TCR affinity analysis to cover a broad spectrum of tolerance behaviours.

Rare codon usage and protein toxicity are well described potential causes of insufficient protein expression in E. coli (Saida, 2007). Rare codon usage describes the fact that some codons are rarely used in E. coli and only small amounts of corresponding transfer-RNAs (tRNAs) are expressed. This problem can normally be overcome by optimisation of codon usage for common tRNAs or by using special E. coli strains as for instance Rosetta 2(DE3) that contain tRNAs for rare codons. However, neither of these two approaches nor the combination of both rescued α*TCR-F grey* expression (see 3.1.2). This makes it unlikely that the insufficient expression is a problem of rare codon usage.

Protein toxicity is more complex and toxic proteins can interfere in multiple ways with the physiological metabolism of E. coli. Typical expression protocols consist of two phases: growth phase and induction phase. During the growth phase, cells are propagated in LB medium. During this phase, it is important to keep the recombinant

gene under repressive conditions to prevent interference of the recombinantly expressed gene product with vital functions of the bacteria. In this thesis this was achieved in a dual way: The T7 RNA polymerase that facilitates production of the recombinant gene, is produced in the E. coli BL21(DE3) host strain under the control of the IPTG-inducible lac UV5 promoter (Studier & Moffatt, 1986). Additionally, a lac repressor that can be inactivated by IPTG, inhibits transcription of the recombinant protein by binding to a lac operator in the T7 promoter region of the pET-30a(+) vector. Both mechanisms ensure particularly low basal transcription of the recombinant gene during growth phase. This is a well-established transcription system that has been used to produce a large variety of different proteins (Saida, 2007). Despite this dually controlled expression system, leaky expression of toxic proteins can sometimes result in loss of the protein encoding plasmid and overgrowth of plasmid free bacteria during the growth phase. However, we observed similar growth rates of α*TCR-F grey* and α*TCR-E salmon* transformed E. coli cultures before induction (**Figure 12**). Furthermore, we measured high plasmid stability quotients (**Figure 13**) that were similar for both TCRs. This indicates that maintaining the plasmid during growth phase was not the critical problem that caused the insufficient expression of α*TCR-F grey*.

In the subsequent induction phase, expression of the recombinant gene is induced. Addition of IPTG to the bacteria culture triggers expression of the T7 RNA polymerase and relieves inhibition of the lac repressor. This leads to transcription of the recombinant protein (Saida, 2007). However, toxic proteins may severely interfere with bacterial functions upon induction before a sufficient amount of recombinant protein is produced (Saida, 2007). We observed that shortly after induction with IPTG α*TCR-F grey* E. coli cultures collapsed (**Figure 12**). Furthermore, we measured high toxicity quotients, defined as the ratio of colony counts on LB-agar plates with and without IPTG, for α*TCR-F grey* close to 100 % in BL21(DE3) E. coli stains (**Figure 13**). This strongly suggests that toxicity of α*TCR-F grey* is the reason for its insufficient recombinant protein expression.

To overcome postinduction toxicity, several approaches were tested. For instance, we extensively altered expression conditions (see 3.1.4) to achieve a slower but

metabolically better controlled and more effective expression. Furthermore, we tested expression in toxicity tolerant *OverExpress*$^{TM}$ strains (see 3.1.5) that have been reported to be better suited for expression of toxic proteins as they show a slower rate of mRNA accumulation (Dumon-Seignovert et al., 2004; Miroux & Walker, 1996). However, none of these approaches to overcome postinduction toxicity of α*TCR-F grey* in E. coli were successful.

In essence, we concluded that changing the expression system to an eucaryotic system might be a more promising approach to successfully express α*TCR-F grey.* For instance, soluble TCRs have been successfully expressed in insect cells using baculovirus transfection (Kappler et al., 1994) or in human HEK293 cells (Walseng et al., 2015). These approaches also have the advantage that production in eukaryotic cells allows post-translational modifications. Expression in eucaryotic cells will hopefully overcome the toxicity problem of *TCR-F grey* and allow affinity measurements by SPR spectroscopy.

## 4.2. TCR functional avidity defines the size of the clonal $T_{reg}$ cell conversion niche.

*In vivo* the interaction between a T cell and an APC is not only affected by the TCR-pMHC interaction but also involves many costimulatory factors and adhesion molecules, all of which may play a role in signal integration . We wanted to investigate how the four TCRs of intrest influence T cell function. To do so, the TCRs were expressed in T hybridoma cells and their functional avidity was measured by *in vitro* peptide stimulation assays. We could show that the T hybridoma cells expressing the four *representative* TCRs could be stimulated by PLP peptide but not by peptides unrelated to the $PLP_{11-19}$ core epitope (e.g., LLO). This indicates that the TCRs of interest are indeed specific for PLP.

### 4.2.1. Higher maximal activation plateaus with $PLP_{1-24}$

For evaluation of the stimulatory potency of the four *representative* TCRs we used both a longer $PLP_{1-24}$ and a shorter $PLP_{9-20}$ peptide. We were interested in the influence of the neighbouring amino acids of the $PLP_{11-19}$ core epitope. The same relative functional avidity hierarchy was measured with both peptides. Yet, we observed that stimulation with the longer $PLP_{1-24}$ peptide led to higher maximal activation plateaus (**Figure 18 C&F**). This was particularly significant for the two TCRs of lower functional avidity (*TCR-L blue* and *TCR-E salmon*). One potential explanation for this observation could be that the four *representative* TCRs recognize different target-epitopes of PLP. However, we deem this unlikely as we found the same stimulation hierarchy for both the longer $PLP_{1-24}$ and the shorter $PLP_{9-20}$ peptide indicating that the core epitope is present in both peptides. Another explanation could be that the longer peptide is more efficiently processed for presentation on APCs (Germain, 1994). Indeed, it is known that in MHC II the antigen binding groove is open ended, so longer peptides can extend beyond it (Brown et al., 1993). As a result, peptides presented on MHC II typically have a range between 12-24 residues (Chicz et al., 1992; Hunt et al., 1992; Rudensky et al., 1991). The 12 amino acid long $PLP_{9-20}$ peptide represents the lower length-limit for presentation on MHC II. The 24 amino acid long $PLP_{1-24}$ peptide is potentially more efficiently processed and/or loaded onto MHC II through direct

exchange of MHC II bound peptides on the surface, so that higher peptide densities on APCs might be achieved using this peptide. These explanations provide possible reasons for the higher plateaus.

### 4.2.2. Correlation between TCR functional avidity and the mode of tolerance

Peptide stimulation assays revealed a reproducible TCR functional avidity hierarchy. *TCR-F grey* had the highest, *TCR-E salmon* had the lowest functional avidity and *TCR-A yellow* and *TCR-L blue* had an intermediate responsiveness (**Figure 18 B/E**):

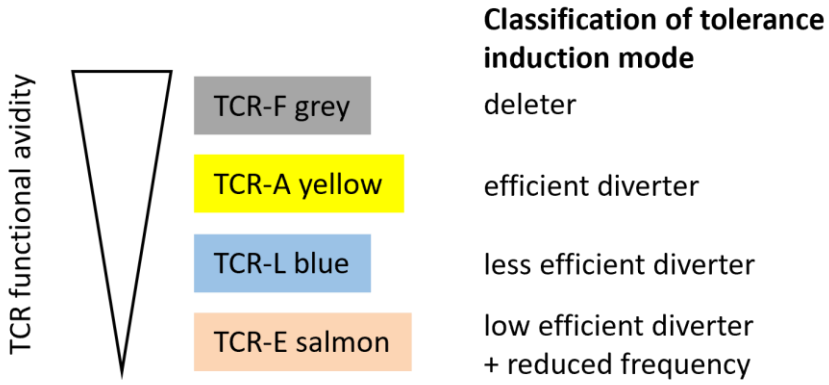


**Figure 33| TCR functional avidity hierarchy:** TCR functional avidity hierarchy was based on measured EC50 in PLP stimulation assays of T hybridoma cells expressing the *representative* TCRs. The classification of tolerance induction against PLP of the *representative* TCRs is based on the repertoire analysis by Hassler et al. (Hassler et al., 2019).

We wanted to examine how TCR function correlates with the results of the repertoire analysis of PLP1 specific T cells (Hassler et al., 2019) (see 1.7.1). Comparative analysis revealed interesting correlations (**Figure 33**). *TCR-F grey*, which was classified as a deleter TCR as it was mostly absent from the PLP tolerant peripheral repertoire albeit being abundant in the uncensored repertoire, had the highest functional avidity. This is in line with a key prediction of the "affinity" model of thymocyte selection which suggests that strong thymic interaction causes negative selection by apoptosis (Klein et al., 2014). For the TCRs of lower functional avidity, negative selection could not be observed in the repertoire analysis. This is reminiscent of the well-defined functional avidity threshold for negative selection observed for $CD8^+$ T cells (Naeher et al., 2007).

TCR entities of intermediate functional avidity, *TCR-A yellow* and *TCR-L blue*, represented the most efficient converter TCRs. Yet, *TCR-A yellow* was more frequent

in the $T_{reg}$ cell compartment than *TCR-L blue*. *TCR-E salmon*, which had the lowest functional avidity of the *representative* TCRs, was only insufficiently converted into the $T_{reg}$ cell compartment. Overall, the frequency of the converter TCRs in the $T_{reg}$ cell repertoire correlated with their relative functional avidity rather than with their abundancy in the uncensored repertoire of thymic precursor cells. This was observed both in the peripheral $T_{reg}$ cell compartment and in the nascent thymic $T_{reg}$ cell compartment. This makes it likely that the correlation between TCR functional avidity and presence in the $T_{reg}$ compartment is not only a result of a survival advantage of more self-reactive T cells in the periphery but reflects different efficiency of $T_{reg}$ cell lineage induction in the thymus based on functional avidity itself.

One possible explanation for this phenomenon could be a limited $T_{reg}$ developmental "niche" as for instance proposed by *Bautista et al*. They examined $T_{reg}$ cell development of a natural occurring thymic TCR clone G113. This TCR is of unknown specificity yet seems to confer self-reactivity based on the observation that G113 TCR expressing cells proliferate when adoptively transferred into lymphopenic and nonlymphopenic hosts. Unexpectedly, in G113 TCR-transgenic $Rag^{-/-}$ mice *Bautista et al.* hardly found any thymic $T_{reg}$ cells which was in apparent contradiction to the findings in a polyclonal setting. This rose the question if polyclonality was crucial for effective $T_{reg}$ cell development. Using G113 TCR-transgenic/WT bone marrow chimeras at different ratios, thereby reducing the frequency of G113 expressing cells within an otherwise polyclonal pool of "bystander" T cells, they showed that the efficiency of $T_{reg}$ cell development was negatively correlated to the clonal frequency of precursors expressing the G113 TCR. With increasing precursor cell numbers, the absolute number of G113 expressing $T_{reg}$ cells reached a plateau (Bautista et al., 2009). This strongly suggested that $T_{reg}$ cell precursors compete for a limiting niche during $T_{reg}$ cell development. Similar approaches came to the same conclusion (Leung et al., 2009). However, the nature of this "niche" is still a matter of active debate. Availability of rare selecting antigens and co-stimulation factors e.g., interleukin-2, are discussed to be of importance (Klein et al., 2019; Lio & Hsieh, 2008).

Our findings in an oligoclonal setting indicate that TCR functional avidity correlates with $T_{reg}$ cell diversion efficiency. This is consistent with the results of previous

experiments by Lee et al. in a bone marrow chimera setting (Lee et al., 2012). They assessed efficiency of $T_{reg}$ cell generation of a panel of TCRs with a broad range of reactivity to OVA when the transgenic TCR is present at low frequency. To do so they transferred TCR-transgenic/WT bone marrow chimera into mice expressing OVA under the control of the insulin promoter. Analysis of the number of $T_{reg}$ cells that were generated demonstrated that the capability of TCRs to mediate $T_{reg}$ cell generation was proportional to their functional avidity. This is in line with our findings that the size or efficiency of the $T_{reg}$ cell diversion "niche" increases with TCR functional avidity. A distinctive feature of the oligoclonal setting used here is that all *representative* T cells are selected in parallel i.e., these cells with different TCRs compete for access to APCs and potentially any other determinant of the limiting $T_{reg}$ cell niche. Furthermore, whereas the OVA-specific bone marrow chimera setting involved an artificial model of a tissue restricted antigen (OVA expression under control of the insulin promotor), we here investigated TCRs specific for PLP i.e., a naturally occurring and physiologically expressed tissue restricted antigen. This makes the results of our comparative approach particularly significant.

Based on these observations, we developed a model to explain the correlation between TCR functional avidity and size of the $T_{reg}$ cell conversion niche: For central tolerance induction it is crucial that the selecting peptide is presented on thymic APCs in particular on medullary thymic epithelial cells (mTEC) (Aschenbrenner et al., 2007; Klein et al., 1998; Oukka et al., 1996). The ectopic expression of otherwise tissue restricted antigens e.g., PLP, in the thymus is controlled by AIRE in a process called promiscuous gene expression. Interestingly, each tissue restricted antigen is only expressed on a small fraction of mTECs (1-3 % in a protein approach (Cloosen et al., 2007) and 2-15 % in an mRNA based approach (Derbinski et al., 2008)). This observation suggests that promiscuous gene expression may entail stochastic processes (Anderson & Su, 2016; Derbinski et al., 2008; Villaseñor et al., 2008). In addition to the paucity of cells expressing a given tissue restricted antigen, it is likely that the density of MHC ligands that present this antigen may vary between APCs (**Figure 34**). Furthermore, we assume that TCRs of low functional avidity can only be stimulated by APCs presenting a high concentration of antigen while TCRs of high

functional avidity can also be stimulated by APCs presenting a low surface density. As a consequence, for T cells expressing a TCR of high functional avidity there is a larger number of thymic APCs that can activate T cells and thereby initiate $T_{reg}$ cell conversion. We propose that the number of APCs that can activate T cells expressing a specific TCR is the determining factor of $T_{reg}$ cell conversion niche size. This model therefore could explain the correlation between $T_{reg}$ cell induction efficiency and TCR functional avidity.

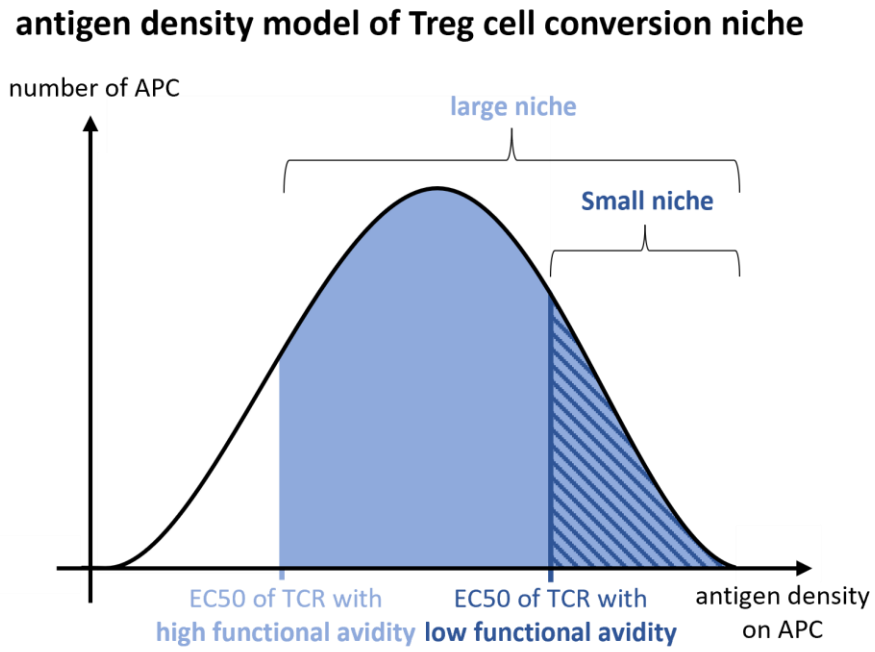


**Figure 34| Niche size for $T_{reg}$ cell development correlates with TCR functional avidity:** Density of tissue restricted antigen presented on APCs are hypothesized to be statistically distributed. According to this model, $T_{reg}$ diversion niche size correlates with the number of APCs that present a corresponding antigen at a density sufficient to trigger $T_{reg}$ cell induction. TCRs of low functional avidity can only be activated by APCs presenting a high concentration of antigen while TCRs of high functional avidity can also be stimulated by APCs presenting a low surface density. Therefore, T cells expressing a TCR with high functional avidity have a larger $T_{reg}$ diversion niche size than T cells expressing a TCR with low functional avidity.

## 4.3. Biophysical characterisation of the T cell-APC interaction

We proposed a model that explains the correlation between functional avidity and niche size for $T_{reg}$ cell conversion. Yet, it still remains elusive what parameters specify the observed threshold between negative selection of *TCR-F grey* with highest functional avidity and the efficient $T_{reg}$ cell conversion of *TCR-A yellow* with an only slightly lower functional avidity. We therefore investigated the binding characteristics of the four *representative* TCRs towards PLP1-$IA^b$ using different biophysical methods. We were interested if this could explain the different modes of tolerance of T cells expressing either of these TCRs.

First, we used the PLP1-tetramer for binding characterisation. Unexpectedly, the deleter *TCR-F grey*, despite displaying the highest functional avidity, displayed a significantly lower PLP1-tetramer staining capacity compared to the other TCRs of interest (**Figure 19**). There are several explanations that may account for this observation. First, T hybridoma cells could express different amounts of TCR. However, this is highly unlikely as we verified by flow cytometry that all hybridoma cells expressed similar amounts of the common β chain and huCD2 (a marker for the individual α chain that could not be stained directly due to a lack of a corresponding antibody) (**Figure 17**). Second, tetramer technology is based on increasing TCR avidity by providing up to four pMHC complexes. Binding of one arm of the tetramer alters the binding kinetics of the other arms as is brings the tetramer and the T cell into closer proximity but might also result in steric tension (Stone et al., 2001). Those effects might be different between *TCR-F grey* and the other TCRs of interest as *TCR-F grey* contains the variable region TRAV9N-3*01 instead of TRAV6D-6*01 that is used by all the other *representative* TCRs. Those variable regions slightly differ in primary and secondary structure. Measurements of TCR affinity by SPR would be necessary to rule out an artifact caused by the specific tetramer structure. Finally, *TCR-F grey* might indeed have a lower TCR affinity despite its high functional avidity. This would contradict the affinity model of thymocyte selection predicting that TCRs which are negatively selected, have a higher affinity than TCRs which are converted into the $T_{reg}$ cell compartment. Several reports demonstrated that tetramer binding capacity and TCR affinity measured by SPR spectroscopy do not necessarily correlate

with T cell function (al-Ramadi et al., 1995; Baker et al., 2000; Kersh et al., 1998). As a consequence, additional factors dictating central tolerance induction would need to be taken into considerations.

For example, the fate decision might be influenced by the TCR-pMHC binding kinetics rather than TCR affinity itself. This is reminiscent of the kinetic proofreading model that was developed to predict T cell function based on TCR-pMHC binding half-life. The model suggests that sufficiently long TCR binding times are necessary to complete intracellular signalling cascades leading to T cell activation (Edwards et al., 2012; McKeithan, 1995; Stepanek et al., 2014; Yousefi et al., 2019).

As a preliminary approach to characterize TCR-pMHC interaction kinetics, PLP1-tetramer binding half-lives were determined. Tetramer binding half-lives of *TCR A yellow*, *TCR-L blue* and *TCR-E salmon* correlated well with the functional avidity hierarchy. Yet, *TCR-F grey*, despite its higher functional avidity, tended (p=0,09) to have a lower PLP1-Tet binding half-life than *TCR-A yellow* (**Figure 21**). At first glance this contradicts the kinetic proofreading model of T cell activation. However, the tetramer dissociation experiment has an extremely complex interaction kinetic that is not only influenced by the TCR-PLP1-$IA^b$ interaction but also by the avidity of the multiple interaction sites of the PLP1-tetramer and the binding kinetic of the capturing antibody. This makes an interpretation of tetramer dissociation experiments difficult in particular as the staining capacity of *TCR-F grey* is significantly lower in comparison to *TCR-A yellow*. SPR would be the better suited technology to determine isolated TCR-pMHC binding half-lives. Unfortunately, the establishment of this technology turned out to be challenging as it was not possible to produce the critical *TCR-F grey* in E. coli due to toxicity (4.1).

Another explanation for the apparent discrepancy of a lower PLP1-tetramer binding half-life of *TCR-F grey* but higher functional avidity in comparison to *TCR-A yellow* could be that such *in vitro* systems do not reflect cellular forces that influence interaction kinetics *in vivo*. Recently, there is accruing evidence that T cell function is better predicted by *in situ* interactions kinetics measured when both the TCR and the pMHC are anchored in membranes and the interaction occurs across the intercellular junction. In particular there have been several reports about “catch-bonds” being

critical for effective T cell activation (Hong et al., 2015; Liu et al., 2014). Catch bonds show unconventional kinetics where application of mechanical forces on a TCR-pMHC interaction counter-intuitively leads to a prolongation of bond lifetime. This is in contrast to a classic slip bond, where mechanic tensions decreases bond lifetime (reviewed in (Kolawole et al., 2020).

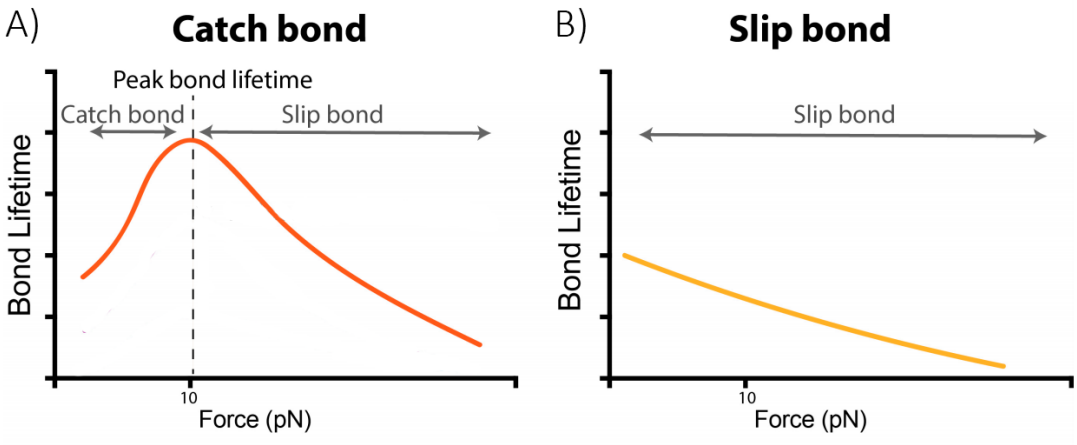


**Figure 35| catch vs. slip bonds: A)** When increasing force is applied to a TCR-pMHC catch bond, bond lifetime increases until a tipping point is reached. Further increasing force above this point leads than to decreased bond lifetime. **B)** In contrast, increasing force on a slip bond continuously decreases bond lifetime. Figure was adapted from *Kolawole et al.* (Kolawole et al., 2020).

It would be interesting to investigate if the deleter *TCR-F grey* forms a catch bond with PLP1-IA$^b$. This would be a potential explanation for the observed highest functional avidity despite the lower *in vitro* tetramer dissociation half-life. Formation of a catch bond could also be the decisive parameter determining the fate decision between $T_{reg}$ conversion und negative selection.

### 4.3.1. Towards measuring TCR-PLP1-IA$^b$ interactions *in situ* using a FRET based microscopic assay.

To measure *in situ* TCR-pMHC interaction kinetics under more physiological conditions we aimed to establish a FRET based microscopic assay based on the experimental setting described by Axmann et al. (Axmann et al., 2015a). To do so it was necessary to develop a novel PLP1-IA$^b$ FRET construct that can be labelled site specifically with a FRET acceptor fluorophore. In our hands the PLP1-IA$^b$-tetramer already proved to be a versatile tool to stain PLP1 reactive T cells. We now wondered if the PLP1-IA$^b$

monomer is suited as a basic structure for the FRET probe. First, we verified stimulatory potency of the PLP1-IA$^b$ monomer coated on the surface of culture plates. Using the PLP1-IA$^b$ monomer as a surrogate ligand, the same stimulatory hierarchy for the *representative* TCRs was observed as in the peptide stimulation assays (**Figure 22**). This strongly indicates that the additional structural motifs in the monomer (biotin tag, 6-histidine tag, the leucin zipper and the linker) have no negative influence on the binding characteristics of PLP1-IA$^b$. We next studied the interaction of PLP1 specific T cells with a functionalized lipid bilayer loaded with the PLP1-IA$^b$ monomer. A "bull's eye arrangement" with clustered TCRs and pMHC in the centre surrounded by a ring of ICAM-1 could be observed microscopically (**Figure 23**). This indicated formation of an immunological synapse. Finally, we proved by intracellular $Ca^{2+}$-flux measurement that functionalized lipid bilayer loaded with the PLP1-IA$^b$ monomer can activate PLP1 specific T cells (**Figure 24**). In conclusion, we could demonstrate that the PLP1-IA$^b$ monomer is a good surrogate ligand and is well suited as a basic structure for FRET experiments.

Next it was necessary to label the PLP1-IA$^b$ monomer site specifically with a FRET acceptor fluorophore. As no structural data of IA$^b$ binding to a TCR labelled with H57 scFv is available a crystal structure of a respective IE$^K$ complex was used as surrogate to predict three mutation sites as anchor point for the FRET probe which would allow a suitable inter-dye distance (**Figure 27**). The corresponding three PLP1-IA$^b$ FRET constructs were successfully expressed in S2 Schneider cells at high yields. This was demonstrated by SDS page in combination with biotin shift assay to verify expression of the alpha chain (**Figure 29**) and Western blot to prove expression of the beta chain (**Figure 30**). All PLP1-IA$^b$ FRET constructs were able to stimulate T hybridoma cells *in vitro* (**Figure 31A**) and T cells *in situ* demonstrated by $Ca^{2+}$ flux measurements (**Figure 31B**). This confirmed functionality of all three PLP1-IA$^b$ FRET constructs. In a final step all three constructs could sufficiently be labelled with the FRET acceptor Alexa Fluor 647 $C_2$-maleimide (3.4.2.3) providing three functional, labelled constructs for FRET experiments.

We next examined the interaction between T cells labelled with a FRET donor by H57 scFv and a functionalized lipid bilayer loaded with either one of the three PLP1-IA$^b$

FRET constructs (**Figure 32**). Despite the proven functionality of the three PLP1-IA$^b$ FRET constructs only low FRET yields were measured. FRET yields were highest (2 %) with the PLP1-IA$^b$ FRET αG28C construct. Unfortunately, this was too low for any quantitative *in situ* affinity analysis. For this, a FRET yield of at least 10 % for an agonistic interaction would have been necessary (Huppa et al., 2010).

Low FRET yields are a rather common problem in FRET based systems, particularly when complex intermolecular interactions are observed (Aoki et al., 2013; Fritz et al., 2013; Miyawaki, 2011). One reason for this difficulty is that both the distance and orientation of donor and acceptor fluorophore influence FRET efficiency.

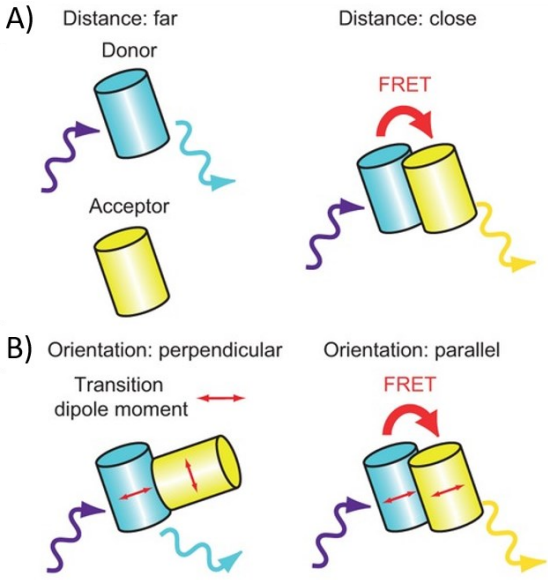


**Figure 36| Principle of FRET:** During FRET, a donor fluorophore transfers energy to an acceptor fluorophore through dipole–dipole coupling**. A)** FRET yield is dependent on the distance and **B)** the relative orientation of the donor and acceptor fluorophore. Figure was adapted from Aoki et al. (Aoki et al., 2013).

Although we had to use a surrogate model to predict the inter-dye distances, we are confident that the inter-dye distance is not the limiting factor as IA$^b$ and IE$^K$ are highly similar in general tertiary structure. However, a general downside of *in silico* modelling is that the orientation of the FRET fluorophores cannot be reliably predicted a priori (Aoki et al., 2013). Hence, FRET yield has to be improved through multiple rounds of trial and error. For this new fluorophore attachment points in the PLP1-IA$^b$ constructs need to be investigated. For example, mutation of G20 of the α chain, in close proximity to the most efficient αG28C mutation, or of G14 of the β chain, in closer proximity to the PLP1 peptide, might be promising candidates for further experiments.

# 5. Conclusion and Outlook

By repertoire comparisons of mice that are tolerant or non-tolerant to PLP, the Klein lab identified four TCRs that behave either as PLP dependent deleters or PLP dependent $T_{reg}$ converters. Aim of this thesis was to investigate which TCR intrinsic binding parameters specify the cell fate decision between negative selection and clonal diversion. Our findings are in line with a model in which tolerance induction is mediated by TCR functional avidity. Negative selection was associated with high functional avidity above a certain threshold. For $T_{reg}$ cell induction, below this threshold, we found a positive correlation between TCR functional avidity and $T_{reg}$ cell induction efficiency. It is thought that $T_{reg}$ cell conversion depends on a limited "niche" but the nature of this "niche" is still a matter of debate. We propose that this "niche" is the number of APCs able to activate $T_{reg}$ precursor cells. Those APCs present selecting peptides at surface densities which we assume to be stochastically distributed across the individual APCs. TCRs of low functional avidity can only be stimulated by APCs presenting a high concentration of antigen while TCRs of high functional avidity can also be stimulated by APCs presenting a low surface density. As a consequence, for T cells expressing a TCR of high functional avidity there is a larger number i.e., "niche", of thymic APCs that can activate T cells and by this initiate $T_{reg}$ cell conversion. This model therefore could explain the correlation between $T_{reg}$ cell induction efficiency and TCR functional avidity.

Yet, it still remains elusive what parameters specify the observed threshold between negative selection and $T_{reg}$ cell conversion. We therefore investigated the binding characteristics of the four *representative* TCRs towards PLP1-$IA^b$ using different biophysical methods. First, we used the PLP1-tetramer as a surrogate ligand for binding characterisation. Analysis of tetramer staining capacity and tetramer dissociation half-lives did not lead to a conclusive explanation of the fate decision. For a more comprehensive analysis of the TCR-pMHCs interaction, measurements of in *vitro* affinity by SPR and *in situ* 2D interaction kinetics by an experimental setup based on FRET would be highly interesting. Unfortunately, establishment of SPR experiments was prevented by postinduction toxicity of *TCR-F grey* and FRET experiments were

limited by low FRET yields. Nevertheless, we successfully expressed three out of four soluble TCRs of interest and proved general feasibility of the FRET experiment with PLP1-IA$^{b}$. This lays the foundation for further optimisation of these assay systems.

Elucidation of the mechanisms of central tolerance induction is of great importance for understanding development of autoimmune diseases like multiple sclerosis. This work contributed to a better understanding of the biophysical mechanisms that control central tolerance induction. We hope that this will ultimately help to understand failures of tolerance induction. This might finally allow early identification and prophylactic treatments of patients at risk for developing autoimmune diseases. This would be a great improvement for patient's health and quality of life.

# 6. Methods & Material

## 6.1. Protein production

### 6.1.1. Overexpression of soluble TCRs in inclusion bodies of E. coli

#### 6.1.1.1. Creation of vectors for expression of soluble TCRs

α and β TCR chains of the soluble TCRs were expressed in bacteria as chimeric proteins. The TCR specific V domains were fused to a human constant α/β region obtained from LC13 T cells, a clone of a human cytotoxic T cell (Newell et al., 2011). The first two amino acids of the constant domains are conserved between humans and mice and functioned as a linker between the mouse variable and the human constant region. To achieve solubility of the complexes, TCR transcription was designed to stop directly before the position where the α and β chain normally form an interchain disulphide bond. Furthermore, the free cysteine at position 186 of the Cβ domain was replaced by an alanine (Clements et al., 2002). This is a common approach to increase efficiency of TCR expression and refolding (Pecorari et al., 1999; van Boxel et al., 2009).

For bacterial overexpression in inclusion bodies, the secretory signal peptide that, in eukaryotes, targets its passenger proteins for translocation across the endoplasmic reticulum, must be removed. To predict the signal peptide sequence, the Phobius-algorithm of the Stockholm bioinformatics center (http://phobius.sbc.su.se) and the SignalP 4.1 algorithm (Petersen et al., 2011) were used.

Gene fragments encoding the signal peptide depleted α chains of *TCR-A yellow*, *TCR-E salmon*, *TCR-F grey* and *TCR-L blue*, and the TCR-PLP1 common β chain were moderately codon optimized for expression in E. coli using the IDT® codon optimization tool (https://eu.idtdna.com/CodonOpt). Final gene fragments (see 7.1) were ordered from IDT® and then cloned using the enzymes Nde1 and Hind3 (in NEBuffer 2.1 New England BioLabs) into the pET-30a(+) expression vector (Novagen). Integrity of the plasmids was checked by gel electrophoresis and sequencing.

#### 6.1.1.2. Transformation of E. coli

Transformation of E. coli was performed by heat shock at 42 °C. For this, competent bacteria were thawed on ice. 10-50 ng plasmid were added to 50 µl competent bacteria solution and the mixture was incubated for 30 minutes on ice. Heat shock was performed in a 42 °C water bath for 45 s for OverExpress™ cells, and for 60 s for BL21(DE3) and Rosetta™ 2(DE3) cells. After heat shock, bacteria were directly returned to ice for 2 minutes. After bacteria cooled down, 250 µl prewarmed TYM medium was added and bacteria were placed into a shaking incubator for 1 h at 180 rpm and 37 °C for recovery. Afterwards, bacteria were placed on LB-agar plates containing the appropriate selection-antibiotic (30 µg/ml kanamycin for pET-30a(+) vector) and were incubated for 14 h at 37 °C. Colonies of successfully transformed bacteria were picked. Successful transformation was double checked by sequencing.

#### 6.1.1.3. Overexpression in E. coli and inclusion body isolation

For production of the soluble TCR chains, a protocol based on the approach published by Clements et al. (Clements et al., 2002) was used. One colony of successfully transformed bacteria was picked and preincubated in 4 ml LB medium with 30 µg/ml kanamycin for 14 h. If not mentioned differently, all incubation steps were performed in a shaking incubator at 180 rpm at 37 °C. The inoculate was diluted into 1 l LB medium with 30 µg/ml kanamycin and was grown to an $OD_{600}$ = 0.6. Protein induction was induced by adding 1 mM IPTG. IPTG activates the T7 RNA polymerase that is encoded in the genome of the competent bacteria and relieves the lac repressor that inhibits T7 transcription of the recombinant protein by binding to a lac operator in the T7 promoter region of the pET-30a(+) vector. For overexpression of protein in inclusion bodies, E. coli were incubated for another 4 hours. Afterwards, bacteria were pelleted and resuspended in 5ml *resuspension buffer*.

For isolation of inclusion bodies, bacteria were lysed by adding 22.5 ml *lysis buffer*. Then, sonication was performed for 3 min (pulsed) on ice using a Branson sonifier®. Inclusion bodies were isolated by centrifugation at 4 °C, 10,000 rpm for 15 min in a Sorvall® SA-600 rotor. The pellet was resuspended in 30 ml *wash buffer*, homogenised, and centrifuged again. This washing step was repeated four times. A final washing step

was performed with 30 ml *wash buffer 2*. Afterwards, inclusion bodies were resuspended in 2 ml *extraction buffer*. Successful protein production was confirmed by Coomassie blue-stained SDS page.

### 6.1.2. Production and purification of labelled PLP1-IA$^b$ FRET in Drosophila S2 cells

For FRET experiments, IA$^b$ loaded with $PLP_{11-19}$ must be labelled site specifically with Alexa Fluor® 647. For this, a free cysteine is needed. As PLP-IA$^b$ already contains a free cysteine at position -2 of the beta chain and this would disturb site specific labelling $Cys_{-2}$ was mutated into alanine for the PLP1-IA$^b$ FRET constructs. Three PLP1-IA$^b$ FRET constructs with new free cysteines at different positions were produced:

| Name | Description | α chain vector | β chain vector |
|---|---|---|---|
| IA$^b$ alpha G28C | glycine at position 28 of the alpha chain was mutated to encode a cysteine | pRMAHa-3 IAb alpha G28C | pRMAHa-3 IAb beta PLP1 C-2A |
| IA$^b$ alpha S90C | serine at position 90 of the alpha chain was mutated to encode a cysteine. | pRMAHa-3 IAb alpha S90C | pRMAHa-3 IAb beta PLP1 C-2A |
| IA$^b$ beta linker G23C | glycine at position 23 in the linker attached to the beta chain was mutated to encode a cysteine. | pRMAHa-3 IAb alpha | pRMAHa-3 IAb beta PLP1 C-2A + linker G23C |

**Table 5| PLP1-IA$^b$ FRET constructs.**

In all constructs, the cysteine at Position -2 of the β chain which would disturb site specific labelling, was mutated into an alanine.

#### 6.1.2.1. Plasmid generation by site directed mutagenesis using polymerase chain reaction (PCR)

Plasmids encoding the PLP1-IA$^b$ FRET constructs were generated by site directed mutagenesis using polymerase chain reaction (PCR), as described before (Cormack, 2001). Source vectors pRMAHa-3 IAb alpha and pRMAHa-3 IAb beta PLP1 encoding the PLP1-IA$^b$ α and β chain, respectively, were kindly provided by Dr. Tobias Hassler.

The following primers were used for site directed mutagenesis:

*pRMAHa-3 IAb alpha G28C*

Primer: IAbα G28C fwd.:
5’ TAAGTGTATATCAGTCTCCTtgtGACATcGGCCAGTACACATTTGAATT

Primer: IAbα G28C ass.:
5’ AATTCAAATGTGTACTGGCCgATGTCacaAGGAGACTGATATACACTTA

Source vector: pRMAHa-3 IAb alpha

*pRMAHa-3 IAb alpha S90C*

primer: IAbα S90C fwd.
5’ TTGGGAGTCTTGACTAAGAGaTCtAATtgtACCCCAGCTACCAATGAGGC

primer: IAbα S90C ass.
5’ GCCTCATTGGTAGCTGGGGTacaATTaGAtCTCTTAGTCAAGACTCCCAA

Source vector: pRMAHa-3 IAb alpha

*pRMAHa-3 IAb beta PLP1 C-2A*

Primer: IAb PLP1 C-2A fwd.
5’ GCAGCCCCGGGACCGAAGGagctCTGGTGGGCGCGCCGTTTGC

Primer: IAb PLP1 C-2A ass.
5’ GCAAACGGCGCGCCCACCAGagctCCTTCGGTCCCGGGGCTGC

Source vector: pRMAHa-3 IAb beta PLP1

*pRMAHa-3 IAb beta PLP1 C-2A + linker G23C*

Primer: IAbβ PLP1 linkerG23C fwd.
5’ CTAGTGGCGGTGGAAGTGGCtgcagTGAAAGGCATTTCGTGTACC

Primer: IAbβ PLP1 linkerG23C ass.
5’ GGTACACGAAATGCCTTTCActgcaGCCACTTCCACCGCCACTAG

Source vector: pRMAHa-3 IAb beta PLP1 C-2A

#### 6.1.2.2. Production of PLP1-IA$^b$ constructs in Gibco® Drosophila S2 Cells

Production and purification of PLP1-IA$^b$ constructs was performed as previously published (Moon et al., 2007) using a protocol of Mark Jenkins' laboratory (http://www.jenkinslab.umn.edu/Jenkins_Lab_2/protocols.html "Jenkins Lab MHC Class II tetramer Production Protocol - 01.08.2016") that describes the process in great detail. In summary, Drosophila S2 cells were transfected with vectors encoding the IA$^b$ α and β chain by calcium phosphate transfection. *In vivo* biotinylation was achieved by co-transfection with an expression plasmid for the E. coli BirA enzyme. A drug resistance gene was encoded on a separate plasmid and was transfected at 10 % the amount of the other genes. This limited the extent of cells gaining drug resistance without expressing the genes of interest. Selection of successfully transfected cells was performed using blasticidin. Cells were upscaled and protein expression was induced by adding 0.8 mM copper, activating a copper-inducible promoter. PLP1-IA$^b$ construct was enriched from cell culture supernatant via nickel affinity chromatography targeting the 6His tag on the C-terminus of the MHC II β chain. The protein was further purified using a monomeric avidin column targeting the biotin tag on the C-terminus of the MHCII α chain and was eluted with excess of biotin. Free biotin was removed by washing using an Amicon Ultra-15 column (Millipore) with a molecular weight cut-off of 30 kD. The purified PLP1-IA$^b$ constructs were stored at -80 °C.

## 6.2. Protein analytics

#### 6.2.1. SDS polyacrylamide gel electrophoresis (SDS page)

SDS page gels were composed of a 4.5 % stacking and a 15 % separation gel. For the separation gel, 5 ml *separation gel buffer*, 10 ml 29.2 % acrylamide/ 0.8 % bis-acrylamide and 5 ml $H_2O$ were mixed. Polymerization was started by adding 100 µl of 10 % tetramethylethylendiamine and 100 µl of 10 % ammoniumpersulfate. The mixture was vortexed and then quickly poured between two glass plates. The top of the gel was layered with isopropanol and the separation gel was left to polymerize for 30 min. Afterwards, isopropanol was carefully removed. For the stacking gel, 2.5 ml

*stacking gel buffer*, 1.5 ml 29.2 % acrylamide/ 0.8 % bis-acrylamide and 6.0 ml $H_20$ were mixed. Polymerization was started by adding 100 µl 10 % tetramethyl-ethylendiamine and 100 µl 10 % ammoniumpersulfate. Mixture was vortexed and then quickly poured onto the separation gel. Combs were put into the gel and the gel was left to polymerize for another 30 min. The finished gels were stored in wet towels at 5 °C.

Samples from soluble TCR production were prepared in 1x *reducing sample buffer* and were preheated to 95 °C for 5 min. Samples from $IA^b$ production were prepared in unreducing 1x *Lam's sample buffer* or 1x *reducing sample buffer.*

Gels were placed in a vertical electrophoresis cell with 1x *SDS-running buffer*, samples were loaded onto the gel and the gel was run at 175 V for approximately 1 h.

After gel electrophoresis, gels were either stained with Coomassie brilliant blue or were used for Western blot.

### 6.2.2. Western blot and Immunodetection

For Western blot, a PVDF Western blotting membrane (Roche) was activated for 1 min in 5 ml methanol and afterwards was equilibrated in 1x *Western blot transfer buffer* for 5 min. 6 blotting paper sheets (Whatman) were soaked with *1x Western blot transfer buffer* and all components were placed in an LKB 2117 Multiphor II electrophoresis unit in the following order:

Cathode carbon pad
3x blotting paper sheets (Whatman)
SDS page gel
PVDF Western blotting membrane (Roche)
3x blotting paper sheets (Whatman)
Anode carbon pad

Proteins were blotted at 80 mA, 50 V for 120 min. Afterwards, the membrane was blocked by incubation in *Western blot blocking solution* for 30 min.

For immunodetection, the membrane was incubated with horseradish peroxidase labelled antibody [10 µg/ml] for 12 h at 4 °C in *Western blot staining solution*. Excessive antibody was removed by washing three times for 30 min with 7.5 ml

*Western blot wash buffer*. For protein detection, the membrane was incubated with SuperSignal® West Pico chemiluminescent substrate (Thermo Scientific) as described in the manufacturer's manual. Chemiluminescence was detected with an RP NEW medical x-ray screen (CEA) using an Optimax® X-Ray Film Processor (ProTec) or with an iBright CL750 Western Blot Imaging System (ThermoFisher).

## 6.3. Stimulation assays of T hybridoma cells

### 6.3.1. General cell culture methods

Unless specified differently, T hybridoma cells were cultured at 37 °C supplemented with 10 % $CO_2$ in complete DMEM (cDMEM) medium containing 8 % FCS. Cells were split when 60-80 % confluent at a 1:6 ratio.

#### 6.3.1.1. T hybridoma cell generation

T hybridoma cells expressing the four *representative TCRs* were generated as previously published (Hassler et al., 2019) and were kindly provided by Christine Federle. In brief, TCRα chains were sub-cloned into the lentiviral vector FUGW harbouring human (hu)CD2 as a marker for effective transduction. The virus was produced into the supernatant of HEK293FT cells. Complete lentivirus was collected and used for transfection of BW58 NFAT-GFP reporter hybridoma cells (Hooijberg et al., 2000) stably expressing the common TCRβ chain.

#### 6.3.1.2. Preparation of bone-marrow derived dendritic cells (BmDC)

BmDC were obtained from C57BL/6 mice carrying the differential *Ptprc*$^a$ pan leukocyte marker commonly known as CD45.1 that is used to unambiguously separate the BmDC that are needed for stimulation from the cells of interest. Mice were euthanized by $CO_2$ asphyxiation. Both hind legs were surgically removed and cleaned from muscles. Bones were stored in PBS for transport. After sterilization of the bones in 70 % ethanol for 1 min, bones were carefully disintegrated in a mortar. Bone marrow cells were resuspended in 2 ml PBS and were passed through a nylon cell strainer. Cells were pelleted by centrifugation at 500 g for 5 min and red blood cells were lysed by

incubation in 1 ml *ACK buffer* for 4 min. After two washing steps, cells were placed in cIMDM with 10 ng/ml granulocyte/macrophage-colony-stimulation-factor (GM-CSF) in uncoated Petri dishes of 10 cm diameter at a concentration of $0.2x10^6$ /ml and a starting volume of 10 ml. The primary cells were cultured for 8 days at 37 °C supplemented with 7 % $CO_2$. On day 3, the culture volume was increased to 20 ml. On day 8, BmDCs were matured by addition of 300 ng/ml E. coli derived LPS. The next day, BmDC were harvested. 5 mM EDTA was used to remove cells from the Petri dish. Before freezing the BmDC, cells were irradiated with 20 gray and the quality of the BmDC was monitored using flow cytometry.

### 6.3.2. Peptide stimulation assay of T hybridoma cells

TCR functional avidity was assessed by stimulating $1.5x10^5$ T hybridoma cells expressing the TCR of interest with titrated amounts of peptide in the presence of $8×10^4$ congenically marked BmDCs in cIMDM. As a positive control, T hybridoma cells were stimulated TCR independently with AntiCD3 antibody. As a negative control, an unrelated peptide (OVA) was applied. Cultures were incubated for 19 h at 37 °C supplemented with 7 % $C0_2$ in a 96-well round bottom microtiter plate. After stimulation, the T hybridoma cells were fixated in 1 % PFA and analysed by flow cytometry. Analysis focused on $CD45.1^-$ $Vb6^+$ $huCD2^+$ cells. Applied gating strategy is depicted in **Figure 37**.

The T hybridoma cells contain an NFAT-GFP reporter system with a dynamic range of GFP expression. To assess functional avidity, the relative amount of $GFP^+$ cells was plotted against lg(peptide concentration). Logarithm was used to account for serial dilution. Data was interpolated with a four-parameter sigmoid dose response curve and lgEC50 of the stimulant (peptide or antibody) was calculated. EC50 is the concentration of the stimulant which induces a response halfway between the baseline and maximum response (**Figure 38**).

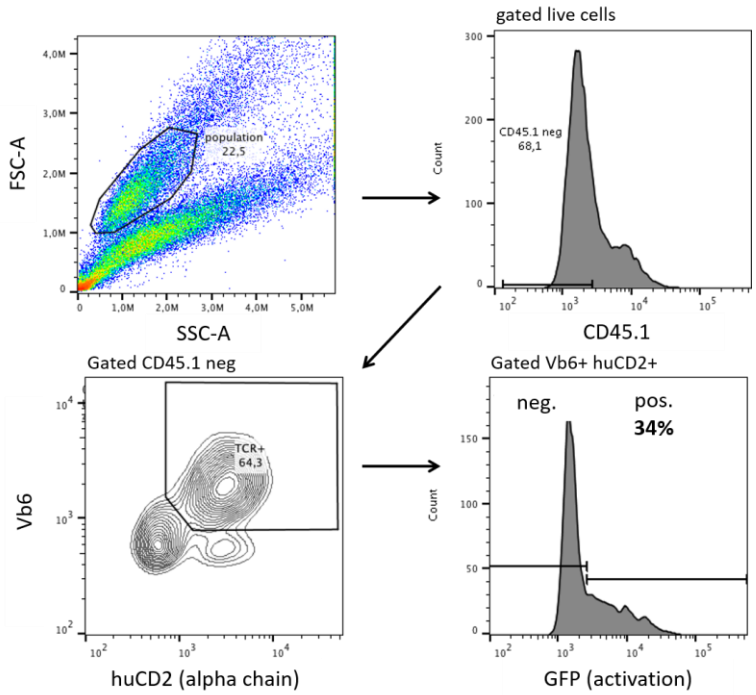


**Figure 37| Gating strategy of stimulation assays**: FSC-A and SSC-A was used to gate for living T hybridoma cells. Analysis was focused on CD45.1$^-$ cells to eliminate congenically marked BmDC and on hybridoma cells efficiently expressing the complete TCR composed of a common β chain βTCR-PLP1 that can be stained with antiVb6 antibody, and an individual αTCR. huCD2 was used as a marker for efficiently αTCR transfected hybridoma cells. Finally, relative amount of GFP$^+$ cells was assessed.

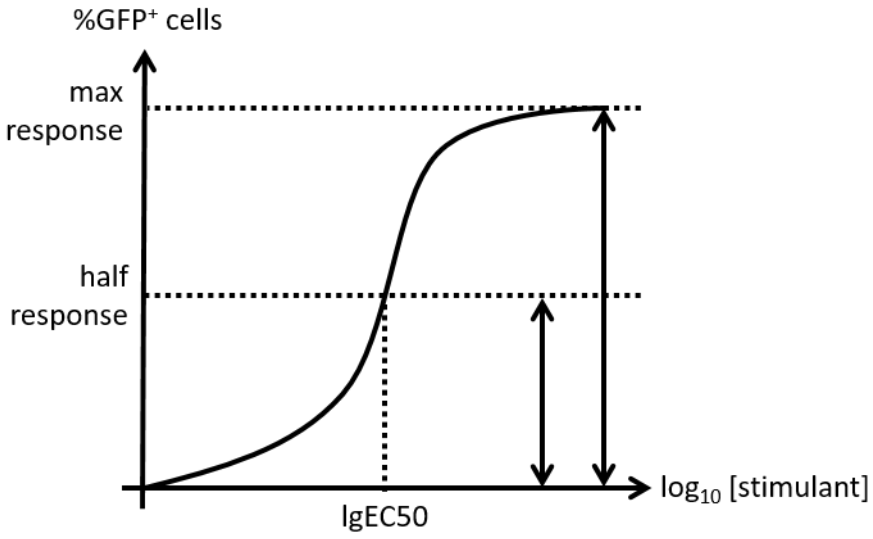


**Figure 38| Calculation of half effective concentration**: T hybridoma cells containing an NFAT-GFP reporter system were stimulated with titrated amounts of peptide. Relative amount of GFP$^+$ cells was plotted against $\log_{10}$ of peptide concentration as depicted in this schematic representation. Data was interpolated with a four-parameter sigmoid dose response curve and lgEC50 was calculated as indicated.

### 6.3.3. PLP1-IA$^b$ stimulation assay of T hybridoma cells

96-well cell culture plates were coated with 50 µl PBS containing PLP1-IA$^b$ at varying concentrations for 6 h. As a negative control, culture plates were coated with no MHC II complex or with IA$^b$ loaded with an PLP unrelated peptide (LLO). After coating was completed, wells were washed three time with PBS to remove uncoated proteins. Afterwards, 1.5x10$^5$ T hybridoma cells in 200 µl cIMDM were added. Cultures were incubated for 12 h at 37°C supplemented with 7% $C0_2$. After stimulation, the T hybridoma cells were fixated in 1 % PFA and analysed by flow cytometry. Analysis was performed as described before for peptide stimulation assays.

## 6.4. Tetramer assays

PLP1-tetramer was produced in our laboratory as previously published (Hassler et al., 2019) and was kindly provided by Dr. Tobias Hassler.

### 6.4.1. Tetramer staining

T hybridoma cells were incubated with 10 nM PLP1-tetramer in *FACS buffer* in the presence of 5 µg/ml AntiCD3 for 30 min at 25 °C and afterwards for 60 min at 4 °C.

### 6.4.2. Tetramer dissociation assay

T hybridoma cells were stained with 10 nM PLP1-tetramer. After 2 washing steps with cold FACS buffer, cells were resuspended in 450 µl cold *dissociation buffer* containing 2 % FCS, 2 mM EDTA and 3.3 µg/ml $IA^b$ capturing antibody (M5/114.15.2, to prevent rebinding) in PBS. PLP1-tetramer dissociation was studied by flow cytometry. Only T hybridoma cells expressing huCD2 (as a marker for expression of the specific TCRα chain) were included. PLP1-tetramer MFI of the T hybridoma cells over time was recorded and data was interpolated with a third order polynomial function:

$$MFI(t) = MFI_0 + B1 * t + B2 * t^2 + B3 * t^3$$

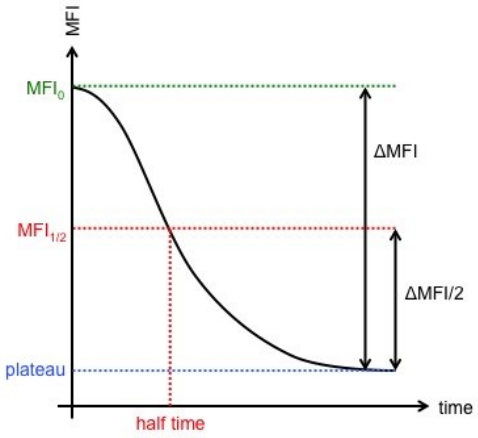


**Figure 39| Schematic representation of tetramer dissociation.**

$MFI_{Plateau}$ was measured after 45 min and ΔMFI was calculated:

$$\Delta MFI = MFI_0 - MFI_{Plateau}$$

PLP1-tetramer half-life $t_{1/2}$ was calculated by solving the following equation:

$$plateau + \Delta MFI/2 = MFI_0 + B1 * t_{1/2} + B2 * t_{1/2}^2 + B3 * t_{1/2}^3$$

$$\{t_{1/2} \in \mathbb{R} \mid t_{1/2} > 0\}$$

If more than one solution is possible, $t_{1/2}$ is the smallest solution.

## 6.5. Lipid bilayer experiments

Lipid bilayer experiments, including $Ca^{2+}$ flux measurements and FRET experiments, were performed as previously published in detail by Axmann et al. (Axmann et al., 2015a, 2015b). A brief description of the experimental setting can be found in the introduction (see 1.6.5).

## 6.6. Statistical analysis

Statistical analysis was performed using GraphPad Prism version 9.1. Details are displayed in the figure legends.

### 6.6.1. Statistical analysis of stimulation assays

To account for serial dilution of the stimulant, statistical evaluation was performed using $log_{(10)}$EC50. For multi comparison analysis of lgEC50, Tukey's multiple comparisons test was used based on the following assumptions:

- Experiments were repeated several times. Each time several treatments were handled in parallel. Since experiment-to-experiment variability was anticipated, data was analysed in such a way that each experiment was treated as a matched set.
- Gaussian distribution was assumed.
- Sphericity was assumed as data represented sets of matched observation.
- There were no missing values.

- For multiple comparison, mean of lgEC50 of each *representative* TCR was compared with mean of lgEC50 of every other TCR.
- Statistical significance was defined using an alpha value of 0.05.

### 6.6.2. Statistical analysis of tetramer dissociation experiments

For multi comparison analysis of $MFI_0$ and half-life of tetramer dissociation experiments, Tukey's multiple comparisons test was used based on the following assumptions:

- Experiments were repeated several times. Each time several treatments were handled in parallel. Since experiment-to-experiment variability was anticipated, data was analysed in such a way that each experiment was treated as a matched set.
- Gaussian distribution was assumed.
- Sphericity was assumed as data represented sets of matched observation.
- As some values were missing due to random experimental failures (e.g., malfunction of the flow cytometer) a mixed effects model was used.
- For multiple comparison mean of MFI/half-life of each *representative* TCR was compared with mean of MFI/half-life of every other TCR.
- Statistical significance was defined using an alpha value of 0.05.

## 6.7. Materials

### 6.7.1. Chemicals

Common chemicals were acquired from Roche and Merck unless otherwise mentioned.

### 6.7.2. Antibodies

*For flow cytometry*

| Epitop | Clone |
|---|---|
| CD3 | 17A2 |
| CD4 | RM4-5 |
| CD45.1 | A20 |
| CD8A | 53-6.7 |
| HUCD2 | RPA-2.10 |
| TCR VB6 | RR4-7 |

Conjugates with different fluorochromes were purchased from BioLegend or BD.

*For protein analysis*

| Epitop | Clone | Manufacturer |
|---|---|---|
| 6-HIS TAG | HIS.H8 | ThermoFisher |

Antibody was labelled with horseradish peroxidase.

### 6.7.3. Enzymes

| Enzyme | Manufacturer |
|---|---|
| Hind III | Pharmacia Biotech |
| Nde I | Fermentas |

### 6.7.4. Plasmids

| Plasmid | Source | Description |
|---|---|---|
| p18 BirA | M. Jenkins | Encodes for BirA enzyme which mediates biotinylation of the BirA signal sequence (Beckett et al., 1999) of the $IA^b$ α chain. |
| pCoBlast | M. Jenkins | Encodes for a resistance gene for Basticidin under control of the copia promotor for expression in S2 cells. |
| pET-30a(+) | Novagen | Was used for production of soluble TCRs in E. coli. Contains a T7 RNA polymerase based expression system. (Vector map see 7.1.6) |
| pRMAHa-3 $IA^b$ alpha | T. Hassler | Encodes for the $IA^b$ α chain |
| pRMAHa-3 $IA^b$ beta PLP1 | T. Hassler | Encodes for the $IA^b$ β chain loaded with $PLP_{11-19}$. |

#### 6.7.4.1. Expression systems

| Bacterial strain | Manufacturer |
|---|---|
| BL21(DE3) Competent E. coli | New England BioLabs Inc. |
| Gibco® Drosophila S2 Cells | Thermofisher Scientific |
| OverExpress C41(DE3) | Lucigen |
| OverExpress C41(DE3) pLys | Lucigen |
| OverExpress C43(DE3) | Lucigen |
| OverExpress C43(DE3) pLys | Lucigen |
| Rosetta™ 2(DE3) | Merck |
| SoloPack® Gold Competent Cells | Agilent Technologies |

### 6.7.5. Commercial kits

| Kit | Manufacturer |
|---|---|
| Alexa Fluor™ 647 C2 Maleimide | ThermoFisher |
| MinElute PCR Purification Kit | Qiagen |
| SuperSignal® West Pico Chemiluminescent Substrate | ThermoFisher |
| Zero Blunt® PCR cloning kit | Invitrogen |

### 6.7.6. Instruments

| Instrument | Trade name | Manufacturer |
|---|---|---|
| Bacterial incubator | Avantgard Line 56 | BD |
| Cell culture incubator | HERAcell 240 | ThermoFischer |
| Centrifuge | Multigufe X3R | Heraeus |
| Electrophoresis Cell | LKB 2117 Multiphor II | LKB/Pharmacia |
| Flow cytometer | FACS Canto II | BD |
| Flow cytometer plate reader | CytoFLEX S | Beckman Coulter |
| High speed centrifuge | RC6+ centrifuge | Sorvall |
| Incubation shaker | Innova 44 | Brunswick |
| Sonicator | Branson sonifier® | Branson Sonic Power Co. |
| Spectrophotometer | BioPhotometer | Eppendorf |
| Vertical Electrophoresis Cell | TetraCell | BioRad |
| Water bath | Isotemp 220 | ThermoFisher |
| Western Blot Imaging System | iBright CL750 | ThermoFisher |

### 6.7.7. Programs

| Program | Task | Manufacturer |
|---|---|---|
| FlowJo v10 | Flow cytometry data analysis | BD |
| Prism 9.1 | statistics | GraphPad |

### 6.7.8. Buffers and Solutions

| Buffers & solutions | Ingredients |
|---|---|
| ACK buffer | 0.15 M $NH_4Cl$<br>10 mM $KHCO_3$<br>0.1 mM EDTA<br>Adjust the pH to 7.2-7.4 |
| Extraction buffer | 20 mM Tris pH 8.0<br>8 M urea<br>0,5 mM EDTA<br>1 mM DTT |
| FACS buffer | PBS containing<br>2 % (v/v) FCS<br>2 mM EDTA |
| Lam's sample buffer (4x) | 60 % (v/v) Glycerol<br>200 mM Tris HCl pH 6.8<br>30 µg/ml Bromphenol-blue<br>in $H_2O$ |

| Buffers & solutions | Ingredients |
|---|---|
| PBS | 0,15 M NaCl,<br>3,0 mM KCl<br>8,0 mM $Na_2HPO_4$<br>2,0 mM $KH_2PO_4$<br>pH adjusted to 7.2-7.4 |
| Reducing sample buffer (3x) | 85 mM Tris HCl pH 6.8<br>11,4 % (v/v) Glycerol<br>2,9 % (w/v) SDS<br>0,05 % (w/v) Bromphenolblue<br>in $H_20$ |
| Resuspension buffer | 50 mM Tris pH 8.0<br>25 % (w/v) sucrose<br>1 mM EDTA<br>10 mM DTT<br>0,2 mM PMSF<br>1 µg/ml pepstatin A |
| SDS-Running buffer (10x) | 0,25 M Tris HCl pH 6<br>1,9 M Glycine<br>35 mM SDS<br>in $H_20$ |
| Separation gel buffer | 1.5 M Tris pH 8,8<br>0,4 % SDS<br>in $H_2O$ |
| Stacking gel buffer | 0.5 M Tris pH 6,8<br>0,4 % SDS<br>In $H_2O$ |
| Wash buffer | 50 mM Tris pH 8.0<br>0,5 % (v/v) Triton X-100<br>100 mM NaCl<br>1 mM EDTA<br>1 mM DTT<br>0,2 mM PMSF<br>1 µg/ml pepstatin A |
| Wash buffer 2 | 50 mM Tris pH 8.0<br>1 mM EDTA<br>1 mM DTT<br>0,2 mM PMSF<br>1 µg/ml pepstatin A |
| Western Blot blocking solution | 5 % (w/v) milk powder<br>in PBS with 0.05 % Tween 20 |
| Western Blot staining solution | 0,5 % (w/v) milk powder<br>in PBS |
| Western Blot Transfer buffer (1x) | 8 % (v/v) Methanol<br>in 1x SDS-Running buffer |
| Western Blot wash buffer | 0,5 % (w/v) milk powder<br>in PBS with 0.05 % Tween 20 |

### 6.7.9. Cell culture media

| Medium | Ingredients |
|---|---|
| cDMEM | 8% (v/v) Fetal calf serum (heat-inactivated, 54 °C for 35 min) (Merck)<br>2 % (v/v) L-Glutamin (Gibco)<br>1 % (v/v) Penicillin (10.000U/ml)/ Streptomycin (10.000 g/ml) (Gibco)<br>1 % (v/v) MEM non-essential amino acids (100x) (Gibco)<br>0,1 % [v/v] β-Mercaptoethanol (Gibco)<br>in Dulbecco's Modified Eagle Medium (Gibco) |
| cIMDM | 8 % (v/v) Fetal calf serum (heat-inactivated, 54°C for 35min) (Merck)<br>2 % (v/v) L-Glutamin (Gibco)<br>1 % (v/v) Penicillin (10.000 U/ml)/ Streptomycin (10.000 g/ml) (Gibco)<br>1 % (v/v) MEM non-essential amino acids (100x) (Gibco)<br>0,1 % [v/v] β-Mercaptoethanol (Gibco)<br>in Iscove's Modified Dulbecco's Medium medium (Gibco) |
| LB agar plate | 2 % (w/v) LB medium (Lennox)<br>1,5 % (w/v) Agar<br>in $H_20$ |
| LB medium | 2 % (w/v) LB medium (Lennox)<br>in $H_20$ |

# 7. Supplement

## 7.1. Cloning sequences for soluble TCR production

mouse variable domain
human constant domain
conserved linker region

### 7.1.1. αTCR-A yellow

Protein sequence:
MGDSVTQTEGPVTVSESESLIINCTYSATSIAYPNLFWYVRYPGEGLQLLLKVITAGQKGSSRGFE
ATYNKETTSFHLQKASVQESDSAVYYCALGAPGGYKVVFGSGTRLLVSPDIQNPDPAVYQLRDS
KSSDKSVCLFTDFDSQTNVSQSKDSDVYITDKCVLDMRSMDFKSNSAVAWSNKSDFACANAFN
NSIIPEDTFFPSPESS*

DNA sequence:
NdeI site
CATATGGGAGATTCCGTGACTCAAACAGAAGGCCCAGTGACCGTCTCAGAAAGCGAGAGC
CTGATCATTAATTGCACGTATTCAGCCACAAGCATTGCTTACCCTAATCTTTTCTGGTATGTT
CGCTATCCTGGAGAAGGTCTGCAACTCTTACTGAAAGTCATTACGGCTGGCCAGAAGGGAA
GCAGCCGCGGGTTTGAAGCCACATACAATAAAGAAACCACCTCCTTCCACTTGCAGAAAGC
CTCAGTGCAAGAGTCAGACTCGGCTGTGTACTACTGTGCTCTGGGTGCCCCCGGAGGCTAT
AAAGTGGTCTTTGGAAGTGGGACTCGCTTGCTGGTAAGCCCTGACATCCAGAACCCGGATC
CTGCCGTGTACCAGCTGCGCGACAGCAAATCCAGTGACAAGTCTGTCTGCTTATTCACCGAT
TTTGATTCTCAAACAAATGTGTCACAAAGTAAGGATTCGGATGTGTATATCACAGACAAATG
TGTGCTGGACATGCGTTCTATGGACTTCAAGAGCAACAGTGCTGTGGCCTGGAGCAACAAA
AGCGACTTTGCATGTGCAAACGCCTTCAACAACAGCATTATTCCAGAAGACACCTTCTTCCC
GAGCCCAGAGAGCTCGTAAGCTT
HindIII site
BamHI site

### 7.1.2. αTCR-L blue

Protein sequence:
MGDSVTQTEGPVTVSESESLIINCTYSATSIAYPNLFWYVRYPGEGLQLLLKVITAGQKGSSRGFE
ATYNKETTSFHLQKASVQESDSAVYYCALGSPGGYKVVFGSGTRLLVSPDIQNPDPAVYQLRDS
KSSDKSVCLFTDFDSQTNVSQSKDSDVYITDKCVLDMRSMDFKSNSAVAWSNKSDFACANAFN
NSIIPEDTFFPSPESS*

DNA sequence:
NdeI site
CATATGGGAGATTCCGTGACTCAAACAGAAGGCCCAGTGACCGTCTCAGAAAGCGAGAGC
CTGATCATTAATTGCACGTATTCAGCCACAAGCATTGCTTACCCTAATCTTTTCTGGTATGTT
CGCTATCCTGGAGAAGGTCTGCAACTCTTACTGAAAGTCATTACGGCTGGCCAGAAGGGAA
GCAGCCGCGGGTTTGAAGCCACATACAATAAAGAAACCACCTCCTTCCACTTGCAGAAAGC
CTCAGTGCAAGAGTCAGACTCGGCCGTGTACTACTGTGCTCTGGGTTCTCCTGGAGGCTATA
AAGTGGTCTTTGGAAGTGGGACTCGCTTGCTGGTAAGCCCTGACATCCAGAACCCGGATCC
TGCCGTGTACCAGCTGCGCGACAGCAAATCCAGTGACAAGTCTGTCTGCTTATTCACCGATT
TTGATTCTCAAACAAATGTGTCACAAAGTAAGGATTCGGATGTGTATATCACAGACAAATGT
GTGCTGGACATGCGTTCTATGGACTTCAAGAGCAACAGTGCTGTGGCCTGGAGCAACAAAA
GCGACTTTGCATGTGCAAACGCCTTCAACAACAGCATTATTCCAGAAGACACCTTCTTCCCG
AGCCCAGAGAGCTCGTAAGCTT
HindIII site
BamHI

### 7.1.3. TCR-E salmon

Protein sequence:
MGDSVTQTEGPVTVSESESLIINCTYSATSIAYPNLFWYVRYPGEGLQLLLKVITAGQKGSSRGFE
ATYNKETTSFHLQKASVQESDSAVYYCALGGPGGYKVVFGSGTRLLVSPDIQNPDPAVYQLRDS
KSSDKSVCLFTDFDSQTNVSQSKDSDVYITDKCVLDMRSMDFKSNSAVAWSNKSDFACANAFN
NSIIPEDTFFPSPESS*

DNA sequence:
NdeI site
CATATGGGAGATTCCGTGACTCAAACAGAAGGCCCAGTGACCGTCTCAGAAAGCGAGAGC
CTGATCATTAATTGCACGTATTCAGCCACAAGCATTGCTTACCCTAATCTTTTCTGGTATGTT
CGCTATCCTGGAGAAGGTCTGCAACTCTTACTGAAAGTCATTACGGCTGGCCAGAAGGGAA
GCAGCCGCGGGTTTGAAGCCACATACAATAAAGAAACCACCTCCTTCCACTTGCAGAAAGC
CTCAGTGCAAGAGTCAGACTCGGCTGTGTACTACTGTGCTCTGGGT**GGC**CCTGGAGGCTAT
AAAGTGGTCTTTGGAAGTGGGACTCGCTTGCTGGTAAGCCCTGACATCCAGAACCCGGATC
CTGCCGTGTACCAGCTGCGCGACAGCAAATCCAGTGACAAGTCTGTCTGCTTATTCACCGAT
TTTGATTCTCAAACAAATGTGTCACAAAGTAAGGATTCGGATGTGTATATCACAGACAAATG
TGTGCTGGACATGCGTTCTATGGACTTCAAGAGCAACAGTGCTGTGGCCTGGAGCAACAAA
AGCGACTTTGCATGTGCAAACGCCTTCAACAACAGCATTATTCCAGAAGACACCTTCTTCCC
GAGCCCAGAGAGCTCGTAAGCTT
HindIII site
BamHI

### 7.1.4. TCR-F grey

Protein sequence:
HMQSVTQPDARVTVSEGASLQLRCKYSYFGTPYLFWYVQYPRQGLQLLLKYYPGDPVVQGVN
GFEAEFSKSNSSFHLRKASVHWSDWAVYFCAVSSNTNTGKLTFGDGTVLTVKPNIQNPDPAVY
QLRDSKSSDKSVCLFTDFDSQTNVSQSKDSDVYITDKCVLDMRSMDFKSNSAVAWSNKSDFAC
ANAFNNSIIPEDTFFPSPESS*

DNA sequence:
Non codon optimized version:
NdeI site
catatgCAGTCAGTGACGCAGCCCGATGCTCGCGTCACTGTCTCTGAAGGAGCCTCTCTGCAG
CTGAGATGCAAGTATTCCTACTTTGGGACACCTTATCTGTTCTGGTATGTCCAGTACCCGCG
GCAGGGGCTGCAGCTGCTCCTCAAGTACTATCCAGGAGACCCAGTGGTTCAAGGAGTGAAT
GGCTTTGAGGCTGAGTTCAGCAAGAGTAACTCTTCCTTCCACCTGCGGAAAGCCTCTGTGCA
CTGGAGCGACTGGGCTGTaTACTTCTGTGCTGTGAGCTCCAACACCAATACAGGCAAATTAA
CCTTTGGGGATGGGACCGTGCTCACAGTGAAGCCAAACATCCAGAACCCGGATCCTGCCGT
GTACCAGCTGCGCGACAGCAAATCCAGTGACAAGTCTGTCTGCTTATTCACCGATTTTGATT
CTCAAACAAATGTGTCACAAAGTAAGGATTCGGATGTGTATATCACAGACAAATGTGTGCT
GGACATGCGTTCTATGGACTTCAAGAGCAACAGTGCTGTGGCCTGGAGCAACAAAAGCGA
CTTTGCATGTGCAAACGCCTTCAACAACAGCATTATTCCAGAAGACACCTTCTTCCCGAGCCC
AGAGAGCTCGTAAGCTT
HindIII site
BamHI

Moderatly codon optimized version:
NdeI site
CATATGCAGTCAGTGACGCAGCCCGATGCTCGCGTCACTGTCTCTGAAGGAGCCTCTCTGCA
GCTGCGCTGCAAGTATTCCTACTTTGGGACACCTTATCTGTTCTGGTATGTCCAGTACCCGC
GCCAGGGGCTGCAGCTGCTCCTCAAGTACTATCCAGGAGACCCAGTGGTTCAAGGAGTGAA
TGGCTTTGAGGCTGAGTTCAGCAAGAGTAACTCTTCCTTCCACCTGCGTAAAGCCTCTGTGC
ACTGGAGCGACTGGGCTGTATACTTCTGTGCTGTGAGCTCCAACACCAATACAGGCAAATT
AACCTTTGGGGATGGGACCGTGCTCACAGTGAAGCCAAACATCCAAAACCCGGATCCTGCC
GTGTACCAGCTGCGCGACAGCAAATCCAGTGACAAGTCTGTCTGCTTATTCACCGATTTTGA
TTCTCAAACAAATGTGTCACAAAGTAAGGATTCGGATGTGTATATCACAGACAAATGTGTGC
TGGACATGCGTTCTATGGACTTCAAGAGCAACAGTGCTGTGGCCTGGAGCAACAAAAGCGA
CTTTGCATGTGCAAACGCCTTCAACAACAGCATTATTCCAGAAGACACCTTCTTCCCGAGCCC
AGAGAGCTCGTAAGCTT
HindIII site
BamHI

Strongly codon optimized version:
NdeI site
CATATGCAGTCAGTGACGCAGCCCGATGCGCGCGTCACTGTCTCGGAAGGTGCCTCACTGC
AGCTGCGCTGCAAGTATAGTTACTTTGGCACCCCTTATCTGTTCTGGTATGTCCAGTACCCGC
GCCAGGGCCTGCAGCTGTTGCTGAAGTACTATCCGGGTGATCCGGTAGTTCAAGGAGTGAA
TGGCTTTGAAGCGGAATTCAGCAAGAGTAATTCGTCATTCCATCTGCGTAAAGCCTCGGTTC
ACTGGAGCGATTGGGCGGTATACTTCTGTGCGGTTAGCTCCAACACCAATACGGGCAAATT
AACCTTTGGCGATGGGACCGTGCTTACTGTTAAGCCAAATATCCAAAACCCGGATCCTGCCG
TGTACCAGCTGCGCGACAGCAAATCCAGTGACAAGTCTGTCTGCTTATTCACCGATTTTGAT
TCTCAAACAAATGTGTCACAAAGTAAGGATTCGGATGTGTATATCACAGACAAATGTGTGCT
GGACATGCGTTCTATGGACTTCAAGAGCAACAGTGCTGTGGCCTGGAGCAACAAAAGCGA
CTTTGCATGTGCAAACGCCTTCAACAACAGCATTATTCCAGAAGACACCTTCTTCCCGAGCCC
AGAGAGCTCGTAAGCTT
HindIII site
BamHI

### 7.1.5. βTCR PLP1

Protein sequence:
MDGGIITQTPKFLIGQEGQKLTLKCQQNFNHDTMYWYRQDSGKGLRLIYYSITENDLQKGDLSE
GYDASREKKSSFSLTVTSAQKNEMAVFLCASSIQGGNTEVFFGKGTRLTVVEDLKNVFPPEVAVF
EPSEAEISHTQKATLVCLATGFYPDHVELSWWVNGKEVHSGVCTDPQPLKEQPALNDSRYALSS
RLRVSATFWQNPRNHFRCQVQFYGLSENDEWTQDRAKPVTQIVSAEAWGRAD*

DNA sequence:
NdeI site
CATATGGATGGTGGCATCATTACTCAGACACCCAAATTCCTGATTGGTCAGGAAGGGCAAA
AACTGACCTTGAAATGTCAACAGAATTTCAATCATGATACAATGTACTGGTACCGCCAGGAT
TCAGGGAAAGGATTGCGTCTGATCTACTATTCAATTACTGAAAACGATCTTCAAAAAGGCG
ATCTGTCTGAAGGCTATGATGCGTCTCGTGAGAAGAAGTCATCTTTTTCTCTCACTGTGACA
TCTGCCCAGAAGAACGAGATGGCCGTTTTTCTCTGTGCCAGCAGTATTCAGGGAGGAAACA
CAGAAGTCTTCTTTGGTAAAGGAACCCGTCTCACAGTTGTAGAGGATTTAAAAAACGTGTTC
CCACCCGAGGTCGCTGTGTTTGAGCCATCAGAAGCAGAGATCTCCCACACCCAAAAGGCCA
CACTGGTATGCCTGGCCACAGGCTTCTACCCCGACCACGTGGAGCTGAGCTGGTGGGTGAA
TGGGAAGGAGGTGCACAGTGGGGTCTGCACAGACCCGCAGCCCCTCAAGGAGCAGCCCGC
CCTCAATGACTCCCGTTACGCCCTGAGCAGCCGCCTGCGTGTCTCGGCCACCTTCTGGCAGA
ACCCCCGCAACCACTTCCGCTGTCAAGTCCAGTTCTACGGGCTCTCGGAGAATGACGAGTG
GACCCAGGATCGCGCCAAACCTGTCACCCAGATCGTCAGCGCCGAGGCCTGGGGGCGCGC
AGACTAAGCTT
HindIIIsite

## 7.1.6. pET-30a (+) vector map (Novagen)

| pET-30a(+) sequence landmarks | |
|---|---|
| T7 promoter | 419-435 |
| T7 transcription start | 418 |
| His•Tag coding sequence | 327-344 |
| S•Tag coding sequence | 249-293 |
| Multiple cloning sites | |
| (*Nco* I - *Xho* I) | 158-217 |
| His•Tag coding sequence | 140-157 |
| T7 terminator | 26-72 |
| *lacI* coding sequence | 826-1905 |
| pBR322 origin | 3339 |
| Kan coding sequence | 4048-4860 |
| f1 origin | 4956-5411 |

The maps for pET-30b(+) and pET-30c(+) are the same as pET-30a(+) (shown) with the following exceptions: pET-30b(+) is a 5421bp plasmid; subtract 1bp from each site beyond *Bam* H I at 198. pET-30c(+) is a 5423bp plasmid; add 1bp to each site beyond *Bam* H I at 198.

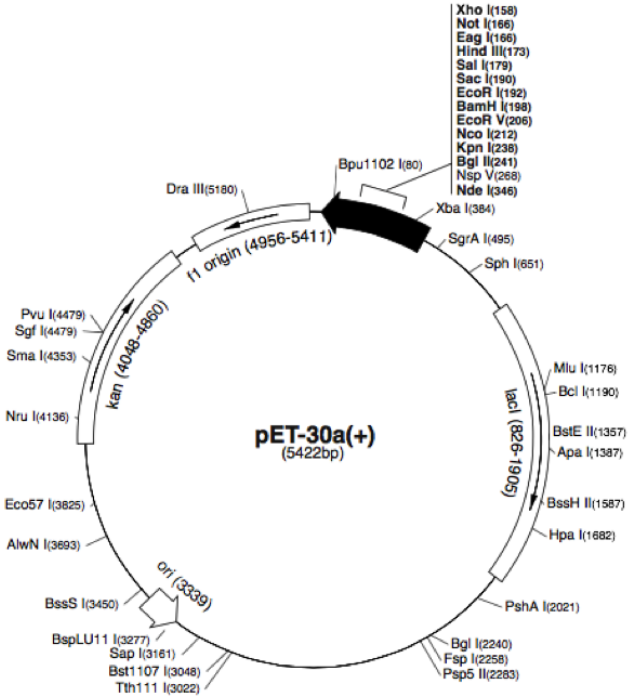


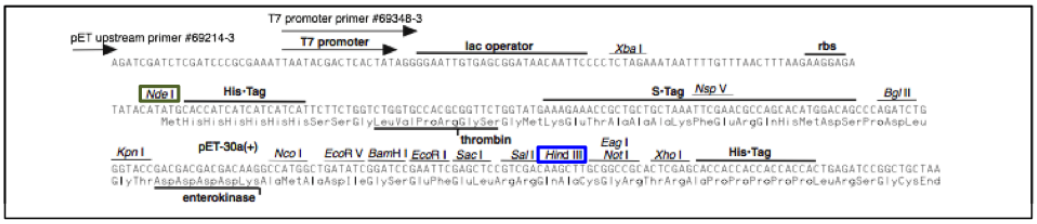

## 7.2. Peptide sequences of myelin proteolipid protein (PLP)

PLP:
MGLLECCARC L**VGAPFASLV** ATGLCFFGVA LFCGCGHEAL TGTEKLIETY FSKNYQDYEY LINVIHAFQY VIYGTASFFF LYGALLLAEG FYTTGAVRQI FGDYKTTICG KGLSATVTGG QKGRGSRGQH QAHSLERVCH CLGKWLGHPD KFVGITYALT VVWLLVFACS AVPVYIYFNT WTTCQSIAFP SKTSASIGSL CADARMYGVL PWNAFPGKVC GSNLLSICKT AEFQMTFHLF IAAFVGAAAT LVSLLTFMIA ATYNFAVLKL MGRGTKF

$PLP_{1-24}$:
GLLECCARCL **VGAPFASLVA** TGLC
Molar mass: 2368 g/mol

$PLP_{9-20}$:
CL**VGAPFASL V**A
Molar mass: 1147 g/mol

$PLP_{FRET}$:
AL**VGAPFASL V**AGGSC
Molar mass: 1420 g/mol

## 7.3. Protein sequences of FRET-IA$^b$ constructs

### 7.3.1. α chains:

**begin crystal structure**
**end crystal structure**
linker
acidic leucine zipper
BirA singal sequence

#### 7.3.1.1. IA$^b$ α (original sequence)

MLSLCGGEDD**IEADH**VGTYGISVYQSPGDIGQYTFEFDGDELFYVDLDKKETVWMLPEFGQLA
SFDPQGGLQNIAVVKHNLGVLTKRSNSTPATNEAPQATVFPKSPVLLGQPNTLICFVDNIFPPVI
NITWLRNSKSVADGVYETSFFVNRDYSFHKLSYLTFIPSDDDIYDCKVEHWGLEEPV**LKHW**EPEI
PAPMSELTETGGGGSTTAPSAQLEKELQALEKENAQLEWELQALEKELAQGGSGGSGLNDIFEA
QKIEWHE*

#### 7.3.1.2. I-A$^b$ α G28C

MLSLCGGEDD**IEADH**VGTYGISVYQSP**C**DIGQYTFEFDGDELFYVDLDKKETVWMLPEFGQLAS
FDPQGGLQNIAVVKHNLGVLTKRSNSTPATNEAPQATVFPKSPVLLGQPNTLICFVDNIFPPVINI
TWLRNSKSVADGVYETSFFVNRDYSFHKLSYLTFIPSDDDIYDCKVEHWGLEEPV**LKHW**EPEIPA
PMSELTETGGGGSTTAPSAQLEKELQALEKENAQLEWELQALEKELAQGGSGGSGLNDIFEAQ
KIEWHE*

#### 7.3.1.3. I-A$^b$ α S90C

MLSLCGGEDD**IEADH**VGTYGISVYQSPGDIGQYTFEFDGDELFYVDLDKKETVWMLPEFGQLA
SFDPQGGLQNIAVVKHNLGVLTKRSN**C**TPATNEAPQATVFPKSPVLLGQPNTLICFVDNIFPPVI
NITWLRNSKSVADGVYETSFFVNRDYSFHKLSYLTFIPSDDDIYDCKVEHWGLEEPV**LKHW**EPEI
PAPMSELTETGGGGSTTAPSAQLEKELQALEKENAQLEWELQALEKELAQGGSGGSGLNDIFEA
QKIEWHE*

### 7.3.2. β chains:

$PLP_{11-19}$ (C-2 to A)
linker
**begin crystal structure**
**end crystal structure**
linker
basic leucine zipper
$His_6$ – tag

#### 7.3.2.1. I-$A^b$ β PLP1

MALQIPSLLLSAAVVVLMVLSSPGTEGCLVGAPFASLVAGGGGTS*GGGSGG*SER**HFVYQFMG**E
CYFTNGTQRIRYVTRYIYNREEYVRYDSDVGEHRAVTELGRPDAEYWNSQPEILERTRAELDTVC
RHNYEGPETHTSLRRLEQPNVVISLSRTEALNHHNTLVCSVTDFYPAKIKVRWFRNGQEETVGV
SSTQLIRNGDWTFQVLVMLEMTPRRGEVYTCHVEHPSLKSPIT**VEWRA**QSESAWSKGGGGST
TAPSAQLKKKLQALKKKNAQLKWKLQALKKKLAQHHHHHH*

#### 7.3.2.2. I-$A^b$ β PLP1 C-2A

MALQIPSLLLSAAVVVLMVLSSPGTEGALVGAPFASLVAGGGGTS*GGGSGG*SER**HFVYQFMG**E
CYFTNGTQRIRYVTRYIYNREEYVRYDSDVGEHRAVTELGRPDAEYWNSQPEILERTRAELDTVC
RHNYEGPETHTSLRRLEQPNVVISLSRTEALNHHNTLVCSVTDFYPAKIKVRWFRNGQEETVGV
SSTQLIRNGDWTFQVLVMLEMTPRRGEVYTCHVEHPSLKSPIT**VEWRA**QSESAWSKGGGGST
TAPSAQLKKKLQALKKKNAQLKWKLQALKKKLAQHHHHHH*

#### 7.3.2.3. I-$A^b$ β PLP1 C-2A linker G23C

MALQIPSLLLSAAVVVLMVLSSPGTEGALVGAPFASLVAGGGGTS*GGGSGC*SER**HFVYQFMG**E
CYFTNGTQRIRYVTRYIYNREEYVRYDSDVGEHRAVTELGRPDAEYWNSQPEILERTRAELDTVC
RHNYEGPETHTSLRRLEQPNVVISLSRTEALNHHNTLVCSVTDFYPAKIKVRWFRNGQEETVGV
SSTQLIRNGDWTFQVLVMLEMTPRRGEVYTCHVEHPSLKSPIT**VEWRA**QSESAWSKGGGGST
TAPSAQLKKKLQALKKKNAQLKWKLQALKKKLAQHHHHHH*

# 8. References


Adams, E. J., & Luoma, A. M. (2013). The adaptable major histocompatibility complex (MHC) fold: structure and function of nonclassical and MHC class I-like molecules. *Annu Rev Immunol*, *31*, 529-561. https://doi.org/10.1146/annurev-immunol-032712-095912

Al-Lazikani, B., Lesk, A. M., & Chothia, C. (2000). Canonical structures for the hypervariable regions of T cell alphabeta receptors. *J Mol Biol*, *295*(4), 979-995. https://doi.org/10.1006/jmbi.1999.3358

al-Ramadi, B. K., Jelonek, M. T., Boyd, L. F., Margulies, D. H., & Bothwell, A. L. (1995). Lack of strict correlation of functional sensitization with the apparent affinity of MHC/peptide complexes for the TCR. *J Immunol*, *155*(2), 662-673.

Altman, J. D., Moss, P. A., Goulder, P. J., Barouch, D. H., McHeyzer-Williams, M. G., Bell, J. I., McMichael, A. J., & Davis, M. M. (1996). Phenotypic analysis of antigen-specific T lymphocytes. *Science*, *274*(5284), 94-96. https://doi.org/10.1126/science.274.5284.94

Anderson, M. S., & Su, M. A. (2016). AIRE expands: new roles in immune tolerance and beyond. *Nat Rev Immunol*, *16*(4), 247-258. https://doi.org/10.1038/nri.2016.9

Anderson, M. S., Venanzi, E. S., Klein, L., Chen, Z., Berzins, S. P., Turley, S. J., von Boehmer, H., Bronson, R., Dierich, A., Benoist, C., & Mathis, D. (2002). Projection of an immunological self shadow within the thymus by the aire protein. *Science*, *298*(5597), 1395-1401. https://doi.org/10.1126/science.1075958

Aoki, K., Kamioka, Y., & Matsuda, M. (2013). Fluorescence resonance energy transfer imaging of cell signaling from in vitro to in vivo: basis of biosensor construction, live imaging, and image processing. *Dev Growth Differ*, *55*(4), 515-522. https://doi.org/10.1111/dgd.12039

Arstila, T. P., Casrouge, A., Baron, V., Even, J., Kanellopoulos, J., & Kourilsky, P. (1999). A direct estimate of the human alphabeta T cell receptor diversity. *Science*, *286*(5441), 958-961.

Aschenbrenner, K., D'Cruz, L. M., Vollmann, E. H., Hinterberger, M., Emmerich, J., Swee, L. K., Rolink, A., & Klein, L. (2007). Selection of Foxp3+ regulatory T cells specific for self antigen expressed and presented by Aire+ medullary thymic epithelial cells. *Nat Immunol*, *8*(4), 351-358. https://doi.org/10.1038/ni1444

Axmann, M., Schutz, G. J., & Huppa, J. B. (2015a). Measuring TCR-pMHC Binding In Situ using a FRET-based Microscopy Assay. *J Vis Exp*(105), e53157. https://doi.org/10.3791/53157

Axmann, M., Schutz, G. J., & Huppa, J. B. (2015b). Single Molecule Fluorescence Microscopy on Planar Supported Bilayers. *J Vis Exp*(105), e53158. https://doi.org/10.3791/53158

Bacchetta, R., Barzaghi, F., & Roncarolo, M. G. (2018). From IPEX syndrome to FOXP3 mutation: a lesson on immune dysregulation. *Ann N Y Acad Sci*, *1417*(1), 5-22. https://doi.org/10.1111/nyas.13011

Baker, B. M., Gagnon, S. J., Biddison, W. E., & Wiley, D. C. (2000). Conversion of a T cell antagonist into an agonist by repairing a defect in the TCR/peptide/MHC interface: implications for TCR signaling. *Immunity*, *13*(4), 475-484. https://doi.org/10.1016/s1074-7613(00)00047-9

Bassing, C. H., Swat, W., & Alt, F. W. (2002). The mechanism and regulation of chromosomal V(D)J recombination. *Cell*, *109 Suppl*, S45-55.

Bautista, J. L., Lio, C. W., Lathrop, S. K., Forbush, K., Liang, Y., Luo, J., Rudensky, A. Y., & Hsieh, C. S. (2009). Intraclonal competition limits the fate determination of regulatory T cells in the thymus. *Nat Immunol*, *10*(6), 610-617. https://doi.org/10.1038/ni.1739

Beckett, D., Kovaleva, E., & Schatz, P. J. (1999). A minimal peptide substrate in biotin holoenzyme synthetase-catalyzed biotinylation. *Protein Sci*, *8*(4), 921-929. https://doi.org/10.1110/ps.8.4.921

Bhandoola, A., von Boehmer, H., Petrie, H. T., & Zuniga-Pflucker, J. C. (2007). Commitment and developmental potential of extrathymic and intrathymic T cell precursors: plenty to choose from. *Immunity*, *26*(6), 678-689. https://doi.org/10.1016/j.immuni.2007.05.009

Bjorkman, P. J., Saper, M. A., Samraoui, B., Bennett, W. S., Strominger, J. L., & Wiley, D. C. (1987). Structure of the human class I histocompatibility antigen, HLA-A2. *Nature*, *329*(6139), 506-512. https://doi.org/10.1038/329506a0

Bromley, S. K., Burack, W. R., Johnson, K. G., Somersalo, K., Sims, T. N., Sumen, C., Davis, M. M., Shaw, A. S., Allen, P. M., & Dustin, M. L. (2001). The immunological synapse. *Annu Rev Immunol*, *19*, 375-396. https://doi.org/10.1146/annurev.immunol.19.1.375

Brown, J. H., Jardetzky, T. S., Gorga, J. C., Stern, L. J., Urban, R. G., Strominger, J. L., & Wiley, D. C. (1993). Three-dimensional structure of the human class II histocompatibility antigen HLA-DR1. *Nature*, *364*(6432), 33-39. https://doi.org/10.1038/364033a0

Brunkow, M. E., Jeffery, E. W., Hjerrild, K. A., Paeper, B., Clark, L. B., Yasayko, S. A., Wilkinson, J. E., Galas, D., Ziegler, S. F., & Ramsdell, F. (2001). Disruption of a new forkhead/winged-helix protein, scurfin, results in the fatal lymphoproliferative disorder of the scurfy mouse. *Nat Genet*, *27*(1), 68-73. https://doi.org/10.1038/83784

Chicz, R. M., Urban, R. G., Lane, W. S., Gorga, J. C., Stern, L. J., Vignali, D. A., & Strominger, J. L. (1992). Predominant naturally processed peptides bound to HLA-DR1 are derived from MHC-related molecules and are heterogeneous in size. *Nature*, *358*(6389), 764-768. https://doi.org/10.1038/358764a0

Clements, C. S., Kjer-Nielsen, L., MacDonald, W. A., Brooks, A. G., Purcell, A. W., McCluskey, J., & Rossjohn, J. (2002). The production, purification and crystallization of a soluble heterodimeric form of a highly selected T-cell receptor in its unliganded and liganded state. *Acta Crystallogr D Biol Crystallogr*, *58*(Pt 12), 2131-2134. http://scripts.iucr.org/cgi-bin/paper?S0907444902015482 http://journals.iucr.org/d/issues/2002/12/00/cy0066/cy0066.pdf

Cloosen, S., Arnold, J., Thio, M., Bos, G. M., Kyewski, B., & Germeraad, W. T. (2007). Expression of tumor-associated differentiation antigens, MUC1 glycoforms and CEA, in human thymic epithelial cells: implications for self-tolerance and tumor therapy. *Cancer Res*, *67*(8), 3919-3926. https://doi.org/10.1158/0008-5472.Can-06-2112

Cormack, B. (2001). Directed mutagenesis using the polymerase chain reaction. *Curr Protoc Mol Biol*, *Chapter 8*, Unit8.5. https://doi.org/10.1002/0471142727.mb0805s37

Davis, M. M., & Bjorkman, P. J. (1988). T-cell antigen receptor genes and T-cell recognition. *Nature*, *334*(6181), 395-402. https://doi.org/10.1038/334395a0

Davis, M. M., Boniface, J. J., Reich, Z., Lyons, D., Hampl, J., Arden, B., & Chien, Y. (1998). Ligand recognition by alpha beta T cell receptors. *Annu Rev Immunol*, *16*, 523-544. https://doi.org/10.1146/annurev.immunol.16.1.523

Derbinski, J., Pinto, S., Rösch, S., Hexel, K., & Kyewski, B. (2008). Promiscuous gene expression patterns in single medullary thymic epithelial cells argue for a stochastic mechanism. *Proc Natl Acad Sci U S A*, *105*(2), 657-662. https://doi.org/10.1073/pnas.0707486105

Derbinski, J., Schulte, A., Kyewski, B., & Klein, L. (2001). Promiscuous gene expression in medullary thymic epithelial cells mirrors the peripheral self. *Nat Immunol*, *2*(11), 1032-1039. https://doi.org/10.1038/ni723

Donskoy, E., & Goldschneider, I. (1992). Thymocytopoiesis is maintained by blood-borne precursors throughout postnatal life. A study in parabiotic mice. *J Immunol*, *148*(6), 1604-1612.

Dumon-Seignovert, L., Cariot, G., & Vuillard, L. (2004). The toxicity of recombinant proteins in Escherichia coli: a comparison of overexpression in BL21(DE3), C41(DE3), and C43(DE3). *Protein Expr Purif*, *37*(1), 203-206. https://doi.org/10.1016/j.pep.2004.04.025

Dustin, M. L. (2014). The immunological synapse. *Cancer Immunol Res*, *2*(11), 1023-1033. https://doi.org/10.1158/2326-6066.Cir-14-0161

Edwards, L. J., Zarnitsyna, V. I., Hood, J. D., Evavold, B. D., & Zhu, C. (2012). Insights into T cell recognition of antigen: significance of two-dimensional kinetic parameters. *Front Immunol*, *3*, 86. https://doi.org/10.3389/fimmu.2012.00086

Famili, F., Wiekmeijer, A. S., & Staal, F. J. (2017). The development of T cells from stem cells in mice and humans. *Future Sci OA*, *3*(3), Fso186. https://doi.org/10.4155/fsoa-2016-0095

Feuerer, M., Jiang, W., Holler, P. D., Satpathy, A., Campbell, C., Bogue, M., Mathis, D., & Benoist, C. (2007). Enhanced thymic selection of FoxP3+ regulatory T cells in the NOD mouse model of autoimmune diabetes. *Proc Natl Acad Sci U S A*, *104*(46), 18181-18186. https://doi.org/10.1073/pnas.0708899104

Fomin, A. B., Pastorino, A. C., Kim, C. A., Pereira, C. A., Carneiro-Sampaio, M., & Abe-Jacob, C. M. (2010). DiGeorge Syndrome: a not so rare disease. *Clinics (Sao Paulo)*, *65*(9), 865-869. https://doi.org/10.1590/s1807-59322010000900009

Fritz, R. D., Letzelter, M., Reimann, A., Martin, K., Fusco, L., Ritsma, L., Ponsioen, B., Fluri, E., Schulte-Merker, S., van Rheenen, J., & Pertz, O. (2013). A versatile toolkit to produce sensitive FRET biosensors to visualize signaling in time and space. *Sci Signal*, *6*(285), rs12. https://doi.org/10.1126/scisignal.2004135

Garboczi, D. N., Ghosh, P., Utz, U., Fan, Q. R., Biddison, W. E., & Wiley, D. C. (1996). Structure of the complex between human T-cell receptor, viral peptide and HLA-A2. *Nature*, *384*(6605), 134-141. https://doi.org/10.1038/384134a0

Garcia, K. C., Degano, M., Stanfield, R. L., Brunmark, A., Jackson, M. R., Peterson, P. A., Teyton, L., & Wilson, I. A. (1996). An alphass T cell receptor structure at 2.5 A and its orientation in the TCR-MHC complex. *Science*, *274*(11), 209-219.

Garcia, K. C., Radu, C. G., Ho, J., Ober, R. J., & Ward, E. S. (2001). Kinetics and thermodynamics of T cell receptor- autoantigen interactions in murine experimental autoimmune encephalomyelitis. *Proc Natl Acad Sci U S A*, *98*(12), 6818-6823. https://doi.org/10.1073/pnas.111161198

Germain, R. N. (1994). MHC-dependent antigen processing and peptide presentation: providing ligands for T lymphocyte activation. *Cell*, *76*(2), 287-299. https://doi.org/10.1016/0092-8674(94)90336-0

Germain, R. N. (2002). T-cell development and the CD4-CD8 lineage decision. *Nat Rev Immunol*, *2*(5), 309-322. https://doi.org/10.1038/nri798

Greer, J. M., & Lees, M. B. (2002). Myelin proteolipid protein--the first 50 years. *Int J Biochem Cell Biol*, *34*(3), 211-215. https://doi.org/10.1016/s1357-2725(01)00136-4

Hassler, T., Urmann, E., Teschner, S., Federle, C., Dileepan, T., Schober, K., Jenkins, M. K., Busch, D. H., Hinterberger, M., & Klein, L. (2019). Inventories of naive and tolerant mouse CD4 T cell repertoires reveal a hierarchy of deleted and diverted T cell receptors. *Proc Natl Acad Sci U S A*, *116*(37), 18537-18543. https://doi.org/10.1073/pnas.1907615116

Hinterberger, M., Aichinger, M., Prazeres da Costa, O., Voehringer, D., Hoffmann, R., & Klein, L. (2010). Autonomous role of medullary thymic epithelial cells in central CD4(+) T cell tolerance. *Nat Immunol*, *11*(6), 512-519. https://doi.org/10.1038/ni.1874

Holmberg, K., Mariathasan, S., Ohteki, T., Ohashi, P. S., & Gascoigne, N. R. (2003). TCR binding kinetics measured with MHC class I tetramers reveal a positive selecting peptide with relatively high affinity for TCR. *J Immunol*, *171*(5), 2427-2434. https://doi.org/10.4049/jimmunol.171.5.2427

Hong, J., Persaud, S. P., Horvath, S., Allen, P. M., Evavold, B. D., & Zhu, C. (2015). Force-Regulated In Situ TCR-Peptide-Bound MHC Class II Kinetics Determine Functions of CD4+ T Cells. *J Immunol*, *195*(8), 3557-3564. https://doi.org/10.4049/jimmunol.1501407

Hooijberg, E., Bakker, A. Q., Ruizendaal, J. J., & Spits, H. (2000). NFAT-controlled expression of GFP permits visualization and isolation of antigen-stimulated primary human T cells. *Blood*, *96*(2), 459-466. http://www.bloodjournal.org/content/bloodjournal/96/2/459.full.pdf

Hori, S., Nomura, T., & Sakaguchi, S. (2003). Control of regulatory T cell development by the transcription factor Foxp3. *Science*, *299*(5609), 1057-1061. https://doi.org/10.1126/science.1079490

Hsieh, C. S., Lee, H. M., & Lio, C. W. (2012). Selection of regulatory T cells in the thymus. *Nat Rev Immunol*, *12*(3), 157-167. https://doi.org/10.1038/nri3155

Hunt, D. F., Henderson, R. A., Shabanowitz, J., Sakaguchi, K., Michel, H., Sevilir, N., Cox, A. L., Appella, E., & Engelhard, V. H. (1992). Characterization of peptides bound to the class I MHC molecule HLA-A2.1 by mass spectrometry. *Science*, *255*(5049), 1261-1263. https://doi.org/10.1126/science.1546328

Huppa, J. B., Axmann, M., Mortelmaier, M. A., Lillemeier, B. F., Newell, E. W., Brameshuber, M., Klein, L. O., Schutz, G. J., & Davis, M. M. (2010). TCR-peptide-MHC interactions in situ show accelerated kinetics and increased affinity. *Nature*, *463*(7283), 963-967. https://doi.org/10.1038/nature08746

Jordan, M. S., Boesteanu, A., Reed, A. J., Petrone, A. L., Holenbeck, A. E., Lerman, M. A., Naji, A., & Caton, A. J. (2001). Thymic selection of CD4+CD25+ regulatory T cells induced by an agonist self-peptide. *Nat Immunol*, *2*(4), 301-306. https://doi.org/10.1038/86302

Josefowicz, S. Z., Lu, L. F., & Rudensky, A. Y. (2012). Regulatory T cells: mechanisms of differentiation and function. *Annu Rev Immunol*, *30*, 531-564. https://doi.org/10.1146/annurev.immunol.25.022106.141623

Kappler, J., White, J., Kozono, H., Clements, J., & Marrack, P. (1994). Binding of a soluble alpha beta T-cell receptor to superantigen/major histocompatibility complex ligands. *Proc Natl Acad Sci U S A*, *91*(18), 8462-8466.

Kappler, J. W., Roehm, N., & Marrack, P. (1987). T cell tolerance by clonal elimination in the thymus. *Cell*, *49*(2), 273-280. https://doi.org/10.1016/0092-8674(87)90568-x

Kersh, G. J., Kersh, E. N., Fremont, D. H., & Allen, P. M. (1998). High- and low-potency ligands with similar affinities for the TCR: the importance of kinetics in TCR signaling. *Immunity*, *9*(6), 817-826. https://doi.org/10.1016/s1074-7613(00)80647-0

Kisielow, P., Blüthmann, H., Staerz, U. D., Steinmetz, M., & von Boehmer, H. (1988). Tolerance in T-cell-receptor transgenic mice involves deletion of nonmature CD4+8+ thymocytes. *Nature*, *333*(6175), 742-746. https://doi.org/10.1038/333742a0

Kjer-Nielsen, L., Clements, C. S., Brooks, A. G., Purcell, A. W., McCluskey, J., & Rossjohn, J. (2002). The 1.5 A crystal structure of a highly selected antiviral T cell receptor provides evidence for a structural basis of immunodominance. *Structure*, *10*(11), 1521-1532.

Klein, L., & Jovanovic, K. (2011). Regulatory T cell lineage commitment in the thymus. *Semin Immunol*, *23*(6), 401-409. https://doi.org/10.1016/j.smim.2011.06.003

Klein, L., Klein, T., Rüther, U., & Kyewski, B. (1998). CD4 T cell tolerance to human C-reactive protein, an inducible serum protein, is mediated by medullary thymic epithelium. *J Exp Med*, *188*(1), 5-16. https://doi.org/10.1084/jem.188.1.5

Klein, L., Klugmann, M., Nave, K. A., Tuohy, V. K., & Kyewski, B. (2000). Shaping of the autoreactive T-cell repertoire by a splice variant of self protein expressed in thymic epithelial cells. *Nat Med*, *6*(1), 56-61. https://doi.org/10.1038/71540

Klein, L., Kyewski, B., Allen, P. M., & Hogquist, K. A. (2014). Positive and negative selection of the T cell repertoire: what thymocytes see (and don't see). *Nat Rev Immunol*, *14*(6), 377-391. https://doi.org/10.1038/nri3667

Klein, L., Robey, E. A., & Hsieh, C. S. (2019). Central CD4(+) T cell tolerance: deletion versus regulatory T cell differentiation. *Nat Rev Immunol*, *19*(1), 7-18. https://doi.org/10.1038/s41577-018-0083-6

Koch, U., & Radtke, F. (2011). Mechanisms of T cell development and transformation. *Annu Rev Cell Dev Biol*, *27*, 539-562. https://doi.org/10.1146/annurev-cellbio-092910-154008

Kolawole, E. M., Lamb, T. J., & Evavold, B. D. (2020). Relationship of 2D Affinity to T Cell Functional Outcomes. *Int J Mol Sci*, *21*(21). https://doi.org/10.3390/ijms21217969

Krangel, M. S. (2009). Mechanics of T cell receptor gene rearrangement. *Curr Opin Immunol*, *21*(2), 133-139. https://doi.org/10.1016/j.coi.2009.03.009

Krueger, A., Zietara, N., & Lyszkiewicz, M. (2017). T Cell Development by the Numbers. *Trends Immunol*, *38*(2), 128-139. https://doi.org/10.1016/j.it.2016.10.007

Lee, H. M., Bautista, J. L., Scott-Browne, J., Mohan, J. F., & Hsieh, C. S. (2012). A broad range of self-reactivity drives thymic regulatory T cell selection to limit responses to self. *Immunity*, *37*(3), 475-486. https://doi.org/10.1016/j.immuni.2012.07.009

Leung, M. W., Shen, S., & Lafaille, J. J. (2009). TCR-dependent differentiation of thymic Foxp3+ cells is limited to small clonal sizes. *J Exp Med*, *206*(10), 2121-2130. https://doi.org/10.1084/jem.20091033

Lind, E. F., Prockop, S. E., Porritt, H. E., & Petrie, H. T. (2001). Mapping precursor movement through the postnatal thymus reveals specific microenvironments supporting defined stages of early lymphoid development. *J Exp Med*, *194*(2), 127-134. https://doi.org/10.1084/jem.194.2.127

Lio, C. W., & Hsieh, C. S. (2008). A two-step process for thymic regulatory T cell development. *Immunity*, *28*(1), 100-111. https://doi.org/10.1016/j.immuni.2007.11.021

Liu, B., Chen, W., Evavold, B. D., & Zhu, C. (2014). Accumulation of dynamic catch bonds between TCR and agonist peptide-MHC triggers T cell signaling. *Cell*, *157*(2), 357-368. https://doi.org/10.1016/j.cell.2014.02.053

Macian, F. (2005). NFAT proteins: key regulators of T-cell development and function. *Nat Rev Immunol*, *5*(6), 472-484. https://doi.org/10.1038/nri1632

Marrack, P., Hannum, C., Harris, M., Haskins, K., Kubo, R., Pigeon, M., Shimonkevitz, R., White, J., & Kappler, J. (1983). Antigen-specific, major histocompatibility complex-restricted T cell receptors. *Immunol Rev*, *76*, 131-145.

McKeithan, T. W. (1995). Kinetic proofreading in T-cell receptor signal transduction. *Proc Natl Acad Sci U S A*, *92*(11), 5042-5046.

Miroux, B., & Walker, J. E. (1996). Over-production of proteins in Escherichia coli: mutant hosts that allow synthesis of some membrane proteins and globular proteins at high levels. *J Mol Biol*, *260*(3), 289-298. https://doi.org/10.1006/jmbi.1996.0399

Miyawaki, A. (2011). Development of probes for cellular functions using fluorescent proteins and fluorescence resonance energy transfer. *Annu Rev Biochem*, *80*, 357-373. https://doi.org/10.1146/annurev-biochem-072909-094736

Modigliani, Y., Thomas-Vaslin, V., Bandeira, A., Coltey, M., Le Douarin, N. M., Coutinho, A., & Salaün, J. (1995). Lymphocytes selected in allogeneic thymic epithelium mediate dominant tolerance toward tissue grafts of the thymic epithelium haplotype. *Proc Natl Acad Sci U S A*, *92*(16), 7555-7559. https://doi.org/10.1073/pnas.92.16.7555

Mombaerts, P., Iacomini, J., Johnson, R. S., Herrup, K., Tonegawa, S., & Papaioannou, V. E. (1992). RAG-1-deficient mice have no mature B and T lymphocytes. *Cell*, *68*(5), 869-877.

Moon, J. J., Chu, H. H., Pepper, M., McSorley, S. J., Jameson, S. C., Kedl, R. M., & Jenkins, M. K. (2007). Naive CD4(+) T cell frequency varies for different epitopes and predicts repertoire diversity and response magnitude. *Immunity*, *27*(2), 203-213. https://doi.org/10.1016/j.immuni.2007.07.007

Murphy, K. M., & Weaver, C. (2017). *Janeway's Immunobiology* (9th ed.).

Naeher, D., Daniels, M. A., Hausmann, B., Guillaume, P., Luescher, I., & Palmer, E. (2007). A constant affinity threshold for T cell tolerance. *J Exp Med*, *204*(11), 2553-2559. https://doi.org/10.1084/jem.20070254

Neefjes, J., Jongsma, M. L., Paul, P., & Bakke, O. (2011). Towards a systems understanding of MHC class I and MHC class II antigen presentation. *Nat Rev Immunol*, *11*(12), 823-836. https://doi.org/10.1038/nri3084

Newell, E. W., Ely, L. K., Kruse, A. C., Reay, P. A., Rodriguez, S. N., Lin, A. E., Kuhns, M. S., Garcia, K. C., & Davis, M. M. (2011). Structural basis of specificity and cross-reactivity in T cell receptors specific for cytochrome c-I-E(k). *J Immunol*, *186*(10), 5823-5832. https://doi.org/10.4049/jimmunol.1100197

Org, T., Chignola, F., Hetényi, C., Gaetani, M., Rebane, A., Liiv, I., Maran, U., Mollica, L., Bottomley, M. J., Musco, G., & Peterson, P. (2008). The autoimmune regulator PHD finger binds to non-methylated histone H3K4 to activate gene expression. *EMBO Rep*, *9*(4), 370-376. https://doi.org/10.1038/sj.embor.2008.11

Oukka, M., Colucci-Guyon, E., Tran, P. L., Cohen-Tannoudji, M., Babinet, C., Lotteau, V., & Kosmatopoulos, K. (1996). CD4 T cell tolerance to nuclear proteins induced by medullary thymic epithelium. *Immunity*, *4*(6), 545-553. https://doi.org/10.1016/s1074-7613(00)80481-1

Pecorari, F., Tissot, A. C., & Plückthun, A. (1999). Folding, heterodimeric association and specific peptide recognition of a murine alphabeta T-cell receptor expressed in Escherichia coli. *J Mol Biol*, *285*(4), 1831-1843. https://doi.org/10.1006/jmbi.1998.2422

Petersen, T. N., Brunak, S., von Heijne, G., & Nielsen, H. (2011). SignalP 4.0: discriminating signal peptides from transmembrane regions. *Nat Methods*, *8*(10), 785-786. https://doi.org/10.1038/nmeth.1701

Porritt, H. E., Gordon, K., & Petrie, H. T. (2003). Kinetics of steady-state differentiation and mapping of intrathymic-signaling environments by stem cell transplantation in nonirradiated mice. *J Exp Med*, *198*(6), 957-962. https://doi.org/10.1084/jem.20030837

Porritt, H. E., Rumfelt, L. L., Tabrizifard, S., Schmitt, T. M., Zúñiga-Pflücker, J. C., & Petrie, H. T. (2004). Heterogeneity among DN1 prothymocytes reveals multiple progenitors with different capacities to generate T cell and non-T cell lineages. *Immunity*, *20*(6), 735-745. https://doi.org/10.1016/j.immuni.2004.05.004

Rosenbluth, J., Nave, K. A., Mierzwa, A., & Schiff, R. (2006). Subtle myelin defects in PLP-null mice. *Glia*, *54*(3), 172-182. https://doi.org/10.1002/glia.20370

Rossjohn, J., Gras, S., Miles, J. J., Turner, S. J., Godfrey, D. I., & McCluskey, J. (2015). T cell antigen receptor recognition of antigen-presenting molecules. *Annu Rev Immunol*, *33*, 169-200. https://doi.org/10.1146/annurev-immunol-032414-112334

Rudensky, Y., Preston-Hurlburt, P., Hong, S. C., Barlow, A., & Janeway, C. A., Jr. (1991). Sequence analysis of peptides bound to MHC class II molecules. *Nature*, *353*(6345), 622-627. https://doi.org/10.1038/353622a0

Saida, F. (2007). Overview on the expression of toxic gene products in Escherichia coli. *Curr Protoc Protein Sci*, *Chapter 5*, Unit 5.19. https://doi.org/10.1002/0471140864.ps0519s50

Sakaguchi, S., Sakaguchi, N., Asano, M., Itoh, M., & Toda, M. (1995). Immunologic self-tolerance maintained by activated T cells expressing IL-2 receptor alpha-chains (CD25). Breakdown of a single mechanism of self-tolerance causes various autoimmune diseases. *J Immunol*, *155*(3), 1151-1164.

Savage, P. A., Boniface, J. J., & Davis, M. M. (1999). A kinetic basis for T cell receptor repertoire selection during an immune response. *Immunity*, *10*(4), 485-492. https://doi.org/10.1016/s1074-7613(00)80048-5

Singer, A., Adoro, S., & Park, J. H. (2008). Lineage fate and intense debate: myths, models and mechanisms of CD4- versus CD8-lineage choice. *Nat Rev Immunol*, *8*(10), 788-801. https://doi.org/10.1038/nri2416

Sobel, R. A., van der Veen, R. C., & Lees, M. B. (1986). The immunopathology of chronic experimental allergic encephalomyelitis induced in rabbits with bovine proteolipid protein. *J Immunol*, *136*(1), 157-163.

Spangrude, G. J., Heimfeld, S., & Weissman, I. L. (1988). Purification and characterization of mouse hematopoietic stem cells. *Science*, *241*(4861), 58-62. https://doi.org/10.1126/science.2898810

Sprent, J., Lo, D., Gao, E. K., & Ron, Y. (1988). T cell selection in the thymus. *Immunol Rev*, *101*, 173-190. https://doi.org/10.1111/j.1600-065x.1988.tb00737.x

Starr, T. K., Jameson, S. C., & Hogquist, K. A. (2003). Positive and negative selection of T cells. *Annu Rev Immunol*, *21*, 139-176. https://doi.org/10.1146/annurev.immunol.21.120601.141107

Steele, C. R., Van Remoortere, K. C., & Hayday, A. C. (2003). Production of a soluble gammadelta T-cell receptor to identify ligands for the murine intestinal intraepithelial gammadelta T cell population. *J Chromatogr B Analyt Technol Biomed Life Sci*, *786*(1-2), 297-304.

Stepanek, O., Prabhakar, A. S., Osswald, C., King, C. G., Bulek, A., Naeher, D., Beaufils-Hugot, M., Abanto, M. L., Galati, V., Hausmann, B., Lang, R., Cole, D. K., Huseby, E. S., Sewell, A. K., Chakraborty, A. K., & Palmer, E. (2014). Coreceptor scanning by the T cell receptor provides a mechanism for T cell tolerance. *Cell*, *159*(2), 333-345. https://doi.org/10.1016/j.cell.2014.08.042

Stone, J. D., Chervin, A. S., & Kranz, D. M. (2009). T-cell receptor binding affinities and kinetics: impact on T-cell activity and specificity. *Immunology*, *126*(2), 165-176. https://doi.org/10.1111/j.1365-2567.2008.03015.x

Stone, J. D., Cochran, J. R., & Stern, L. J. (2001). T-cell activation by soluble MHC oligomers can be described by a two-parameter binding model. *Biophys J*, *81*(5), 2547-2557. https://doi.org/10.1016/s0006-3495(01)75899-7

Studier, F. W., & Moffatt, B. A. (1986). Use of bacteriophage T7 RNA polymerase to direct selective high-level expression of cloned genes. *J Mol Biol*, *189*(1), 113-130. https://doi.org/10.1016/0022-2836(86)90385-2

van Boxel, G. I., Stewart-Jones, G., Holmes, S., Sainsbury, S., Shepherd, D., Gillespie, G. M., Harlos, K., Stuart, D. I., Owens, R., & Jones, E. Y. (2009). Some lessons from the systematic production and structural analysis of soluble (alpha)(beta) T-cell receptors. *J Immunol Methods*, *350*(1-2), 14-21. https://doi.org/10.1016/j.jim.2009.08.008

van Gent, D. C., Ramsden, D. A., & Gellert, M. (1996). The RAG1 and RAG2 proteins establish the 12/23 rule in V(D)J recombination. *Cell*, *85*(1), 107-113.

Vigano, S., Utzschneider, D. T., Perreau, M., Pantaleo, G., Zehn, D., & Harari, A. (2012). Functional avidity: a measure to predict the efficacy of effector T cells? *Clin Dev Immunol*, *2012*, 153863. https://doi.org/10.1155/2012/153863

Vignali, D. A., Collison, L. W., & Workman, C. J. (2008). How regulatory T cells work. *Nat Rev Immunol*, *8*(7), 523-532. https://doi.org/10.1038/nri2343

Villaseñor, J., Besse, W., Benoist, C., & Mathis, D. (2008). Ectopic expression of peripheral-tissue antigens in the thymic epithelium: probabilistic, monoallelic, misinitiated. *Proc Natl Acad Sci U S A*, *105*(41), 15854-15859. https://doi.org/10.1073/pnas.0808069105

von Boehmer, H. (2005). Unique features of the pre-T-cell receptor alpha-chain: not just a surrogate. *Nat Rev Immunol*, *5*(7), 571-577. https://doi.org/10.1038/nri1636

Walseng, E., Wälchli, S., Fallang, L. E., Yang, W., Vefferstad, A., Areffard, A., & Olweus, J. (2015). Soluble T-cell receptors produced in human cells for targeted delivery. *PLoS One*, *10*(4), e0119559. https://doi.org/10.1371/journal.pone.0119559

Wang, L., Winnewisser, J., Federle, C., Jessberger, G., Nave, K. A., Werner, H. B., Kyewski, B., Klein, L., & Hinterberger, M. (2017). Epitope-Specific Tolerance Modes Differentially Specify Susceptibility to Proteolipid Protein-Induced Experimental Autoimmune Encephalomyelitis. *Front Immunol*, *8*, 1511. https://doi.org/10.3389/fimmu.2017.01511

Wirnsberger, G., Hinterberger, M., & Klein, L. (2011). Regulatory T-cell differentiation versus clonal deletion of autoreactive thymocytes. *Immunol Cell Biol*, *89*(1), 45-53. https://doi.org/10.1038/icb.2010.123

Yague, J., Blackman, M., Born, W., Marrack, P., Kappler, J., & Palmer, E. (1988). The structure of V alpha and J alpha segments in the mouse. *Nucleic Acids Res*, *16*(23), 11355-11364. https://www.ncbi.nlm.nih.gov/pmc/articles/PMC339015/pdf/nar00165-0402.pdf

Yousefi, O. S., Günther, M., Hörner, M., Chalupsky, J., Wess, M., Brandl, S. M., Smith, R. W., Fleck, C., Kunkel, T., Zurbriggen, M. D., Höfer, T., Weber, W., & Schamel, W. W. (2019). Optogenetic control shows that kinetic proofreading regulates the activity of the T cell receptor. *Elife*, *8*. https://doi.org/10.7554/eLife.42475

Zadran, S., Standley, S., Wong, K., Otiniano, E., Amighi, A., & Baudry, M. (2012). Fluorescence resonance energy transfer (FRET)-based biosensors: visualizing cellular dynamics and bioenergetics. *Appl Microbiol Biotechnol*, *96*(4), 895-902. https://doi.org/10.1007/s00253-012-4449-6

# 9. List of abbreviations

| | |
|---|---|
| **2D** | two dimensional / in situ (1.6.4) |
| **3D** | three-dimensional (1.6.4) |
| **ACK (buffer)** | ammonium-chloride-potassium (buffer) |
| **AIRE** | autoimmune-regulator |
| **APC** | antigen presenting cell |
| **APS1** | autoimmune polyendocrinopathy syndrome type 1 |
| **BirA** | E. coli biotin ligase |
| **BmDC** | bone marrow derived dendritic cells |
| **C** | constant (domain) |
| **CD** | cluster of differentiation |
| **cDMEM** | complete Dulbecco's modified eagle's medium |
| **CDR** | complementarity determining region |
| **cIMDM** | Complete Iscove modified Dulbecco media |
| **D** | diversity (segment) |
| **DC** | dendritic cell |
| **DN** | double negative ($CD4^-$ & $CD8^-$) |
| **DNA** | deoxyribonucleic acid |
| **DP** | double positive ($CD4^+$ & $CD8^+$) |
| **EAE** | experimental autoimmune encephalitis |
| **EC50** | Half maximal effective concentration |
| **EDTA** | ethylenediaminetetraacetic acid |
| **ETP** | early thymic progenitors |
| **FAB** | antigen binding fragment |
| **FACS** | fluorescence-activated cell scanning |
| **fixed-β** | $TCR\beta^-$ $PLP1^{tg}$ $TCR\alpha^{+/-}$ $Foxp3^{gfp}$ |
| **Foxp3** | forkhead box P3 |
| **FRET** | Förster resonance energy transfer |
| **FSC-A** | forward Scatter area |
| **GFP** | green fluorescent protein |
| **GM-CSF** | granulocyte/macrophage-colony-stimulation-factor |
| **H3L4** | histone 3 lysine 4 |
| **H57 scFv-Cy3** | h57 single chain variable fragment linked to Cy3 fluorophore |
| **HSC** | hematopoietic stem cell |
| **huCD2** | human CD2 |
| **$IA^b$** | Mouse MHC class II I-Ab |
| **ICAM-1** | Intercellular adhesion molecule **1** |
| **$IE^K$** | Mouse MHC class II I-Ek |
| **IPTG** | isopropyl-β-d-thiogalactopyranoside |
| **J** | joining segment |
| **kana** | kanamycin |
| **KD** | dissociation constant |
| **KO** | knockout |

| | |
|---|---|
| **$k_{off}$** | off-rate |
| **$k_{on}$** | on-rate |
| **Lac I operon** | Lactose Operon 1 |
| **LB** | lysogeny broth |
| **Lck** | lymphocyte-specific protein tyrosine kinase |
| **LFA-1** | Lymphocyte function-associated antigen 1 |
| **LPS** | Lipopolysaccharide |
| **MFI** | mean fluorescence intensity |
| **MHC** | major histocompatibility complex |
| **mRNA** | messenger ribonucleic acid |
| **mTEC** | medullary thymic epithelial cell |
| **NFAT** | nuclear factor of activated t cells |
| **OD600** | optical density measurements at a wavelength of 600 nm |
| **OVA** | ovalbumin |
| **PBS** | phosphate-buffered saline |
| **PCR** | *polymerase chain reaction* |
| **PFA** | Perfluoroalkoxy alkanes |
| **PLP** | myelin proteolipid protein |
| **Plt.** | plateau |
| **pMHC** | peptide loaded major histocompatibility complex |
| **PVDF** | Polyvinylidene fluoride |
| **RAG** | recombination activating gene |
| **RNA** | Ribonucleic acid |
| **scFv** | single-chain variable fragment |
| **SCID** | severe combined immunodeficiency |
| **SD** | standard deviation |
| **SDS page** | sodium dodecyl sulfate polyacrylamide gel electrophoresis |
| **SP** | single positive ($CD4^+$ $CD8^-$ or $CD8^+$ $CD4^-$) |
| **SPR** | surface plasmon resonance |
| **SSC-A** | side scatter area |
| **t1/2** | half-life |
| **TCR** | T cell receptor |
| **TEC** | thymic epithelial cell |
| **Tet** | tetramer |
| **tg** | transgene |
| **TIRF** | Total internal reflection fluorescence |
| **Treg** | Regulatory T cell |
| **tRNA** | Transfer ribonucleic acid |
| **TSP** | thymus seeding progenitors |
| **V** | variable (domain) |
| **WT** | Wild type |

# 10. Appendix

## 10.1. List of figures


**Figure 1| Structure of MHC I and MHC II** 12

**Figure 2| T cell receptor** 13

**Figure 3| Thymic T cell development** 15

**Figure 4| Affinity model of thymocyte selection** 18

**Figure 5| Interaction between TCR and peptide loaded MHC complex (pMHC)** 19

**Figure 6| FRET-based assay to quantify TCR-pMHC binding *in situ*** 22

**Figure 7| $IA^b$ restricted epitopes of PLP** 24

**Figure 8| Schematic representation of PLP1-tetramer** 25

**Figure 9| PLP1-tetramer specific repertoire analysis** 28

**Figure 10| Schematic representation of a soluble TCR** 30

**Figure 11| Expression of soluble TCRs under "standard" conditions** 32

**Figure 12| Collapse of α*TCR-F grey* cultures upon induction** 33

**Figure 13| Plasmid stability and toxicity in BL21(DE3) E. coli** 35

**Figure 14| Stable *OverExpress™* E. coli cultures upon induction** 36

**Figure 15| Plasmid stability and toxicity in OverExpress™ C41pLys E. coli** 37

**Figure 16| Expression of α*TCR-F grey* was not detectable in OverExpress™ cells** 38

**Figure 17| Quality control of T hybridoma cell lines** 40

**Figure 18| *In vitro* stimulation assay with PLP peptide** 40

**Figure 19| PLP1-tetramer surface staining of T hybridoma cells** 43

**Figure 20| Schematic representation of tetramer dissociation** 44

**Figure 21| PLP1-tetramer dissociation** 45

**Figure 22| PLP1-$IA^b$ monomer stimulates T hybridoma cells** 48

**Figure 23| Interaction of *TCR-F grey* T cells with a functionalized, glass supported lipid bilayer with or without PLP1-$IA^b$ monomer** 50

**Figure 24| A lipid bilayer functionalized with PLP1-$IA^b$ monomer activates T cells** 51

**Figure 25| Partial amino acid sequence PLP1-IAb** 52

**Figure 26| Mutation of cysteine at position -2 of PLP-$IA^b$ monomer does not influence stimulatory potency** 53

**Figure 27| Prediction of 3 potential FRET acceptor fluorophore positions in PLP1-$IA^b$ monomer** 54

**Figure 28| 12% SDS page of PLP1-$IA^b$ FRET constructs** 55

**Figure 29| Identification of the α chain by streptavidin shift assay** 56

**Figure 30| Identification of the β chain by western plot** 56

**Figure 31| PLP1-$IA^b$ constructs were functional** 57

**Figure 32| PLP1-IA$^b$ FRET constructs resulted in low FRET signals** **58**
**Figure 33| TCR functional avidity hierarchy** **63**
**Figure 34| Niche size for $T_{reg}$ cell development correlates with TCR functional avidity** **66**
**Figure 35| catch vs. slip bonds** **69**
**Figure 36| Principle of FRET** **71**
**Figure 37| Gating strategy of stimulation assays** **82**
**Figure 38| Calculation of half effective concentration** **82**
**Figure 39| Schematic representation of tetramer dissociation** **84**

## 10.2. List of tables

**Table 1| Classification of *representative* TCRs** **27**
**Table 2| Statistical comparison of lgEC50** **42**
**Table 3| Summary of mean of measured tetramer dissociation parameters** **46**
**Table 4| Statistical comparison of $MFI_0$ and half-life** **46**
**Table 5| PLP1-IA$^b$ FRET constructs** **76**

# 11. Curriculum Vitae

**Personal Details:**

| | |
|---|---|
| Name: | Emanuel Urmann |
| Date of birth: | 01.03.1995 |
| Nationality: | Germany |
| E mail: | emanuel1urmann@gmail.com |

**Education:**

| | |
|---|---|
| 2010 – 2013 | Abitur at Internatsschule Schloss Hansenberg, Geisenheim |
| 2013-2020 | medical degree at LMU Munich |
| December 2020 | Approbation |

**Experience:**

| | |
|---|---|
| 2017-2021 | scientist at Institute for Immunology LMU Munich, AG Klein |
| Since June 2021 | research assistant and physician at University hospital Mainz |

**Scholarships**

| | |
|---|---|
| 2013-2020 | scholarship of the Konrad-Adenauer-Stiftung |
| 2017-2018 | MD scholarship of the ‚*Integrated Research Training Group*' of the SFB 1054 |

**Volunteer work**

| | |
|---|---|
| June 2014 | international culture and sport exchange with japan (Yoro-Cho sports club) |
| 2014-2018 | CEO of the Hansenberg Alumni Verein (e.V.) |
| 2016/2017 | Groupspeaker of Konrad-Adenauer-Stiftung |
| 2018-2021 | CEO of the Ehemaligenstiftung Hansenberg |

**Publications:**

| | |
|---|---|
| 2018 | Emanuel Urmann et al. „How does TCR affinity influence the mechanisms of central tolerance induction“ poster: DGFI Spring School on Immunology, Ettal. |
| 09/2019 | Tobias Hassler, Emanuel Urmann et al. „Inventories of naive and tolerant mouse CD4 T cell repertoires reveal a hierarchy of deleted and diverted T cell receptors.” Proc Natl Acad Sci USA. 2019 Sep 10;116(37):18537-18543. DOI: 10.1073/pnas.1907615116 |

# 12. Affidavit

LMU LUDWIG-MAXIMILIANS-UNIVERSITÄT MÜNCHEN | Promotionsbüro Medizinische Fakultät | MMRS

**Eidesstattliche Versicherung**

Emanuel Urmann

Name, Vorname

Ich erkläre hiermit an Eides statt, dass ich die vorliegende Dissertation mit dem Titel:

*TCR functional avidity defines the size of the clonal $T_{reg}$ cell conversion niche*

selbständig verfasst, mich außer der angegebenen keiner weiteren Hilfsmittel bedient und alle Erkenntnisse, die aus dem Schrifttum ganz oder annähernd übernommen sind, als solche kenntlich gemacht und nach ihrer Herkunft unter Bezeichnung der Fundstelle einzeln nachgewiesen habe.

Ich erkläre des Weiteren, dass die hier vorgelegte Dissertation nicht in gleicher oder in ähnlicher Form bei einer anderen Stelle zur Erlangung eines akademischen Grades eingereicht wurde.

Mainz, 07.07.2022 — Emanuel Urmann

Ort, Datum — Unterschrift Doktorandin bzw. Doktorand